

# Investigation of Orbital Debris Situational Awareness with Constellation Design and Evaluation

Ethan B. Ohriner

Thesis submitted to the Faculty of the  
Virginia Polytechnic Institute and State University  
in partial fulfillment of the requirements for the degree of

Masters of Science  
In  
Aerospace Engineering

Jonathan T. Black, Chair  
Kevin Shinpaugh  
Matt VanDyke

11 December 2020  
Blacksburg, Virginia

Keywords: orbital debris, laser debris removal, constellation design, space situational awareness

Copyright 2020, Ethan B. Ohriner

# Investigation of Orbital Debris Situational Awareness with Constellation Design and Evaluation

Ethan B. Ohriner

## ABSTRACT

Orbital debris is a current and growing threat to reliable space operations and new space vehicle traffic. As space traffic increases, so does the economic impact of orbital debris on the sustainability of systems that increasingly support national security and international commerce. Much of the debris collision risk is concentrated in specific high-density debris clusters in key regions of Low Earth Orbit (LEO). A potential long-term solution is to employ a constellation of observation satellites within these debris clusters to improve monitoring and characterization efforts, and engage in Laser Debris Removal (LDR) as means of collision mitigation. Here we adapted and improved a previous methodology for evaluating such designs. Further, we performed an analysis on the observer constellations' effectiveness over a range of circular, elliptical, and self-maneuvering designs. Our results show that increasingly complex designs result in improved performance of various criteria and that the proposed method of observation could significantly reduce the threat orbital debris poses to space operations and economic growth.

# Investigation of Orbital Debris Situational Awareness with Constellation Design and Evaluation

Ethan B. Ohriner

## GENERAL AUDIENCE ABSTRACT

Orbital debris is defined as all non-operational, man-made objects currently in space. US national space regulations require every new satellite to have a de-orbit plan to prevent the creation of new debris, but fails to address the thousands of derelict objects currently hindering space operations. As space traffic increases, so does the economic impact of orbital debris on the sustainability of systems that increasingly support national security and commercial growth. While orbital debris is usually assessed by looking at the full volume of space, most massive debris objects are concentrated in high-density clusters with a higher than normal probability for collision. A potential solution to the growing orbital debris problem is to place a group of observation satellites within these debris clusters to both improve monitoring capabilities and provide a means for preventing potential collisions by engaging with debris via Laser Debris Removal (LDR). This research presents a methodology for comparing and contrasting different observer satellite constellation designs. Our results show that increasingly complex orbit designs improve various performance criteria, but ultimately orbits that more closely match those of the debris objects provide the best coverage. The proposed method of observation and engagement could significantly reduce the threat orbital debris poses to space operations and economic growth.

# Table of Contents

<b>I.</b>	<b>Introduction</b> .....	1
A.	Background.....	1
B.	Problem Statement.....	2
C.	Research Objectives, Questions, and Hypothesis.....	4
<b>II.</b>	<b>Background</b> .....	6
A.	Debris Clusters.....	6
B.	Laser Debris Removal.....	8
1.	Literature Review.....	10
2.	L'ADROIT.....	11
3.	Spaceborne, Pulsed UV Laser System.....	13
4.	Summary.....	14
<b>III.</b>	<b>Methodology</b> .....	16
A.	Modeling.....	16
1.	Approach.....	16
2.	Preliminary Analysis.....	17
B.	Metrics.....	18
C.	Code Structure.....	20
1.	Satellite Initialization.....	20
2.	Maneuvering Cases.....	22
2.1	Phasing Maneuver Logic.....	23
2.2	RAAN Maneuver Logic.....	26
3.	Conjunction Data Generation.....	28
4.	Metrics.....	29
4.1	Percent Coverage (PC).....	30
4.2	Time Average Gap (TAG).....	31
4.3	Mean Duration (MD).....	31
4.4	Mean Response Time (MRT).....	31
4.5	Metric Rollup.....	32
<b>IV.</b>	<b>Analysis and Results</b> .....	34
A.	Static Circular Cases.....	34
B.	Static Elliptical Cases.....	40

C. Phasing Maneuver Cases .....	47
D. RAAN Maneuver Cases.....	51
<b>V. Conclusion</b> .....	<b>55</b>
<b>References</b> .....	<b>57</b>
<b>Appendix A: Cluster Information</b> .....	<b>58</b>
<b>Appendix B: Simulation Code</b> .....	<b>74</b>

## List of Figures

Fig. 1	Cluster Spatial Density and Location, with Total Cluster Mass [2] .....	6
Fig. 2	L'ADROIT LDR System for Orbital Debris Removal. [4] .....	11
Fig. 3	Code Structure Flowchart .....	20
Fig. 4	STK 3D Graphics Window .....	22
Fig. 5	Phasing Maneuver Flowchart.....	24
Fig. 6	Phasing Maneuver .....	25
Fig. 7	Phasing Maneuver Targeted with STK Astrogator .....	25
Fig. 8	RAAN Maneuver, Changing the Node [12].....	27
Fig. 9	RAAN Maneuver Targeted with STK Astrogator, $\Omega_i = 0^\circ$ , $\Omega_f = 5^\circ$ , $i = 74^\circ$ .....	27
Fig. 10	Conjunction Data Structure.....	28
Fig. 11	Metric Rollup Flowchart .....	33
Fig. 12	Cluster 1 Circular Static Total Score.....	35
Fig. 13	Cluster 2 Circular Static Total Score.....	35
Fig. 14	Cluster 3 Circular Static Total Score.....	36
Fig. 15	Cluster 1 Circular Static Metrics .....	38
Fig. 16	Cluster 2 Circular Static Metrics .....	39
Fig. 17	Cluster 3 Circular Static Metrics .....	39
Fig. 18	Cluster 1 Elliptical Static Total Score .....	41
Fig. 19	Cluster 2 Elliptical Static Total Score .....	42
Fig. 20	Cluster 3 Elliptical Static Total Score .....	42
Fig. 21	Cluster 1 Circular Phasing Maneuver Total Score .....	48
Fig. 22	Cluster 1 Elliptical Phasing Maneuver Total Score .....	48
Fig. 23	Spherical Coverage Gaps .....	52
Fig. 24	Cluster 1 Circular RAAN Maneuver Total Score .....	53
Fig. 25	Cluster 1 Elliptical RAAN Maneuver Total Score.....	53

## List of Tables

Table 1	Debris Cluster Characteristics .....	7
Table 2	STK Astrogator Mission Segments .....	23
Table 3	Cluster 1 Circular Static Performance Results .....	37
Table 4	Cluster 2 Circular Static Performance Results .....	37
Table 5	Cluster 3 Circular Static Performance Results .....	38
Table 6	Circular vs. Elliptical Result Statistics .....	43
Table 7	Cluster 1 Elliptical Static Performance Results.....	44
Table 8	Cluster 2 Elliptical Static Performance Results.....	45
Table 9	Cluster 3 Elliptical Static Performance Results.....	46
Table 10	Cluster 1 Circular Phasing Maneuver Performance Results .....	49
Table 11	Cluster 1 Elliptical Phasing Maneuver Performance Results.....	50
Table 12	Cluster 1 Circular RAAN Maneuver Performance Results .....	54
Table 13	Cluster 1 Elliptical RAAN Maneuver Performance Results .....	54

# 1. Introduction

## A. Background

It is globally accepted that orbital debris is a growing hazard that threatens space operations and the future of space traffic management. In 2017, The United States Congress acknowledged as part of the NASA Transition Authorization Act, S.442\*, that "... orbital debris poses serious risks to the operational space capabilities of the U.S.; an international commitment and integrated strategic plan are needed to mitigate the growth of orbital debris wherever possible." There have already been multiple documented events in which debris impact has resulted in the termination of an active satellite. Numerous other spacecraft anomalies are also suspected to have been caused by collisions with untracked debris.

A collision between space debris objects would have an immediate impact on space flight safety, causing a deterioration of payload operations and a reduction in the operational lifetimes of satellites. Past satellite collisions have already demonstrated the amount of additional debris that is generated from a high velocity impact. The Iridium-Cosmos collision in 2009 involved a total mass of 1600 kg and produced over 3000 trackable fragments and likely 30,000 non-trackable fragments.[1, 2] Further, the 850kg Fengyun-1C destruction resulted in roughly 2,200 trackable fragments and likely over 25,000 non-trackable fragments.[2] The debris from these collisions will remain in orbit for decades, creating an ongoing collision threat for objects in Low Earth Orbit (LEO).

The amount of debris created from a collision is directly proportional to the total mass involved, meaning increased attention should be placed on the most massive at-risk objects. While much of the orbital debris collision risk is usually assessed by looking at the full volume of LEO, most

---

\* S.442 – National Aeronautics and Space Administration Transition Authorization Act of 2017. 115<sup>th</sup> Congress. Public Law No: 115-10 (03/21/2017)



massive debris objects are located in tightly clumped clusters with a higher probability for collision due to their overlapping altitudes and inclinations. These clusters are composed of mostly abandoned rocket bodies that are up to 8,300kg each. Three of these clusters account for almost 30% of all derelict mass in LEO. The massive size of these objects combined with the increased probability of collision makes these clusters one of the most immediate risks posed by orbital debris.[2]

To properly address this looming threat, a new approach to space traffic management must be developed that can monitor and characterize these massive debris objects in their operational environment, while simultaneously focusing on preventing a catastrophic collision that could hinder space operations for decades.

## **B. Problem Statement**

Ground based monitoring of these debris clusters is not adequate enough to properly mitigate their inherent risk. Space based sensors can improve Space Situational Awareness (SSA) capabilities beyond what is achievable with ground based sensors. Close up characterization can help identify if large derelicts have existing damage from collisions with non-trackable debris, while monitoring for new damage in an effort to delineate the location of currently non-trackable debris. In addition to providing a higher level of monitoring and characterization, a space based SSA constellation integrated within the debris clusters allows for faster intervention in the event a potential collision is determined.

The risk of collision between the massive objects within these clusters can be properly mitigated with a system capable of reliably performing Just-In-Time Collision Avoidance (JCA). This method involves predicting potential collisions and intervening by nudging the orbit of one of the involved objects. Various methods of performing JCA have been explored for a number of years,

such as deploying talcum powder or a cloud of gas in a satellites path via sounding rockets.[3] One of the more promising and economically viable options for JCA is Laser Debris Removal (LDR) in which a laser is used to heat up material on a derelict satellite, creating an ejection of plasma roughly perpendicular to the surface.[4] This ejection imparts momentum onto the debris, effectively raising or lowering its orbit. LDR can be performed over a wide scope of ranges, and could be effectively applied by a constellation of observer satellites.

One of the challenges with developing SSA capabilities is determining what level of coverage and interaction between the observer satellites (OBS) and the resident space objects (RSO) is adequate. Any constellation of observer satellites must be able to monitor every object within the cluster with enough quality and timeliness to accurately predict all potential collisions, but also provide a full scope LDR system capable of reliably intervening. The principal challenge for LDR systems operating in the LEO environment is the relative velocities between OBSs and RSOs, which make it difficult to maintain access for a long enough duration to fully re-position non-cooperative debris.

Research reported in “*Geostationary Orbit Development and Evaluation for Space Situational Awareness*” [5] developed a methodology for evaluating near-GEO observation satellite constellations to optimize their SSA capabilities. We have adapted and improved this methodology to evaluate different constellation designs for the purpose of determining the optimal configuration capable of mitigating the collision risk within the debris clusters in LEO. Different approaches, including circular, eccentric, and self-maneuvering designs are considered.

This research focuses on analyzing the methods for evaluating the performance of LEO SSA and collision intervention LDR of space debris clusters. While specific focus is placed on three particular debris clusters, the intent is not to fully develop a sensor suite and LDR system. But

rather, focus on a broad approach to highlight the achievable coverage of an observation constellation, demonstrate the collision mitigation potential, and further develop a methodology that can be applied to any SSA or interaction-based spacecraft constellation. Range, illumination, and line-of-sight based criteria will be used to assess periods of access between the OBS constellation and debris RSOs, derived from researched LDR operating constraints.

### **C. Research Objectives, Questions, and Hypothesis**

The primary aim of this research is to zero in on a constellation architecture that can most effectively mitigate the collision risk within the debris clusters by providing timely, quality, and efficient coverage. To achieve this goal, a number of research questions need to be answered. Are there certain classes of constellation designs that outperform in any of the grading metrics? This will provide insight into niche designs that could be effectively employed for specific SSA needs, such as a cluster with highly inclined objects. Additionally, will maneuvering constellations improve performance in any metrics, and will those improvements justify their fuel and  $\Delta V$  costs? Maneuvers can be costly, especially when constant maneuvering is expected. Even if maneuvering satellites improve the SSA coverage of a constellation, are the  $\Delta V$  requirements too prohibitive to consider feasibly implementing?

We hypothesize that an investigation of constellation design capabilities will result in multiple options that are able to meaningfully impact the threat orbital debris poses to space operations and economic growth. Further, the investigation will demonstrate the range of applications that the tools and methodology showcased in this research have with regards to addressing SSA and space traffic management needs. Our research shows that increasingly complex designs result in improved performance for some grading metrics, but designs that more closely mirror the specific orbits of the objects being observed offer the best results. *We expect designs that implement*

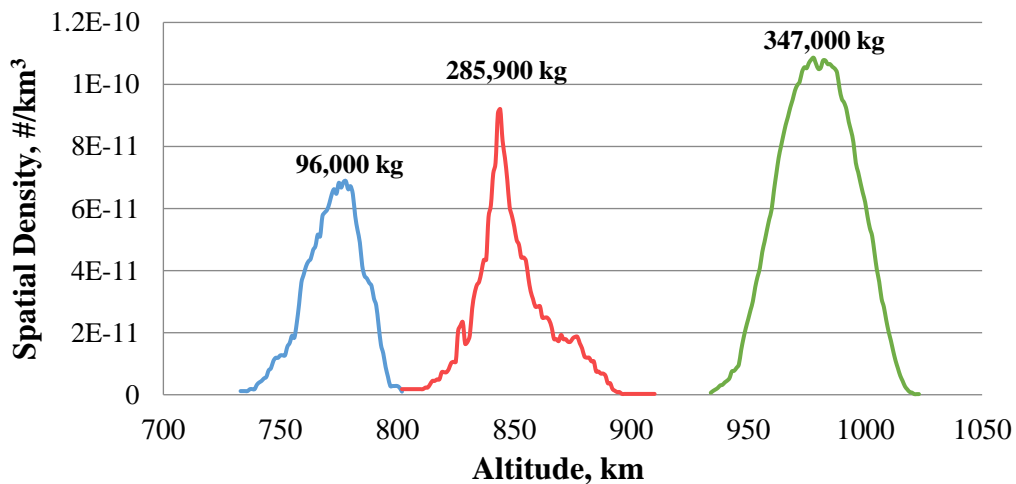
*maneuvers will improve the overall coverage of the debris clusters, but that the improvements are tempered by the significant fuel costs.* Cost and mission lifetime are important factors in a mission's ultimate success. Finally, while the same constellation architecture is expected to provide the best performance for all three clusters analyzed, it is hypothesized that the specific altitude and eccentricity that best meets the mission criteria will be different for each cluster, based on their differences in altitude, inclination, and derelict RSO dispersion.

## 2. Background

### A. Debris Clusters

For this research effort, the constellation design methodology will be applied to three independent debris clusters. Satellites are considered a ‘cluster’ when they orbit with small variations in their inclinations and altitudes. Analyses have shown that interaction between the members of these clusters is higher than typical satellite interaction statistics indicate.[4] The close proximity of the objects leads to a higher probability of collision, while the massive size of the objects magnifies the scientific and economic impact a potential collision would have on space operations in their vicinity.

Figure 1 shows the spatial density, total mass, and average altitude of each cluster. The combined mass of the clusters accounts for close to 30% of the total derelict mass in LEO.[2] Table 1 contains basic characteristics of the clusters being evaluated, including the probability of collision in one year, and the estimated debris produced from a collision. The clusters are comprised of mostly Russian rocket bodies, though other payloads also contribute to the high mass concentration. A detailed list of all objects included in each cluster is provided in Appendix A.



**Fig. 1 Cluster Spatial Density and Location, with Total Cluster Mass [2]**

**Table 1 Debris Cluster Characteristics**

Cluster Altitude	Cluster	Approximate Mass (kg) <sup>1</sup>	#	L/D (m)	Altitude Extremes		Inclination	Mass Span (kg/km)	PC/Year <sup>2</sup>	Produced From a Collision <sup>3</sup>	
					High	Lowest				Cataloged	Lethal, Nontrackable (LNT)
775km	SL-8 R/B	1,434	44	7/2.4	793	733	74	1052	1/413	2868	43020
	SL-8 Payloads	850	44	3/2	802	742	74	623		3400	42500
850km	SL-16 R/B	8,300	18	11/3.9	860	814	71	3248	1/548	16600	249000
	SL-16 Payloads	3,250	18	4/2	868	823	71	1300		13000	162500
	Other Payloads	2,000	39	4/2	910	795	80	678		8000	100000
975km	SL-8 R/B	1,434	144	7/2.4	1020	935	83	2429	1/92	2868	43020
	SL-8 Payloads	800	142	3/2	1024	934	83	1262		3200	40000
	Other Payloads	1500	18	4/2	997	905	64	293		6000	75000

1. Mass and size values are approximate as the variety of sources used did not have identical consensus - there is some uncertainty in these values. Where there are different mass objects, the approximate mass represents an average.
2. Probability of Collision (PC) is calculated using a ‘Probability Calculator’, based on number of objects, collision cross section, collision impact velocity, exposure time, volume of cluster, etc.[2]
3. Rocket Body (R/B) on R/B collisions use 1x mass for cataloged object production (but also 2x to capture both objects involved) and 15x mass for LNT. Payload (P/L) on P/L uses 2x/25x for cataloged/LNT and R/B on P/L uses 1.5x/20x. [2]

*A single collision between two 8300 kg SL-16 rocket bodies would produce an estimated 16,600 cataloged objects, and an estimated 249,000 lethal non-trackable (LNT) objects in its vicinity.*

Catalogued debris is any object greater than 10 cm, while LNTs are any debris objects smaller than 10 cm. This collision would have a much larger impact on space operations than any other recent collision event, as it would nearly double the current catalogued debris population, which is approximately 23,000 objects. The 975 km cluster has the highest probability for collision. With 304 objects, the cumulative probability of collision each year is ~1%. Debris created from a collision in either of these clusters will remain in orbit for decades. This much debris would impact

all satellites near the collisions orbit, and create a hazard for any space vehicle traveling through the debris field. Due to the similar orbits of the objects within these clusters, a single collision could lead to a runaway effect causing further impact and generating even more debris.[6]

Despite the increased risk and consequence of a collision, no group is specifically monitoring collision potential within these clusters.[2] The Combined Space Operations Center (CSpOC) is tasked with monitoring possible collisions with all operational satellites, but no attention is currently given to collisions between derelict satellites despite only 6% of catalogued space debris being operational.[6] The potential impact on operational satellites from a collision between massive derelicts makes them just as important to monitor.

## **B. Laser Debris Removal**

Laser ablation has been studied for the purpose of orbital debris mitigation for over 25 years. Materials, if heated above a specific fluence threshold ( $J/m^2$ ), will vaporize and eject plasma, imparting momentum onto the target.[7] From ground-based to space-based systems, lasers provide a promising and economic means for reducing orbital debris impact. ORION, a NASA ground-based concept validation study concluded that LDR is not only feasible, but is economically modest compared to alternative debris mitigation options, such as shielding or replacing high-value spacecraft.[8, 9] In a 2014 study, the International Coherent Amplifying Network (ICAN) developed a fiber based laser architecture to de-orbit small debris. They concluded that space-based operation of LDR systems is achievable and efficient.[10] Based on their success, ICAN researchers held the first workshop to discuss laser solutions for orbital debris in 2015.

Space based LDR systems provide many advantages over ground based systems. The space environment provides a comparatively large target access rate, which in turn permits the system to

use smaller and lighter optics while providing superior performance. Space also provides a black background, making for better target detection and acquisition. The main advantage a space based system offers, though, is in reducing the operating range between laser aperture and target. A shorter range reduces the average operating power, since the laser pulse energy is more efficient at producing momentum on the target.[7]

The measure of laser pulse energy efficiency is captured in the coupling factor ( $C_m$ ), Eq. (1), defined by laser radiation parameters including the irradiation  $I$  ( $\text{W}/\text{m}^2$ ), pulse duration  $\tau$  (s), and wavelength  $\lambda$  (m).[7]

$$C_m = \frac{C_{m0}}{(I \cdot \lambda \cdot \sqrt{\tau})^{1/4}} \quad (1)$$

$C_{m0}$  is a coefficient dependent on the target material, as a function of the average atomic mass and charge state in the ablated plasma.[7] While radiation parameter selection is crucial in the successful application of LDR systems, adjustments made on orbit mean a single system is capable of adapting to handle different sizes of debris and operating at different ranges. For larger targets, the same laser optics can be effective by increasing the pulse energy needed for smaller targets. Beam focal spot size can also be adjusted to generate the optimal fluence for any specific target.

The coupling factor is a direct measure of how effective the laser optics are at changing the targets velocity. Based on this value, Eq. (2) can be used to calculate  $\Delta V$  capabilities of the optics;  $\mu$  ( $\text{kg}/\text{m}^3$ ) represents the targets mass density,  $\Phi$  ( $\text{J}/\text{m}^2$ ) represents fluence, and  $\eta_c$  represents an impulse transfer efficiency term based on thrust direction and target orientation.[7]



$$\Delta V = \frac{\eta_c \cdot C_m \cdot \Phi}{\mu} \quad (2)$$

### 1. Literature Review

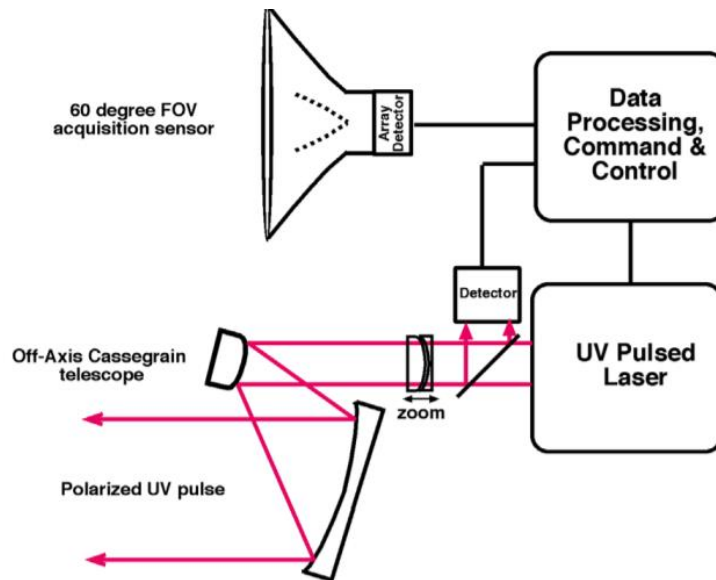
The intention of this research is not to develop a fully designed LDR system, but rather to contrast different constellation designs to find the architecture that provides the best platform for space based SSA and LDR mitigation within debris clusters. Literature review is relied on to provide reference and context for expected operating ranges, laser engagement duration expectations, and  $\Delta V$  capabilities for the high mass derelict objects within the clusters. These reference metrics will help guide the constellation judging criteria, and dictate access constraints such as range and illumination.

Two primary research articles were relied on as references with respect to space based orbital debris mitigation. First, “*L’ADROIT – A spaceborne ultraviolet laser system for space debris clearing*” [4] by Phipps and Bonnal develops a high fidelity LDR system capable of handling small and large debris. The detail of L’ADROIT (Laser Ablative Debris Removal by Orbital Impulse Transfer) incorporates realistic target detection rate, minimum and maximum operating ranges for small and large debris, and per-object cost estimates for nudging and removal. Further, “*A spaceborne, pulsed UV laser system for re-entering or nudging LEO debris, and re-orbiting GEO debris,*” [7] also by Phipps, provides an in-depth look at how the L’ADROIT system can be tweaked and applied to orbital debris mitigation on multiple levels. Various approaches to large derelict nudging are discussed, including LEO collision avoidance and GEO debris re-orbiting. Range and duration requirements for debris nudging on the scale of 10 km to 300 km are examined.

## 2. L'ADROIT

In L'ADROIT, Phipps states that “pulsed laser active debris removal using laser ablation jets on target is the most cost-effective way to re-enter [debris]”. LDR removed the need for orbit matching that most other debris removal methods require. Phipps claims that the L'ADROIT system would cost roughly \$280,000 to alter a 1-ton object's orbit by 40 km.[4]

L'ADROIT consists of two solar powered sensors; a wide field of view passive sensor for target acquisition and a narrow field of view active laser for tracking and firing. The acquisition sensor has a 60 degree field of view, with a  $70 \mu\text{rad}$  /pixel resolution that identifies targets with solar illumination. Once a target is acquired, the active laser will engage while progressively increasing its pulse energy. The laser pointing direction is guided via feedback based on plasma flashes on the target. Target position along the beam can be determined to  $\pm 7.5\text{mm}$ , giving feedback as to when a target has had its orbit altered by the desired amount.[4] Figure 2 shows the components of the L'ADROIT system, and how the two sensors work together. The zoom mirror helps focus the beam focal spot size to optimize target material ablation.



**Fig. 2 L'ADROIT LDR System for Orbital Debris Removal. [4]**

A number of factors are considered when determining the optimal operating range for the system. Reasonable pulse energy based on power consumption combined with appropriate laser spot diameter are the key factors. Good acquisition rate based on relative velocities is also important, considering transverse angular rates to maintain line of sight with the target. With all of these factors, the range for large targets is set at  $600 \pm 300$  km. The lower end of the operating range is chosen primarily based on avoiding transverse angular rates, assuming a relative velocity of 15 km/s. Though reasonable, this range is chosen based on optics intended for addressing small debris as well. The operating range for small targets is chosen as  $250 \pm 75$  km. Without the added constraint of optimizing the optics for both small and large debris, the optics could be more fine-tuned for large debris at longer ranges.[4]

For our research, a minimum range is not used to limit target access intervals, since improving general observation and SSA is also an objective. It is assumed LDR operation will occur during reasonable ranges and windows of operation. While the LDR operating windows may be shorter than recorded object access durations, the primary goal is to contrast the performance of various constellation designs, and longer duration access still implies more robust LDR operation capabilities.

The expected performance for large orbital debris intervention using L'ADROIT is estimated with a typical target  $\Delta V$  of 8.3 cm/s per 40s duration of laser interaction with a 1000 kg target.[4] This means 625 interactions are needed to achieve 43 m/s  $\Delta V$ , which is the target  $\Delta V$  needed to re-orbit the objects by 40 km. Phipps estimates it would take roughly 4 years to complete this process on 2000 one ton objects. Many of the derelict objects within the evaluated clusters in our research are around 1000kg with relative velocities at or below 15 km/s, making the performance expectations for L'ADROIT an appropriate metric for reference. However, 40 km is conservative

when considering the degree of orbit adjust necessary for collision avoidance. Shorter durations and fewer interactions could still be effective in collision mitigation.

### 3. Spaceborne, Pulsed UV Laser System

In this research, Phipps addresses the variety of impacts orbital debris have on space operations. Collisions between massive derelicts threaten space flight safety, small debris are hard to track but still pose a high risk, and large GEO derelicts occupy limited orbital slot availability. The system outlined in L'ADROIT defines an architecture for laser debris removal that can be tuned and adapted to address each unique threat orbital debris poses. Phipps explores specific, conservative radiation parameters for a variety of optics that optimize LDR effectiveness in each area.

Parameter tuning is based around implementation on a space based system, with consideration to typical derelict materials and expected operating ranges. Optimal ranges can be determined based on Eq. (3), defined by the pulse energy  $E_L$  (J), optimal fluence  $\Phi_{opt}$  ( $J/m^2$ ), mirror diameter  $D$  (m), wavelength  $\lambda$  (m), and non-dimensional beam quality  $M^2$  of the laser optics. A beam quality of  $M^2 = 1$  is the best achievable, though values closer to 2 are more realistic.[7]

$$L_{MAX} = \sqrt{\frac{\pi \cdot E_L}{\Phi_{opt}}} \cdot \frac{D}{2 \cdot M^2 \cdot \lambda} \quad (3)$$

For the GEO debris removal scenario, it is estimated that large derelicts can be adjusted by 100 km in roughly 75 days. Within this time frame, however, multiple targets can be engaged, meaning 75 days per derelict re-orbit is a highly conservative time estimate. This includes orbit circularization for any target maneuvered into a graveyard orbit. This scenario considers a 3m mirror capable of up to 6.8 kJ energy pulses, operating at a maximum range of 2400 km.[7]

For LEO derelict nudging, Phipps considers 10 km of orbit adjustment sufficient to ensure successful intervention in a potential collision. Engaging the debris from an average distance of 1600 km, nudging a 1000kg object would require 2000 pulses of 3.2 kJ. With the optics described, this would be achievable over 830 seconds of laser engagement. It is worth noting that a single engagement of 830 seconds is not necessary, and that the re-orbiting could be accomplished over multiple passes by the same observer satellite, or multiple engagements from different satellites. For a 1000 kg object at a 760 km altitude, the corresponding  $\Delta V$  to nudge by 10 km equals 0.52 m/s.[7]

#### *4. Summary*

Some aspects of LDR require further investigation before a fully developed system could be launched. While additional research is necessary though, these obstacles do not threaten the core concept. A key aspect of LDR is how effective the plasma ablation is at imparting momentum onto the target. The plasma ejection needs to be perpendicular to the target, meaning orientation of the vehicle is an important consideration. However, studies have shown that orientation errors and non-orthogonal plasma ejection can be considered as an overall momentum efficiency loss. Even with an efficiency loss, impulses in a counter-velocity direction will still lead to a semi-major axis reduction. Another important factor with object orientation is negating all angular movement to prevent tumbling of the target. This can be accomplished with closed-loop laser tracker control based on observed movement to guide impact zone selection. A common criticism of space laser technology is the difficulty in distinguishing the power beam from weaponry. It is assumed that as long as LDR systems are presented as clearly commercial and are operated in a suitable manner, weapon distinctions will not be a serious concern. Finally, further research is needed into the

ablation of target materials, such as MLI blankets and thermal protections. Without successful ablation of the target materials, momentum transfer is uncertain.[7]

Implementation of a space based LDR system with an observer satellite constellation inside of high risk debris clusters is feasible, practical, and economical. Though specifics for each cluster are not being determined, such as precise  $\Delta V$  requirements, laser duration statistics, and valid operating ranges, the reference metrics stand as appropriate benchmarks from which to extrapolate similar metrics. Three tiers of access ranges are based on the laser engagement estimates discussed in the literature review: 2400 km, 600 km, and 100 km. Though 100 km is less than the low end of the ranges discussed, it still provides a benchmark for close range laser interaction and will better characterize general satellite observation opportunities. Illumination will also be a constraint for target access, only using line-of-sight when the RSO is in direct sunlight or penumbra. Average access duration statistics for each RSO will be evaluated based on total duration time and average duration gap, as a way of ensuring engagements with large time gaps are weighted lower than constellations that provide more consistent coverage.

### **3. Methodology**

#### **A. Modeling**

A combination of Matlab and Systems Tool Kit (STK) is used for the simulation and modeling environment for this research. STK is a software package that allows for complex analysis of satellite systems, and is commercially available and integrates well with other analysis software. In determining the analysis method for this investigation, software tools were chosen that could effectively and accurately model the space environment and output all necessary data. STK is also useful in loading the debris object ephemerides by using TLE sets for any defined simulation timeframe. The TLE sets allow a constellation to be easily evaluated over multiple scenario durations and at any point in the clusters life. Lastly, STK can be commanded and operated via Matlab scripts, which allows for automation of the analysis process and easier management of the resulting data. All data processing and data management was conducted using Matlab and Microsoft Excel.

#### *1. Approach*

The three-tiered approach to the range constraint for this analysis was chosen to align with the methodology adapted from Ref. 5. Comparing the constellation designs based on their overall performance across all three access ranges ensures the robustness of the constellation is appropriately captured. Each subsequent Tier represents a benchmark for ensuring more efficient LDR capabilities and increasingly exquisite target characterization. The Tiers are easily configurable within the simulation, and can be altered to assess their impact on the success of a constellation design.

## *2. Preliminary Analysis*

When first creating the simulation environment, a number of design options were considered. The first step involved creating randomly generated clusters to refine the metrics and data collection aspect of the simulation. This work was beneficial in achieving a better understanding of the orbital motion of objects within clusters of similar altitudes and inclinations. This preliminary work was also useful for developing the maneuvers used in the constellation designs by exploring what maneuvers would be possible to implement, and which could be most effective at improving constellation performance.

The preliminary analysis stage also involved taking one of the clusters, and varying a number of core simulation parameters to assess their impact on the accuracy of the results. First, the number of observer satellites in the constellation was varied to assess the impact on cluster coverage. The typical constellation evaluated in this research has eight evenly spaced satellites, but every option down to four OBS constellations were considered and compared. The number of satellites in the constellation ultimately had no effect on the relative performance between different cases, but as expected adding observer satellites to the constellation enhances performance across the board. While the number of satellites will have an impact on the performance metrics, it will not impact how cases compare to each other. An assessment of the impact of simulation length was also conducted, comparing constellation performance when run for three, six, and 12 months. Longer scenario timeframes increase the simulation runtime drastically, so reducing the scenario time while maintaining accuracy is important. Results were consistent for all scenario lengths analyzed, indicating constellation performance will not change when examined over a three month time frame versus a 12 month time frame. Finally, the impact of Tier selection was tested to ensure different ranges wouldn't produce wildly different results. Though based on specific ranges



derived from the literature review, the Tiers are by no means absolute ranges at which each constellation can be considered effective or not, so ensuring constellations would perform relatively similar with alternate Tiers is important.

## **B. Metrics**

A core aspect of this research is how well the grading metrics capture the performance of the constellations. The metrics characterize the scope of the analysis, so it's important each metric captures a key part of the mission goal and that the relative weighing of the metrics is successfully comprehensive. The intention of this research is to determine the constellation architecture that is best suited for space based SSA and LDR collision mitigation of massive debris clusters. In this sense, the most important design choice is the range to target that defines each Tier. The closer an optical sensor is to a target, the better the characterization is regardless of sensor selection. The same is true for LDR in that regardless of laser parameters, the closer the system is to a target the more efficient the transfer of momentum will be. The range selection for each Tier combined with the selection of metrics must encompass the scope of the mission. A strong performance across all metrics is required for a successful constellation architecture. The four metrics, equally weighed, are Percent Coverage (PC), Time Average Gap (TAG), Mean Response Time (MRT), and Mean Duration (MD).

Percent Coverage is a measure of the overall time-based coverage between the constellation and the debris cluster. The total access durations for each RSO are summed and divided by the total simulation time. Maintaining contact between the RSOs and OBSs is a key aspect of SSA and LDR. A lower percent coverage metric indicates a constellation will have less constant coverage of the debris clusters and overall poorer characterization.

Time Average Gap is a measure of the mean gap duration averaged over time for each RSO. It is “the average length of the gap we would find if we randomly sampled the system”.[11] While percent coverage provides a measure of the total engagement time, TAG makes sure there is consistent coverage throughout the simulation. A constellation with large gaps in RSO coverage is not robust enough to fully mitigate the risk of debris collision. If a predicted collision were to occur during a gap in coverage for both RSOs, JCA would not be possible without maneuvering at least one of the observer satellites.

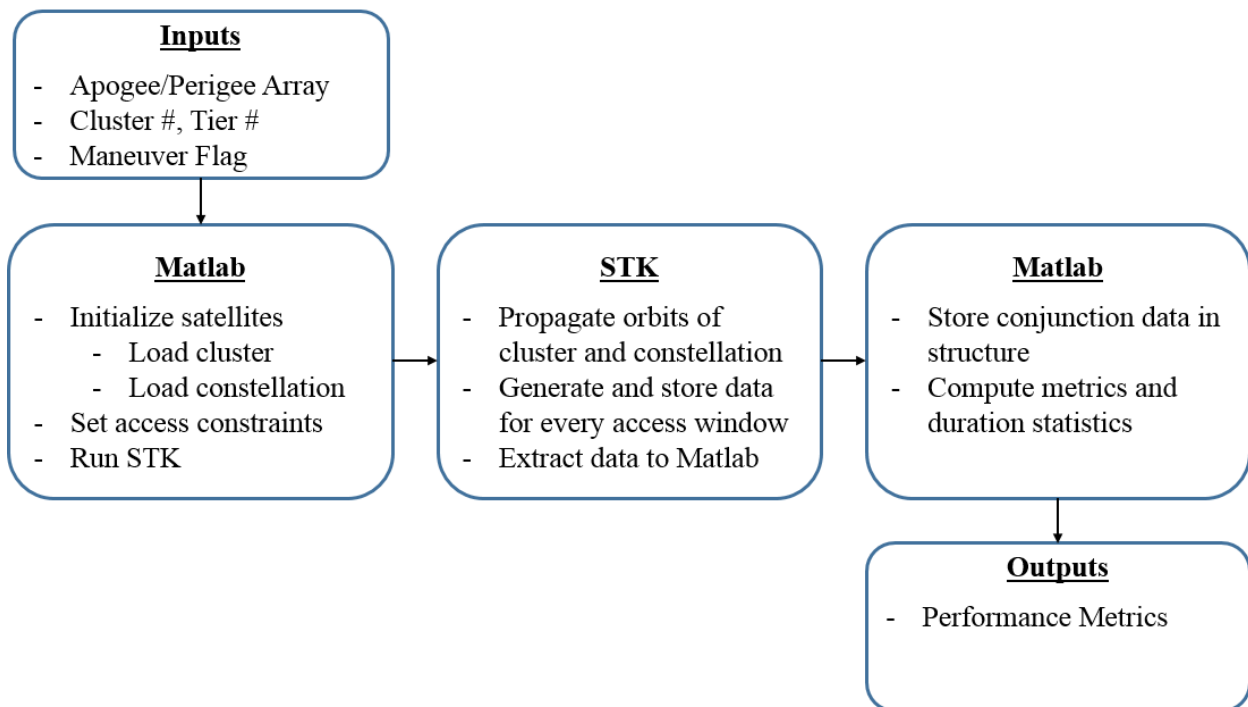
Mean Response Time “takes into account both coverage and gap statistics in trying to determine the whole systems responsiveness”[11]. MRT is a measure of how effectively a constellation is able to respond to instantaneous requests for LDR or SSA engagement.

Mean Duration is the average of every access interval for each RSO. This metric is particularly important for LDR due to the lengthy total engagement times needed to nudge large derelicts successfully into new orbits. Although PC already acts as a way of comparing the total duration times, longer individual durations means fewer conjunctions are needed to nudge a debris object which leads to overall shorter total engagement time.

These metrics can be updated and shaped to fit the goals of any constellation design analysis. For example, if exquisite characterization of RSOs is a primary mission goal, minimizing the range at closest approach could be prioritized by adding a metric that averages the closest conjunction distances for each RSO. By fitting the metrics for the mission, the methodology used in this research could be applied to any satellite grouping that would benefit from space based coverage to ensure the optimal design is found. Equations defining these metrics are found in section IV.C.4.

### C. Code Structure

The primary code is a Matlab script that uses the actxserver function to connect to STK, build the scenario, run the full simulation, and calculate all grading metrics. Data is extracted from STK during the simulation and stored in a data structure with metrics for each RSO in the scenario. The script is set up to easily change the structure of the scenario based on user inputs, including scenario length, cluster selection, maneuver flags, and constellation parameters. Once the scenario is loaded, each RSO records every conjunction with an observer satellite that meets the range, illumination, and line-of-site access criteria over the full scenario time frame. Figure 3 below outlines the flow of information for the simulation process. Each component of the analysis is explained in further detail in the following sections.



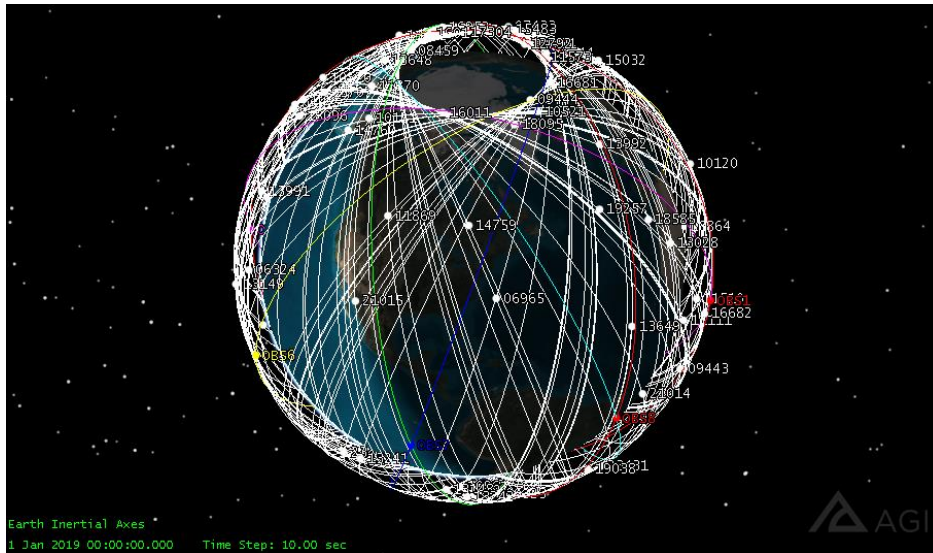
**Fig. 3 Code Structure Flowchart**

#### 1. Satellite Initialization

The first section of the code initializes the selected debris cluster by loading an array of five-digit satellite catalog numbers into STK. The Simplified General Perturbations (SGP4) propagator

in STK uses two-line element (TLE) sets to propagate each debris object by generating ephemerides based on the epoch of each TLE. SGP4 considers perturbations due to Earth oblateness, solar and lunar gravitational effects, gravitational resonance effects, and drag induced orbital decay. After initializing in STK, each RSO is configured with range and illumination constraints to define conditions for access intervals with OBSs. The range constraint is set with a maximum distance dependent on the Tier. The illumination constraint is set to only consider a conjunction if the RSO is in either direct sunlight or penumbra, as lighting is a crucial aspect of both LDR engagement and optics based observation.

The observer satellites are then initialized in the simulation based on if they are maneuvering or non-maneuvering. Maneuvering satellites build their trajectories using the STK Astrogator module and will be discussed in more detail in the following section, while non-maneuvering satellites are set up by defining their classical orbital elements (COE) and using the high precision orbit propagator (HPOP). HPOP is a numerical integration propagator that is derived using full algorithms, correct ephemerides, and is the highest fidelity propagator included in STK. Each OBS orbit is defined by an apogee, perigee, inclination, and true anomaly. All satellites in the constellation are evenly spaced around the Earth to most effectively cover the debris cluster. A range constraint is also set to ensure RSO access is limited based on the Tier. Illumination constraints are not necessary since the only lighting requirement is that the debris itself is illuminated from the perspective of the OBS. Figure 4 shows the STK 3D graphics window with Cluster 3 and an 8-object circular constellation loaded and propagated. The 304 debris objects in the cluster have their orbits shown in white, while the OBS constellation has the orbits of its 8 satellites shown in color. The constellation has an inclination of 83 degrees and a central altitude of 7346 km.



**Fig. 4 STK 3D Graphics Window**






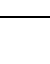
## 2. *Maneuvering Cases*

Maneuvering satellites use the STK Astrogator tool, which aids with interactive orbit maneuvering and trajectory design. Astrogator supports a wide variety of options for modeling and targeting satellite trajectories, including impulsive and finite burns, and utilizes HPOP for propagation around the trajectory design. The maneuvering satellites are initialized with COE, propagated to configured stopping conditions, determine the required  $\Delta V$  maneuver, and then repeat the process for the duration of the scenario. Maneuvering satellites attempt to improve their engagement with the debris clusters by adjusting their orbits to better interact with the debris. To be effective, however, the performance improvements must justify the  $\Delta V$  and fuel usage. Propellant is often a substantial portion of the mass budget for a satellite, and reducing  $\Delta V$  requirements extends the life of the mission.

Two types of maneuvers are considered in this research, an in-plane perigee-shift phasing maneuver to adjust the satellites position within their orbital plane and an out-of-plane Right Ascension of the Ascending Node (RAAN) maneuver to rotate the orbital plane. Table 2 identifies

all of the mission segments for STK’s Astrogator tool. These segments are used to create a mission profile for any satellite, and are capable of coordinating conditional maneuvers with a targeting sequence. All setup and commanding for maneuvering cases is handled via the Matlab interface.

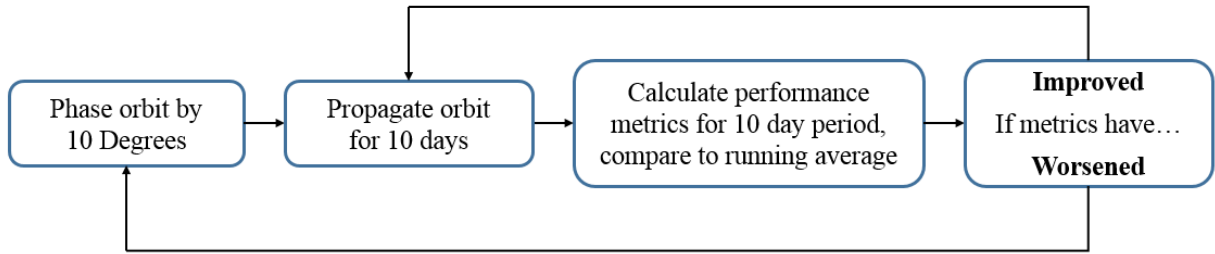
**Table 2 STK Astrogator Mission Segments**

Mission Segments	Icon	Definition	Options
Initial State		Define the initial conditions of the mission sequence.	Coordinate Frame, Initial Conditions, Orbit Epoch, Fuel Tank Parameters, Perturbations
Launch		Model a simple spacecraft launch from Earth or another central body.	Central Body, Ascent Type, Launch location, Fuel Tank Parameters, Perturbations
Follow		Set the spacecraft to follow another vehicle at a specified offset.	Offset, Join and Separation Parameters, Fuel Tank Parameters, Perturbations
Maneuver		Model a spacecraft maneuver.	Attitude Control and Orientation, $\Delta V$ Magnitude, Impulsive vs. Finite, Engine Type, Fuel Usage
Propagate		Model the movement of the spacecraft along its current trajectory until meeting specified stopping conditions.	Propagator (HPOP default), Stopping Conditions, Tolerance, Duration
Target Sequence		Run targeting profiles to converge on specified satellite conditions. Useful when stopping conditions are not easily defined.	Convergence Parameters, Iterations, Tolerances, Targeting Parameters

### 2.1 Phasing Maneuver Logic

The intention of the phasing maneuver is to reposition each satellite in the optimal position within its orbit. Phasing maneuvers are typically used in an attempt to rendezvous with another spacecraft, but are utilized in this research to improve overall performance metrics by repositioning the spacecraft to more reliably conjunct with the debris objects. The observer satellites executing the phasing maneuver will phase their orbit by 10 degrees, orbit for 10 days, and then conduct an analysis to conclude if performance has improved. On the condition performance has improved, it will orbit for another 10 days and then repeat the analysis process. On the condition that

performance has worsened, it will first perform another 10 degree phasing maneuver and then repeat the process. Over a yearlong simulation, this gives each observer satellite the chance to phase over a full 360 degrees and determine the optimal position within its orbit. Performance over each 10 day period is compared to a running average of the performance up until that point. Any satellite that executes a phasing maneuver is doing so because its performance over the 10 day propagation period has lowered its overall performance metrics. Figure 5 shows an algorithmic representation of the phasing maneuver in a flowchart.



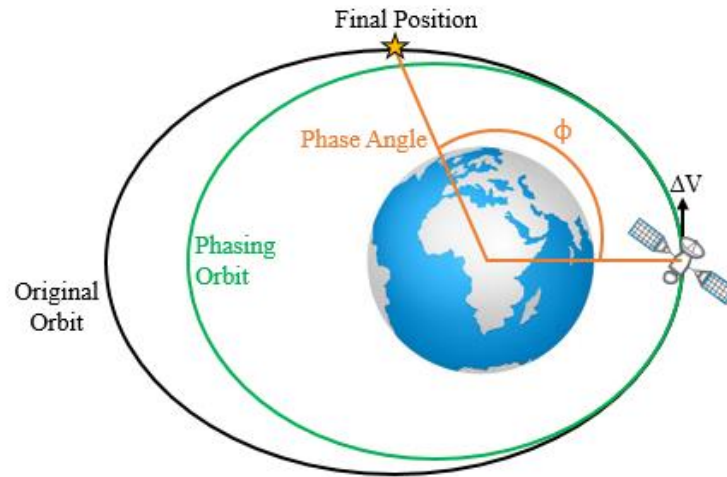
**Fig. 5 Phasing Maneuver Flowchart**

The phasing maneuver is executed using STK Astrogator’s targeting sequence function. Each maneuver involves two burns at apogee that shift the satellites perigee, one to place the satellite in a phasing orbit for a single period and a second to return the satellite to its original orbit. The semi-major axis (SMA) of the phasing orbit is determined by the desired change in period ( $T$ ). Astrogator’s targeting sequence is able to target a desired SMA, and converge on the required  $\Delta V$ . For the second burn, the original SMA is targeted. Eqs. (4-5) are used to calculate the SMA of the phasing orbit, which is used to target the maneuver.

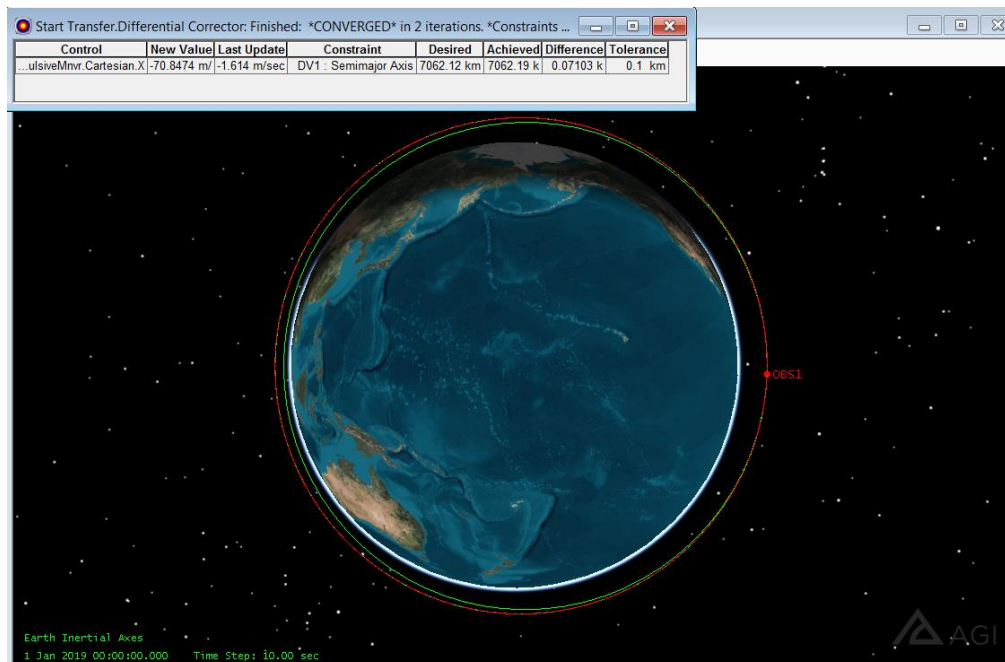
$$T_{phasing} = T_{original} \cdot \left( \frac{360 - \phi}{360} \right) \quad (4)$$

$$SMA_{phasing} = \sqrt[3]{\mu_E \cdot \frac{T_{phasing}^2}{2\pi}} \quad (5)$$

In Eq. (4),  $\phi$  equals the phasing angle and  $T_{\text{original}}$  is solved for using the original orbits SMA. Figure 6 illustrates a typical phasing maneuver intended to reposition the satellite further along its orbit. Figure 7 shows an example of the maneuver being targeted with STK.



**Fig. 6 Phasing Maneuver**



**Fig. 7 Phasing Maneuver Targeted with STK Astrogator**



## 2.2 RAAN Maneuver Logic

The intention of the RAAN ( $\Omega$ ) maneuver is to achieve more comprehensive spherical coverage of the debris clusters. The debris objects in each cluster are spread over a large range of RAANs, requiring out of plane maneuvers to ensure complete coverage. With observer satellites evenly spaced by their RAAN, there are large areas of each cluster that are unmonitored. By continually increasing the RAAN of each satellite by a small amount, the cluster should be able to provide full coverage of the debris clusters. Plane change maneuvers are one of the more costly maneuvers for spacecraft to perform, but necessary to improve spherical coverage of the debris clusters.

Plane change maneuvers can only be executed at the two points of intersection between the original plane and the desired plane. Applying a change in velocity at any point other than the common points will change both the inclination and the RAAN. First, an observer satellite is propagated to the initial argument of latitude ( $\mu_i$ ) as determined by Eqs. (6-8) [12], based on the inclination ( $i$ ) and desired RAAN change angle ( $\Delta\Omega$ ). The Astrogator tool is then used to target the new argument of latitude ( $\mu_f$ ), with the result converging on the appropriate  $\Delta V$  in the out-of-plane direction. For circular orbits, this singular burn results in a pure RAAN maneuver. For elliptical orbits, this maneuver additionally alters the perigee and requires a second burn to then correct back to the initial constellation shape.

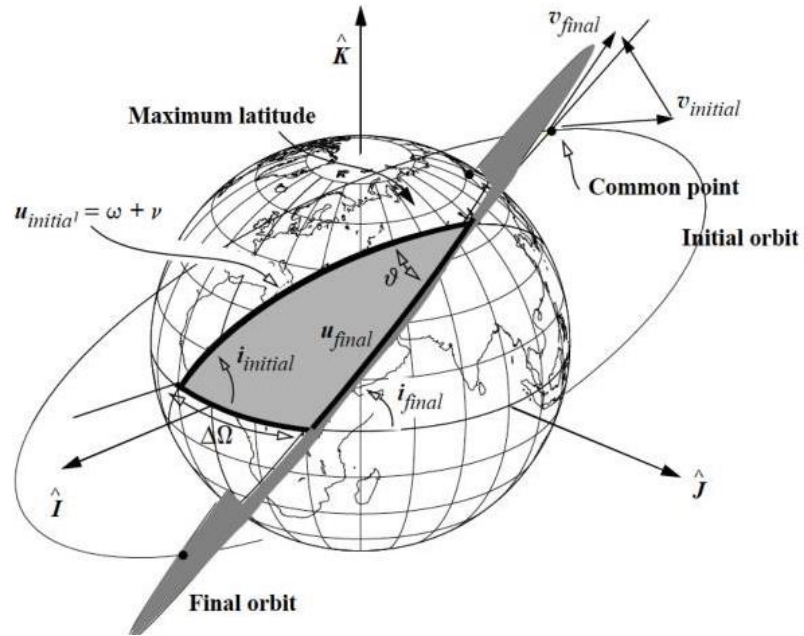
$$\cos(v) = \cos^2(i) + \sin^2(i) \cos(\Delta\Omega) \quad (6)$$

$$\cos(\mu_i) = \tan(i) \left( \frac{\cos(\Delta\Omega) - \cos(v)}{\sin(v)} \right) \quad (7)$$

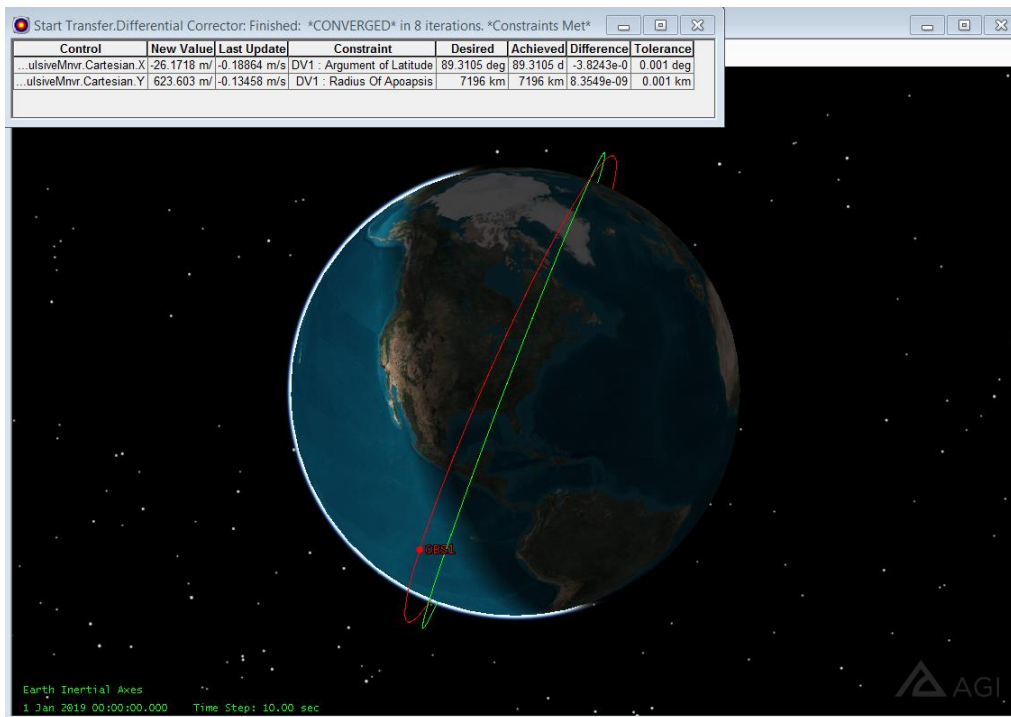
$$\cos(\mu_f) = \cos(i) \sin(i) \left( \frac{1 - \cos(\Delta\Omega)}{\sin(v)} \right) \quad (8)$$

In Eqs. (6-8),  $v$  represents the angle through which the orbital plane must rotate, and  $\mu$  represents the argument of latitude at the point of intersection before and after the maneuver. Eq. (6) is first

used to solve for  $v$ , and then Eqs. (7-8) are used to solve for  $\mu_i$  and  $\mu_f$ . Figure 8 illustrates a RAAN change maneuver, and Figure 9 shows the RAAN maneuver being targeted with STK.



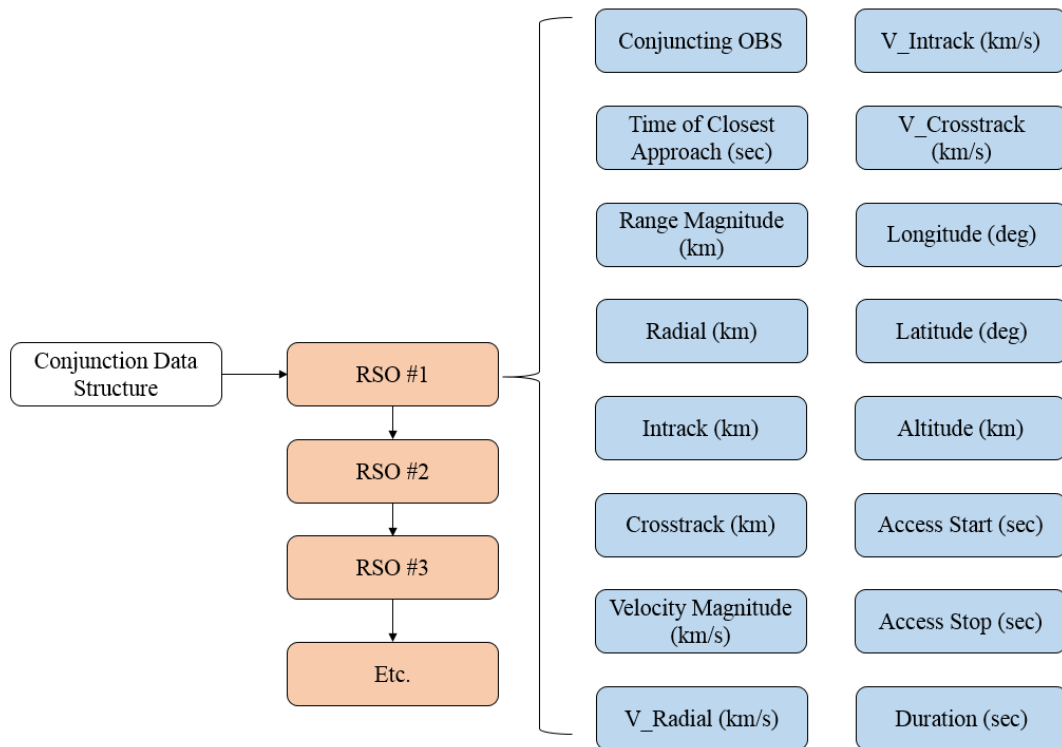
**Fig. 8 RAAN Maneuver, Changing the Node [12]**



**Fig. 9 RAAN Maneuver Targeted with STK Astrogator,  $\Omega_i = 0^\circ$ ,  $\Omega_f = 5^\circ$ ,  $i = 74^\circ$**

### 3. Conjunction Data Generation

The Conjunction Data Generation section loops through each RSO in the debris cluster and computes its access to every OBS in the constellation. This is achieved by creating a displacement vector between the two satellites in the Radial, In-Track, Cross-Track (RIC) frame and corresponding vector magnitude calculation to determine the times and ranges of each access interval. A velocity vector is then created by taking the derivative of the position vector in the Earth-Centered-Earth-Fixed (ECEF) and RIC frames. A wide range of data is collected for each access interval, including total duration, time of closest contact, position, and velocity broken into RIC frame components. The longitude, latitude, and altitude of the RSO at the time of closest approach is also recorded. Figure 10 outlines the data structure used in the analysis.



**Fig. 10 Conjunction Data Structure**

#### 4. Metrics

Once all of the conjunction data has been exported from STK into Matlab, access intervals are sorted in order of occurrence to make it easier to calculate accurate metric statistics. It is common for multiple observer satellites to be in conjunction with the same RSO at the same time, leading to double or triple counting portions of access durations in the percent coverage metric. As conjunctions overlap with each other, they are combined and counted as a single duration for that RSO. While multiple OBSs could theoretically engage an RSO at the same time, it is unlikely that would be part of normal operating procedure. Multiple LDR systems engaging a target at the same time would make it difficult to coordinate beam placement on the RSO so as to avoid canceling out each other's momentum or tumbling the target. In the context of SSA, multiple angles of observation lead to improved RSO characterization, so overlapping conjunctions are indicative of good constellation performance and are not discounted in the other metrics. Mean duration in particular would be skewed if overlapping conjunctions were merged into a single, long access interval. If the final conjunction ends before the end of the simulation, the remaining simulation time is considered a single duration gap. In this way, an RSO with no conjunctions is considered to have a single, long duration gap that equals the full simulation time.

Each constellation is evaluated based on its performance as a whole, and not according to the performance of individual observation satellites. Metrics are first calculated from the perspective of each RSO, and are then aggregated into overall system statistics that represent the performance of the constellation. Statistical analysis of each constellations performance in each metric are also recorded.

Additional metrics for judging the performance of each constellation are calculated, but not included in the official weighing scheme. Metrics that do not contribute to the relative grading

scheme, but are still important to meet a minimum level of performance. It is crucial that every RSO has some form of consistent access with at least one of the observer satellites. If a constellation does not provide coverage for every RSO in the cluster, it would not meet the requirements of a successful design, even if it were to outweigh other designs in some of the metrics. A cluster conjunction (CC) percentage is calculated and included with the results to capture this behavior. It is also important to remove constellation designs that may be constrained by onboard sensors ability to track an RSO. Relative angular rates between the OBS and RSO are recorded to ensure slew rates are not too large.

The method for calculating each metric is described in the following sections. Most of the metrics are based on those used in the methodology adapted from Ref. 5, and are further referenced in *Space Mission Analysis and Design (SMAD)*. [11] Yates and Spanbauer used an iteration based simulation model for their analysis, so some of the calculations had to be modified from versions used in their research. For scenarios where there was no contact between the RSOs and the OBSs, such as cases where the semi major axes are greater than the range constraint, default metrics are used. Percent Coverage is calculated as 0%, Mean Duration is calculated as 0 sec, and Time Average Gap and Mean Response Time are both calculated as the total simulation time.

#### *4.1 Percent Coverage (PC)*

Percent Coverage is the percentage of total simulation time that each RSO is in contact with at least 1 OBS. Higher values for percent coverage are associated with a stronger constellation performance, but can be associated with lower revisit rates. Equation 9 includes the AccessDuration set, which is an array of each conjunction duration in order or occurrence.

$$PC = \frac{\sum(\text{AccessDuration})}{\text{TotalSimTime}} \quad (9)$$

#### 4.2 Time Average Gap (TAG)

Time average gap is “the average length of the gap we would find if we randomly sampled the system”.[11] It’s calculated by assembling an array of all the coverage gap durations, and then taking the sum of the squares. The sum of the squares value is then divided by the total simulation time to produce an average time gap metric.

$$TAG = \frac{\sum(\text{DurationGaps}^2)}{\text{TotalSimTime}} \quad (10)$$

#### 4.3 Mean Duration (MD)

The mean duration is a simple calculation that captures a different aspect of the duration intervals than percent coverage. An array of all the access intervals is averaged to find the mean length of access for each RSO. The value for each RSO is then averaged to get a single value to represent the mean duration for each constellation.

$$MD = \frac{\sum \text{AccessDuration}}{\#\text{Durations}} \quad (11)$$

#### 4.4 Mean Response Time (MRT)

Two values are required for computing MRT, a response time counter and response summation. In a simulation based on timesteps, for each timestep that an RSO is not in contact with an OBS, the response summation is incremented by the full value of the current response time. For each

conjunction gap, the response time counter keeps track of a growing average that weighs incremental time. For a simulation not based on timesteps, the nth triangle number is used to compute the summation of the current response time.

Mean response time focuses on how long it takes the observer satellites to reengage the RSO by incrementing a response time variable by the full duration of the gap every second. This is accomplished by using a numerical summation equation to solve for the response summation, and dividing by the full simulation time. The MRTsum is calculated by taking the sigma summation of each component of the DurationGaps array. Each gap interval has the nth triangle number computed and added to the MRTsum array, which is ultimately summed and divided by the total simulation time. Eq. (12) below is used to compute the MRTsum array, while Eq. (13) is used to calculate the final metric.

$$\sum_{N=1}^K N = \frac{K(K+1)}{2} \quad (12)$$

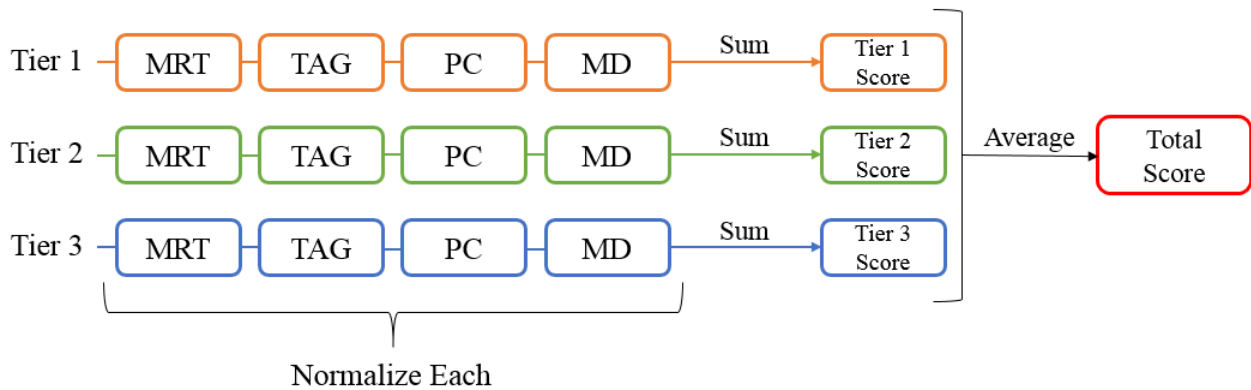
$$MRT = \frac{\sum MRTsum}{TotalSimTime} \quad (13)$$

#### 4.5 Metric Rollup

To directly compare and contrast the performances of the different constellations, a method of generating a single, succinct score was developed that encapsulates the performance of a constellation in each metric across all 3 Tiers. The total score represents the average performance of every RSO in the constellation with respect to all four grading metrics.

Within each Tier, the results for each metric are normalized by the best score, and then summed for each constellation for a best possible score of 4. A 4 is achieved by a single case having the

best performance in all four metrics. The scores for each Tier are then averaged together for a single rating for each constellation design. Every case analyzed for a cluster is normalized to the same values, making the scoring consistent across each category of cases. Figure 11 illustrates the metric rollup process. The normalization process occurs uniformly across all constellation types within a cluster, but is done independently for each cluster. Table 3 in Section IV.A shows the results for Cluster 1 circular cases, and showcases the metric rollup used as a comparison tool.



**Fig. 11 Metric Rollup Flowchart**

The scoring is intended to make the comparison process objective and enable a fair judgement to be made across all considered constellations. There are many different factors that go into deciding if a constellation design will be effective, and reducing each designs' performance into a single score is intended to provide an objective way to determine the optimal design. A well performing constellation based on these metrics is certain to provide adequate coverage based on the mission's scope. A constellation that is successful in only one Tier is unlikely to have a favorable final score, just as a constellation that performs great in a single metric but poorly in other metrics is also unable to achieve a relatively high final score.



## 4. Analysis and Results

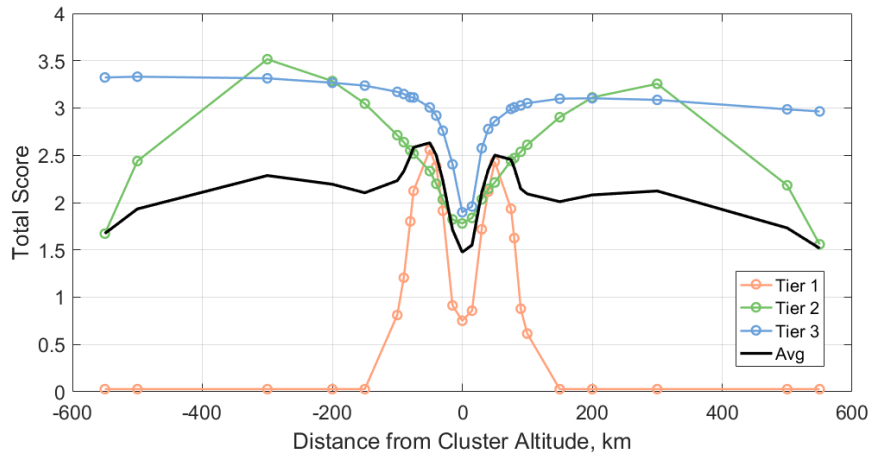
This research focuses on comparing and contrasting constellation designs for the purpose of orbital debris mitigation through LDR and SSA observation. The evaluation breaks the analysis into three maximum-range Tiers representing 100 km, 600 km, and 2400 km. Each constellation has a separate simulation run for each Tier, with different set conjunction constraints. Results from each Tier are normalized and combined into a single value that represents the performance of each case, with each Tier having equal impact on the total score. The principal metrics of interest used to evaluate the different constellation designs are MRT, TAG, PC, and MD. Color coding is used in all tables and graphics to make comparison easier, with Tier 1 results shown in orange, Tier 2 results shown in green, and Tier 3 results shown in blue.

It was hypothesized that ideal LDR constellation designs would have different orbital parameters for each RSO cluster, given the differences in inclination and altitude. All three clusters, however, produced remarkably similar results, with the best performing case for each being the non-maneuvering, circular, -50 km offset constellation. The results also show the same trends in metrics and constellation performance, with mostly symmetrical behavior. Based on the similarity between clusters in static cases, maneuvering cases were only analyzed for Cluster 1.

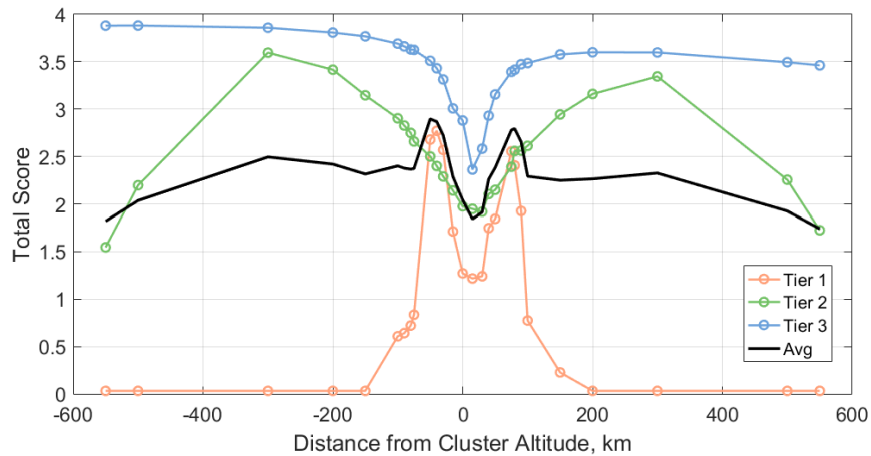
### A. Static Circular Cases

The first set of constellations evaluated were static, circular orbits with varying offsets from the central altitudes of each cluster. All constellations evaluated contain eight satellites evenly distributed around the Earth by RAAN. Figures 12-14 depict the total score of each case for each cluster, providing a summary of the performance of each constellation. Tables 3-5 show the full performance results for each cluster, while Figures 15-17 plot each of the metrics at all three Tiers. Tables 3-5 display all metrics for each case, and include a cluster conjunction (CC) percentage

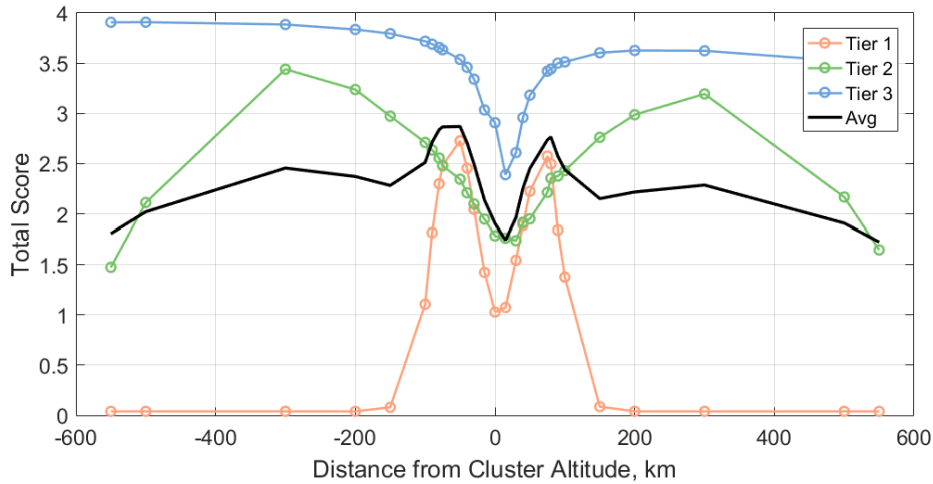
which represents the percentage of RSOs that had a conjunction. It was determined early on in the analysis that any constellations with offsets greater than the Tier 2 maximum conjunction distance perform significantly worse than other cases. As a result, the range of cases analyzed includes a large distribution of altitudes between -550 km and +550 km. Offsets greater than the Tier 1 maximum conjunction distance also perform worse overall, since they engage in no conjunctions in Tier 1. All of the best performing circular scenarios have altitude offsets less than 100 km, but including larger altitude offset cases is important for comparing how the metrics improved with higher Tiers.



**Fig. 12 Cluster 1 Circular Static Total Score**



**Fig. 13 Cluster 2 Circular Static Total Score**



**Fig. 14 Cluster 3 Circular Static Total Score**

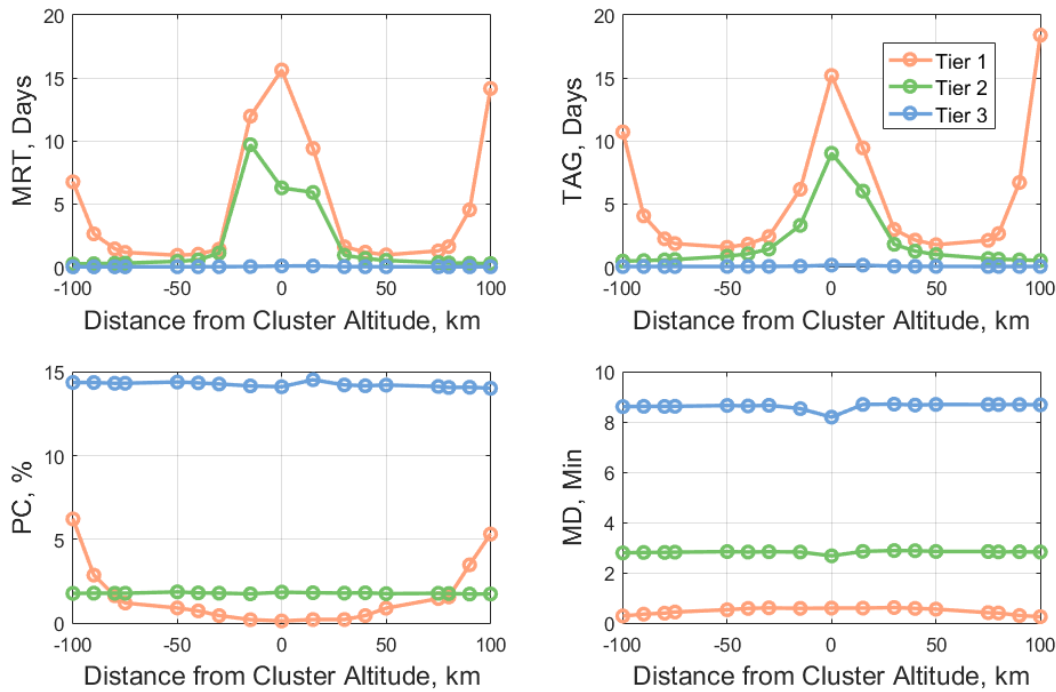
The relationships are roughly symmetric for all three clusters, with peaks in constellation performance at 50% of maximum range for Tiers 1 and 2, and fairly steady performance in Tier 3. Cases with larger offsets perform well in Tier 3, but as expected provide no capability at the lower Tier levels. Also as expected, higher Tiers provide exceptionally better performance for every case examined as this results in longer conjunction intervals.

Almost all cases perform well in Tier 3, with MRTs and TAGs under an hour and PCs of about 14%. Tier 3 also shows an average conjunction duration of almost 9 minutes. The Tier 2 metrics have much more variation in the performance of each case, with the  $\pm 300$  km cases performing the best. Constellations centered exactly at the debris cluster altitude perform the worst. This is expected since no altitude offset means a lower drift rate and less relative movement between the OBSs and RSOs within the cluster, leading to less interaction between the satellites. The best performing cases within Tier 2 have MRTs and TAGs around 5 hours and PCs under 2%. Tier 1 metrics show the most variation in performance as well as the worst performing metrics. All MDs were lower than 1 minute, but the best performing cases in Tier 1 still have favorable MRTs and TAGs of under 2 days.

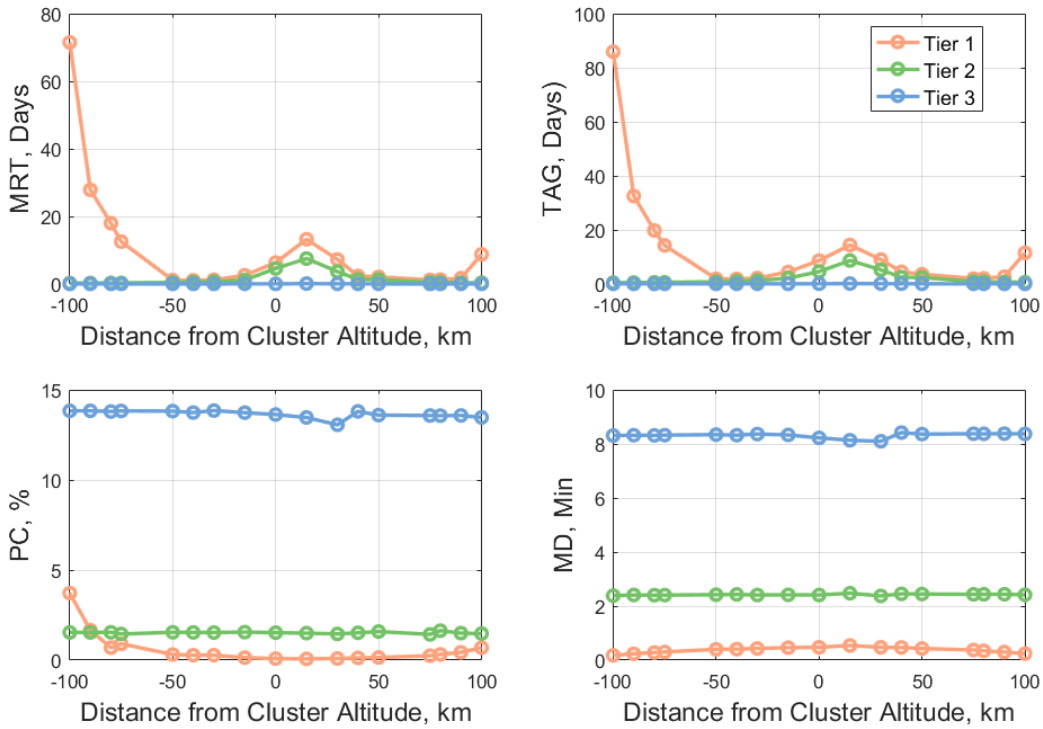


**Table 5 Cluster 3 Circular Static Performance Results**

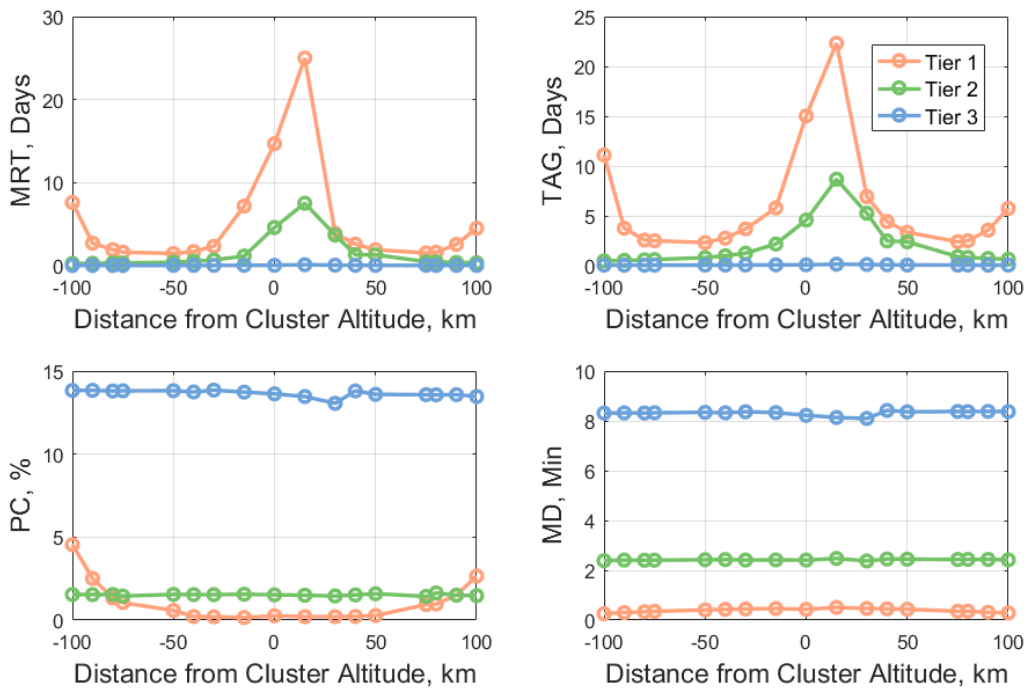
Case	Tier 1: 100 km						Tier 2: 600 km						Tier 3: 2400 km						Total Score
	MRT (days)	TAG (days)	PC (%)	MeanD (min)	CC (%)	Score	MRT (days)	TAG (days)	PC (%)	MeanD (min)	CC (%)	Score	MRT (days)	TAG (days)	PC (%)	MeanD (min)	CC (%)	Score	
circ +550km 8obj OMan	90.00	90.00	0.00	0.00	0	0.041	0.300	0.547	0.628	1.148	100	1.648	0.026	0.049	12.287	8.194	100	3.486	<b>1.725</b>
circ +500km 8obj OMan	90.00	90.00	0.00	0.00	0	0.041	0.215	0.395	0.712	1.475	100	2.167	0.025	0.048	12.431	8.230	100	3.519	<b>1.909</b>
circ +300km 8obj OMan	90.00	90.00	0.00	0.00	0	0.041	0.152	0.279	1.212	2.159	100	3.193	0.025	0.047	12.999	8.347	100	3.623	<b>2.286</b>
circ +200km 8obj OMan	90.00	90.00	0.00	0.00	0	0.041	0.194	0.352	1.397	2.337	100	2.986	0.025	0.047	13.262	8.370	100	3.626	<b>2.217</b>
circ +150km 8obj OMan	88.979	89.028	0.658	0.005	91	0.088	0.241	0.442	1.458	2.390	100	2.761	0.025	0.048	13.425	8.376	100	3.603	<b>2.151</b>
circ +100km 8obj OMan	4.499	5.746	2.660	0.289	100	1.377	0.356	0.648	1.473	2.418	100	2.429	0.027	0.051	13.469	8.370	100	3.512	<b>2.439</b>
circ +90km 8obj OMan	2.560	3.556	1.508	0.313	100	1.842	0.392	0.723	1.498	2.438	100	2.376	0.027	0.052	13.578	8.382	100	3.500	<b>2.573</b>
circ +80km 8obj OMan	1.615	2.499	0.970	0.360	100	2.497	0.453	0.827	1.636	2.436	100	2.354	0.028	0.054	13.569	8.373	100	3.441	<b>2.764</b>
circ +75km 8obj OMan	1.533	2.395	0.932	0.355	100	2.574	0.479	0.901	1.429	2.435	100	2.213	0.029	0.055	13.575	8.376	100	3.419	<b>2.736</b>
circ +50km 8obj OMan	1.914	3.352	0.276	0.436	100	2.224	1.305	2.399	1.587	2.447	100	1.951	0.035	0.065	13.598	8.363	100	3.181	<b>2.452</b>
circ +40km 8obj OMan	2.589	4.429	0.222	0.455	100	1.891	1.320	2.479	1.517	2.455	100	1.916	0.043	0.083	13.803	8.418	100	2.958	<b>2.255</b>
circ +30km 8obj OMan	3.889	6.937	0.208	0.469	100	1.544	3.680	5.258	1.455	2.377	100	1.739	0.059	0.111	13.059	8.097	100	2.609	<b>1.964</b>
circ +15km 8obj OMan	25.010	22.323	0.208	0.510	100	1.075	7.516	8.676	1.498	2.475	100	1.763	0.113	0.147	13.466	8.136	100	2.389	<b>1.742</b>
circ +0km 8obj OMan	14.687	15.027	0.263	0.432	100	1.030	4.599	4.583	1.525	2.411	100	1.786	0.046	0.080	13.629	8.223	100	2.907	<b>1.907</b>
circ -15km 8obj OMan	7.178	5.792	0.155	0.465	100	1.424	1.160	2.168	1.557	2.417	100	1.948	0.040	0.075	13.733	8.331	100	3.034	<b>2.136</b>
circ -30km 8obj OMan	2.328	3.686	0.199	0.449	100	2.045	0.679	1.251	1.534	2.411	100	2.098	0.031	0.059	13.852	8.367	100	3.340	<b>2.494</b>
circ -40km 8obj OMan	1.695	2.765	0.217	0.432	100	2.454	0.539	0.991	1.537	2.431	100	2.209	0.028	0.054	13.740	8.324	100	3.458	<b>2.707</b>
circ -50km 8obj OMan	1.469	2.314	0.580	0.409	100	2.726	0.410	0.806	1.547	2.422	100	2.344	0.027	0.051	13.818	8.343	100	3.537	<b>2.869</b>
circ -75km 8obj OMan	1.625	2.496	1.051	0.352	100	2.484	0.322	0.607	1.451	2.408	100	2.478	0.025	0.049	13.811	8.325	100	3.633	<b>2.865</b>
circ -80km 8obj OMan	1.929	2.576	1.334	0.335	100	2.299	0.314	0.575	1.546	2.405	100	2.555	0.025	0.047	13.800	8.316	100	3.656	<b>2.837</b>
circ -90km 8obj OMan	2.710	3.748	2.508	0.303	100	1.817	0.286	0.525	1.536	2.411	100	2.635	0.024	0.047	13.838	8.322	100	3.689	<b>2.713</b>
circ -100km 8obj OMan	7.603	11.098	4.547	0.258	99.333	1.107	0.261	0.485	1.541	2.386	100	2.710	0.024	0.046	13.833	8.311	100	3.718	<b>2.511</b>
circ -150km 8obj OMan	87.091	87.374	0.540	0.004	99	0.081	0.191	0.362	1.396	2.329	100	2.972	0.023	0.044	13.845	8.271	100	3.794	<b>2.282</b>
circ -200km 8obj OMan	90.00	90.00	0.00	0.00	0	0.041	0.161	0.297	1.430	2.265	100	3.237	0.022	0.043	13.815	8.225	100	3.835	<b>2.371</b>
circ -300km 8obj OMan	90.00	90.00	0.00	0.00	0	0.041	0.132	0.243	1.255	2.074	100	3.439	0.022	0.041	13.824	8.118	100	3.885	<b>2.455</b>
circ -500km 8obj OMan	90.00	90.00	0.00	0.00	0	0.041	0.225	0.359	0.680	1.292	100	2.112	0.021	0.040	13.750	7.873	100	3.908	<b>2.021</b>
circ -550km 8obj OMan	90.00	90.00	0.00	0.00	0	0.041	0.335	0.559	0.570	0.924	100	1.475	0.021	0.040	13.661	7.800	100	3.907	<b>1.808</b>



**Fig. 15 Cluster 1 Circular Static Metrics**



**Fig. 16 Cluster 2 Circular Static Metrics**



**Fig. 17 Cluster 3 Circular Static Metrics**

Figures 15-17 indicate that the MRT and TAG metrics show the most variation, and therefore have the largest impact on total score. PC and MD are relatively steady across all cases, with the exception of Tier 1 PC, which begins to increase at the edge of the Tier 1 range constraint. The metric figures only display cases for offsets up to  $\pm 100$  km to highlight the region of interest. Offsets larger than 100 have no conjunctions in Tier 1, as seen in Tables 3-5, and negatively affect the scale of the figures. Tier 1 MRT and TAG performance is best in the  $\pm 50$  km cases, which is driving the overall results. The results indicate that constellation performance is more dependent on the access focused metrics than the coverage focused metrics. With substantial relative movement between RSOs and OBSs, the access metrics are much more dependent on relative altitude.

Based solely on the circular constellation results, a constellation of observer satellites placed at the ideal altitude offset would have highly effective coverage of the debris cluster. On average, each RSO would have a Tier 3 level conjunction every hour with a long enough duration to engage in meaningful LDR, and a Tier 1 conjunction every day capable of close range SSA observation and characterization.

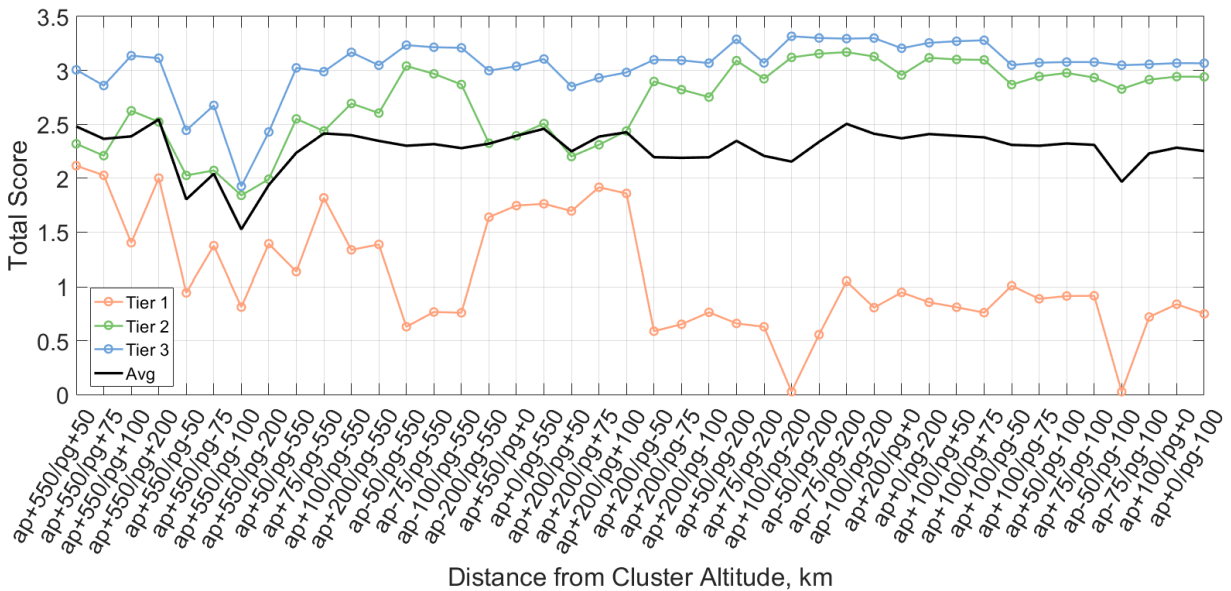
## **B. Static Elliptical Cases**

Elliptical constellations increase the OBS to RSO relative movement within the debris clusters, and allow for more frequent conjunctions with the debris objects. Generally, elliptical cases do improve performance compared to the circular cases. However while the results show that on average the elliptical cases perform better, the top performing circular case for each cluster outperformed every single elliptical case analyzed.

For Cluster 1, the average performance of all circular constellations was 2.13 with a standard deviation of 0.33, while the elliptical constellations have an average performance of 2.29 with a

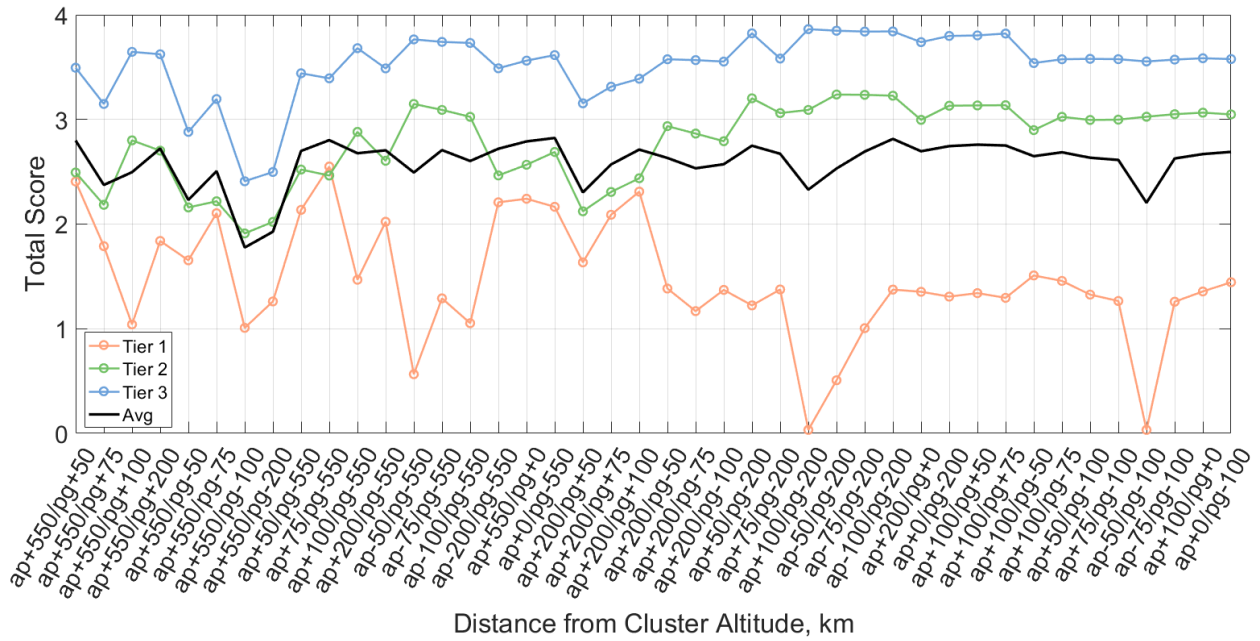
standard deviation of 0.18. The top performing circular case, -50 km offset, has a score of 2.632, while the top performing elliptical case, -50 km apogee / -100 km perigee offset, has a score of 2.545. There is only a small difference between these two cases, but the main distinction is in their Tier 1 performance, where the circular case outperforms the elliptical case in every metric. The elliptical constellations test set includes apogee/perigee combinations over the full range of circular cases analyzed. One area where elliptical constellations do perform better than circular cases though, is more frequent close conjunctions. The grading metrics are geared towards constellations that offer prolonged contact with the debris, but for a mission where achieving the closest possible approach is desired, the best performing case may be elliptical.

Figures 18-20 depict the total score of each case for each cluster, providing a summary of the performance for each constellation. Tables 7-9 show the full performance results for each cluster. The best performing circular case is included in the elliptical results tables as a reference for comparison.

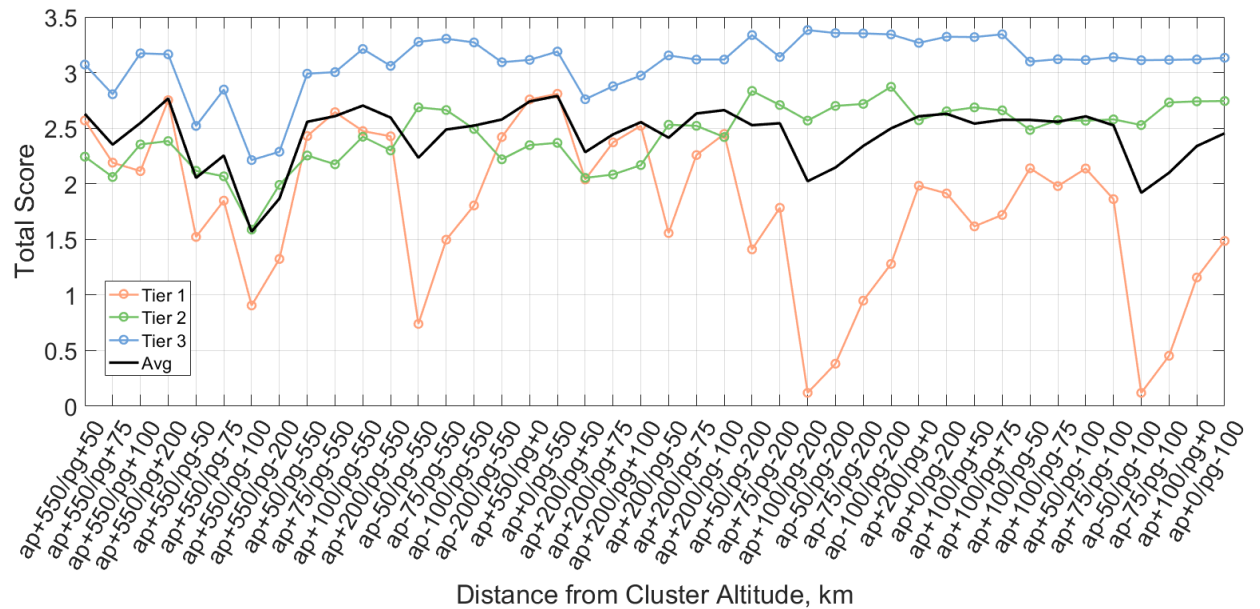


**Fig. 18 Cluster 1 Elliptical Static Total Score**





**Fig. 19 Cluster 2 Elliptical Static Total Score**



**Fig. 20 Cluster 3 Elliptical Static Total Score**

Results for Clusters 2 and 3 closely resemble those for Cluster 1, with overall improved performance from elliptical cases, but the best performing case still being the -50 km circular constellation. The best performing Cluster 2 and Cluster 3 elliptical constellation is the 50 km apogee / -200 km perigee case. The average performance of all Cluster 2 circular constellations is 2.33 with a standard deviation of 0.32, while the elliptical constellations have an average performance score of 2.59 with a standard deviation of 0.22. The average performance of all Cluster 3 circular constellations is 2.34 with a standard deviation of 0.35, while the elliptical constellations have an average performance score of 2.44 with a standard deviation of 0.26. The results are mostly consistent between all 3 clusters, and are compared in Table 6.

**Table 6 Circular vs. Elliptical Result Statistics**

Cluster	Circular		Elliptical	
	Total Score	1 $\sigma$ Std	Total Score	1 $\sigma$ Std
1	2.13	0.33	2.29	0.18
2	2.33	0.32	2.59	0.22
3	2.34	0.35	2.44	0.26

Given that the debris clusters themselves contain exclusively circular orbits, the circular designs more closely match the orbits of the debris objects. When positioned in an ideal offset from the cluster, circular cases offer more prolonged observation capabilities as a larger percentage of their time is spent within the conjunction distance of the debris objects. The metrics are geared towards finding the cases that best fit the mission parameters, and prolonged contact provides a better LDR operating environment. Comparatively though, elliptical constellations with large or poor performing altitude offsets still intersect the clusters and allow for conjunctions with the debris objects. Cases such as the elliptical 550 km apogee / -200 km perigee constellation perform better than either of its circular counterparts.



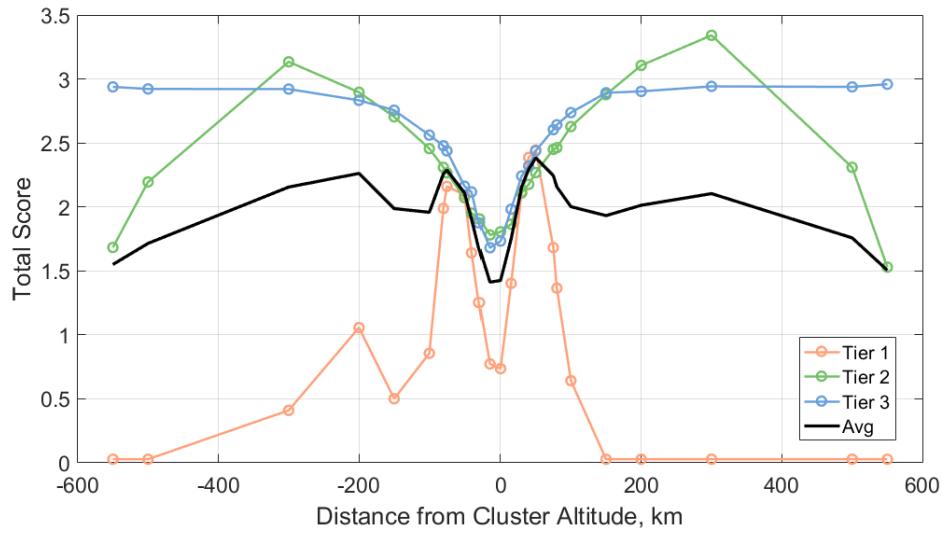




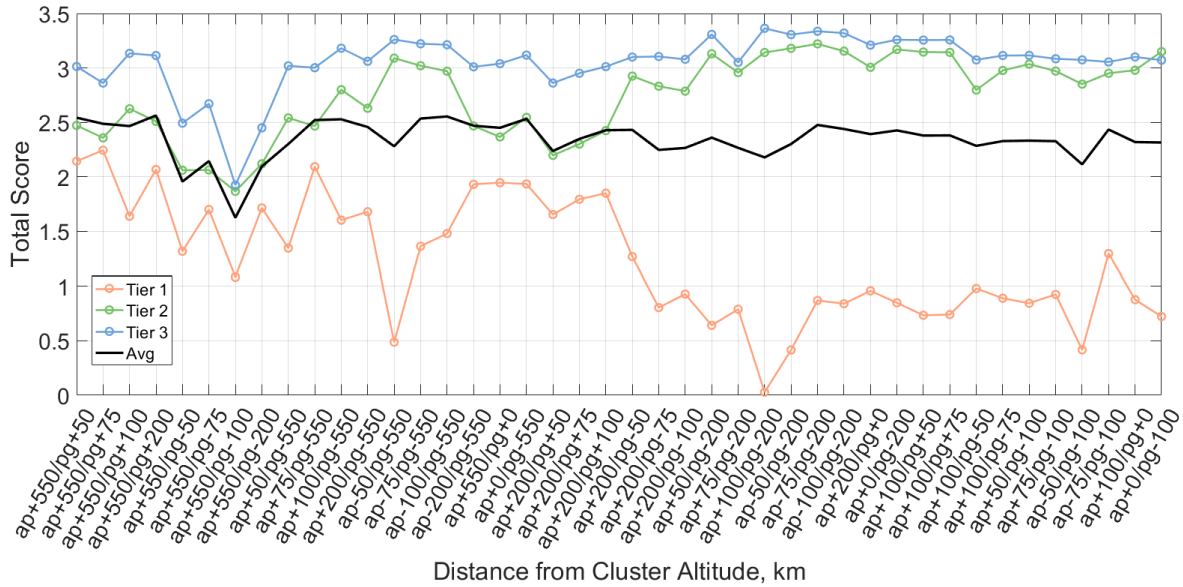
### **C. Phasing Maneuver Cases**

Based on the similarity between all three clusters in examining the non-maneuvering circular and elliptical cases, the impact of maneuvering cases is only analyzed for Cluster 1. The impact that maneuvering has on Cluster 1 performance can be assumed consistent with the other 2 clusters. For the phasing maneuver, each OBS propagates its orbit for 10 days before analyzing its performance over those 10 days. If the performance lowers the overall average, the satellite will maneuver and phase 10 degrees along its orbit. If the 10 days of propagation improve its performance, it will continue to orbit for another 10 days and then reevaluate.

The maneuvering cases were hypothesized to allow the OBSs to settle on the optimal position within their orbit, thereby improving the performance for every case. The results show that maneuvering cases have mixed results, but overall perform worse than non-maneuvering cases for circular constellations and perform slightly better for elliptical constellations. There is not a drastic difference in their performance, but maneuvering cases spend a large portion of time on their phasing orbits, and tend to not conjunct with any debris objects while phasing. Even though OBS performance is mostly improved after maneuvers, improvement is only slight and their time spent phasing increases their average response time. The TAG and MRT metrics decreased, but PC and MD metrics increased across every Tier. Despite time spent phasing reducing the overall conjunction time, the phasing maneuvers increase the PC metric enough for a net gain. Figures 21-22 show the total score for each Tier. Tables 10-11 contain the full performance results for circular and elliptical cases.



**Fig. 21 Cluster 1 Circular Phasing Maneuver Total Score**



**Fig. 22 Cluster 1 Elliptical Phasing Maneuver Total Score**

It holds true for the phasing maneuver cases that elliptical constellations as a whole have better performance results than circular cases, but the best overall constellation remains the static, circular -50 km offset case. Comparing the static and maneuvering cases for circular constellation designs, the static cases have an average score of 2.13 with a standard deviation of 0.33, while the

maneuvering cases have an average score of 1.99 with a standard deviation of 0.31. The largest impact on the metrics was a doubling of the average Tier 3 TAG metric from 1.37 hours to 2.58 hours. The improvement in the PC metric is only slight, with a 4.8% increase in Tier 3 being the largest improvement.

Comparing the static and maneuvering cases for elliptical constellation designs, the static cases have an average score of 2.28 with a standard deviation of 0.19, while the maneuvering cases have an average score of 2.35 with a standard deviation of 0.17. Improvement is only slight, and with a  $\Delta V$  of roughly 140 m/s per maneuver, a steep improvement in at least one of the metrics is necessary for this maneuver to be considered a viable consideration in the constellation design. By any measure, adding a phasing maneuver to the constellation architecture does not provide an improvement in constellation performance.

**Table 10 Cluster 1 Circular Phasing Maneuver Performance Results**

Case	Tier 1: 100 km						Tier 2: 600 km						Tier 3: 2400 km						Total Score
	MRT (days)	TAG (days)	PC (%)	MeanD (min)	CC (%)	Score	MRT (days)	TAG (days)	PC (%)	MeanD (min)	CC (%)	Score	MRT (days)	TAG (days)	PC (%)	MeanD (min)	CC (%)	Score	
circ -50km 8obj 0Man	0.938	1.573	0.905	0.534	100	2.556	0.454	0.857	1.865	2.849	100	2.333	0.026	0.050	14.408	8.669	100	3.006	<b>2.632</b>
circ +550km 8obj 1Man	90.00	90.00	0.00	0.00	0	0.028	0.263	0.483	0.675	1.323	100	1.683	0.026	0.051	13.456	8.522	100	2.938	<b>1.550</b>
circ +500km 8obj 1Man	90.00	90.00	0.00	0.00	0	0.028	0.197	0.356	0.804	1.717	100	2.195	0.027	0.051	13.741	8.525	100	2.922	<b>1.715</b>
circ +300km 8obj 1Man	79.03	78.71	8.73	0.03	98.864	0.410	0.147	0.275	1.400	2.524	100	3.134	0.027	0.053	14.368	8.652	100	2.921	<b>2.155</b>
circ +200km 8obj 1Man	61.23	65.77	17.85	0.31	96.591	1.057	0.193	0.357	1.589	2.711	100	2.896	0.030	0.057	14.693	8.688	100	2.833	<b>2.262</b>
circ +150km 8obj 1Man	66.314	72.021	6.804	0.195	96.591	0.501	0.242	0.443	1.676	2.768	100	2.704	0.031	0.061	14.671	8.689	100	2.756	<b>1.987</b>
circ +100km 8obj 1Man	5.413	8.095	4.206	0.328	100	0.856	0.336	0.631	1.747	2.812	100	2.456	0.038	0.073	15.106	8.685	100	2.561	<b>1.958</b>
circ +80km 8obj 1Man	1.221	2.071	1.382	0.417	100	1.988	0.427	0.797	1.747	2.826	100	2.309	0.041	0.079	14.954	8.695	100	2.478	<b>2.258</b>
circ +75km 8obj 1Man	1.115	1.920	1.257	0.464	100	2.161	0.455	0.847	1.724	2.833	100	2.266	0.043	0.082	14.817	8.698	100	2.438	<b>2.288</b>
circ +50km 8obj 1Man	1.165	2.140	0.639	0.543	100	2.094	0.704	1.336	1.739	2.811	100	2.072	0.062	0.119	15.160	8.686	100	2.162	<b>2.110</b>
circ +40km 8obj 1Man	1.636	2.993	0.330	0.545	100	1.641	1.021	1.883	1.702	2.808	100	1.951	0.066	0.127	15.204	8.645	100	2.117	<b>1.903</b>
circ +30km 8obj 1Man	2.908	4.943	0.191	0.623	100	1.253	1.731	3.124	1.757	2.893	100	1.907	0.112	0.187	14.256	8.768	100	1.876	<b>1.679</b>
circ +15km 8obj 1Man	10.399	15.574	0.135	0.594	100	0.773	4.881	7.687	1.807	2.710	100	1.781	0.250	0.468	15.141	8.658	100	1.681	<b>1.412</b>
circ +0km 8obj 1Man	12.654	10.484	0.258	0.516	100	0.736	3.821	5.702	1.736	2.830	100	1.806	0.203	0.383	15.182	8.796	100	1.733	<b>1.425</b>
circ -15km 8obj 1Man	2.379	3.895	0.698	0.594	100	1.403	2.174	2.378	1.718	2.794	100	1.865	0.083	0.150	14.542	8.623	100	1.982	<b>1.750</b>
circ -30km 8obj 1Man	1.166	2.121	0.611	0.566	100	1.220	0.691	1.245	1.794	2.798	100	2.109	0.057	0.109	15.726	8.681	100	2.242	<b>2.157</b>
circ -40km 8obj 1Man	1.028	1.725	0.683	0.552	100	2.387	0.585	1.041	1.791	2.800	100	2.176	0.049	0.094	15.117	8.630	100	2.320	<b>2.294</b>
circ -50km 8obj 1Man	0.960	1.643	0.881	0.490	100	2.445	0.461	0.866	1.756	2.823	100	2.268	0.043	0.083	15.233	8.645	100	2.438	<b>2.384</b>
circ -75km 8obj 1Man	1.618	2.440	1.295	0.418	100	1.682	0.339	0.631	1.751	2.798	100	2.450	0.037	0.069	15.253	8.628	100	2.604	<b>2.245</b>
circ -80km 8obj 1Man	2.165	3.275	1.768	0.392	100	1.365	0.331	0.607	1.726	2.802	100	2.463	0.035	0.067	15.207	8.620	100	2.642	<b>2.157</b>
circ -100km 8obj 1Man	23.156	27.547	7.511	0.248	98.864	0.642	0.269	0.497	1.739	2.777	100	2.628	0.032	0.062	15.252	8.603	100	2.737	<b>2.002</b>
circ -150km 8obj 1Man	90.000	90.000	0.000	0.000	0	0.028	0.201	0.374	1.666	2.711	100	2.878	0.028	0.055	15.114	8.560	100	2.892	<b>1.932</b>
circ -200km 8obj 1Man	90.000	90.000	0.000	0.000	0	0.028	0.163	0.305	1.603	2.650	100	3.106	0.027	0.055	14.693	8.591	100	2.903	<b>2.013</b>
circ -300km 8obj 1Man	90.000	90.000	0.000	0.000	0	0.028	0.130	0.241	1.447	2.401	100	3.341	0.026	0.053	14.368	8.552	100	2.942	<b>2.104</b>
circ -500km 8obj 1Man	90.000	90.000	0.000	0.000	0	0.028	0.173	0.309	0.754	1.576	100	2.309	0.026	0.051	13.741	8.516	100	2.938	<b>1.758</b>
circ -550km 8obj 1Man	90.000	90.000	0.000	0.000	0	0.028	0.293	0.486	0.583	1.141	100	1.529	0.025	0.051	13.456	8.518	100	2.959	<b>1.505</b>





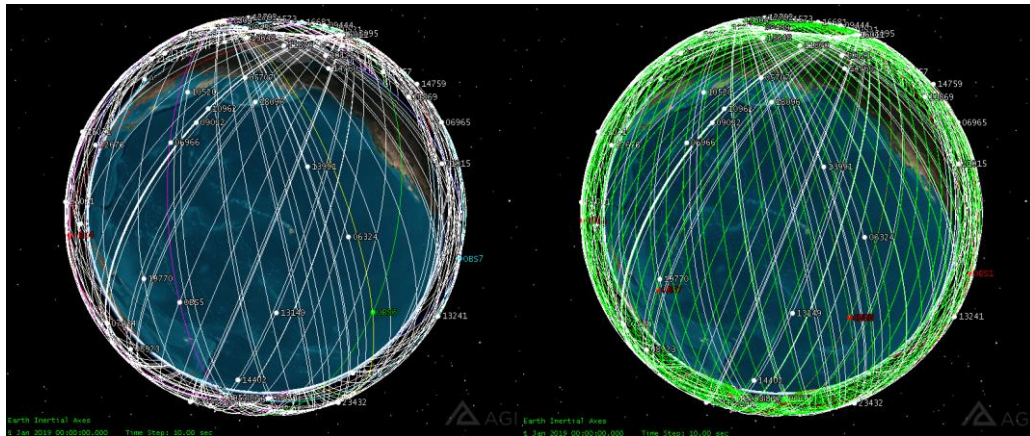
An interesting area of note is how the phasing maneuver impacted the performance of each Tier differently. For both circular and elliptical constellations, the smaller the range constraint is, the better impact phasing maneuvers have on the performance metrics. Circular constellations have a 9% improved Tier 1 performance with phasing maneuvers, while Tier 2 and 3 performance decreased by 4.4% and 15.2%, respectively. Similarly, elliptical constellations have a 13.5%, 1.5%, and 0.4% improved performance for Tiers 1, 2, and 3. This suggests that if increased weight is placed on lower Tiers, for example if a mission were focused more on minimizing the range at closest approach, phasing maneuvers could offer significantly better performance improvements than these results indicate. Especially since it has been shown that Tier 1 has a larger impact on the total score than Tiers 2 and 3.

A potential improvement that could be implemented in future research would be to calculate a different phasing angle for each maneuver that will position the OBS within each clusters' altitude range for the majority of the phasing orbit. The method used in this research phased each OBS by 10 degrees regardless of the constellation offset, which is what led to most observer satellites having no debris conjunctions while phasing. If the phase angle were targeted based on OBS offset, the phasing orbit could be tuned so phasing OBS pass through the cluster altitude range for the majority of the phasing orbit, hopefully increasing conjunction rate while phasing.

#### **D. RAAN Maneuver Cases**

As with the phasing maneuver, the RAAN maneuvering cases are only analyzed for Cluster 1. Large portions of the debris clusters surface area are unmonitored by OBSs, meaning conjunctions near the minimum and maximum latitudes are relied on for many of the RSOs conjunctions. RAAN maneuvers are intended to improve the spherical coverage of the clusters. Figure 23 highlights this gap in coverage, comparing a non-maneuvering constellation on the left with a RAAN-

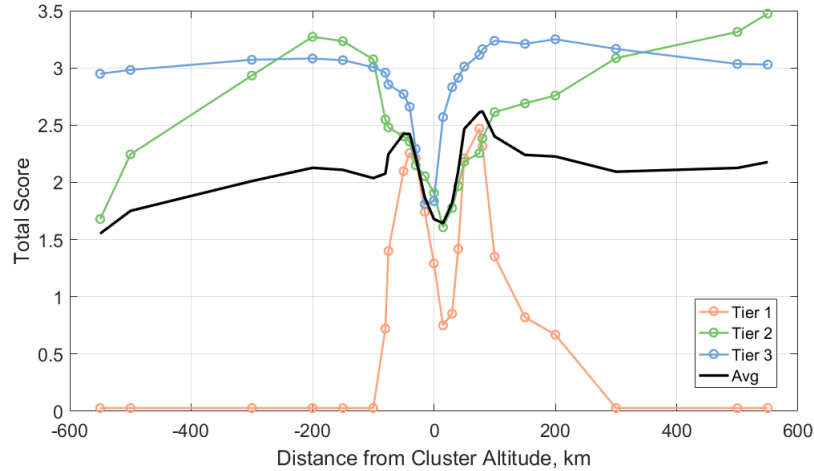
maneuvering constellation on the right. The orbit path for all maneuvering observer satellites are shown in green, to highlight the improved spherical coverage. RAAN maneuvers are executed by performing a 5 degree  $\Delta\Omega$  shift every 15 days of orbit propagation, to rotate each orbit a total of 120 degrees over a yearlong simulation.



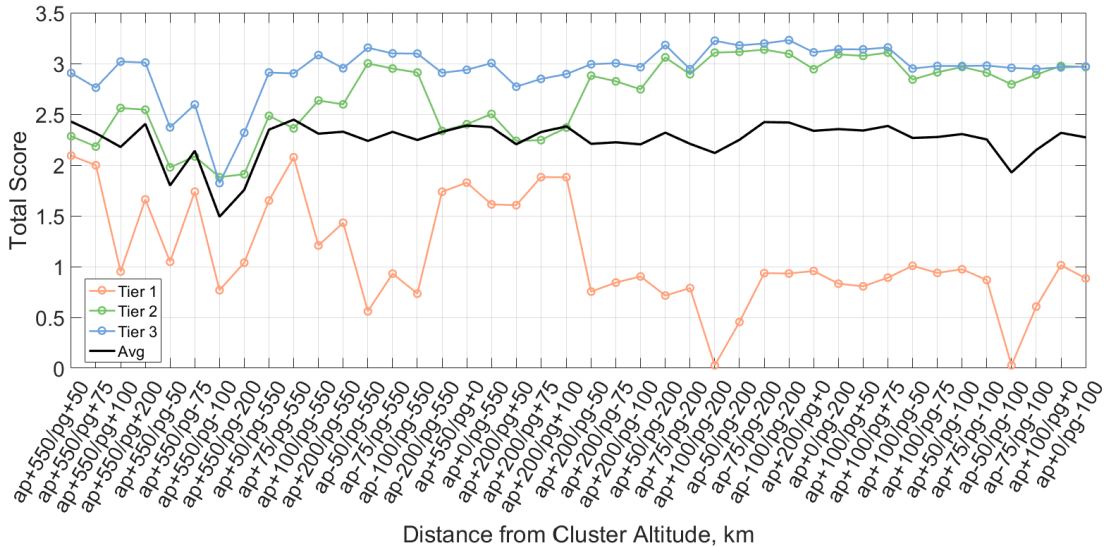
**Fig. 23 Spherical Coverage Gaps**

The results show that RAAN maneuvering cases performed similar to the phasing maneuver cases, with mixed results but an overall worse performance than static cases for both circular and elliptical constellations. RAAN maneuvers outperformed phasing maneuver cases, but ultimately the static circular cases provide the best performance based on the grading metrics. With RAAN maneuvers, observer satellites do not spend time on phasing orbits like they do with phasing maneuvers, reducing the impact on conjunction gaps. Figures 24-25 show the total score for each Tier. Tables 12-13 contain the full performance results for circular and elliptical cases.

Comparing the static and maneuvering cases for circular constellation designs, the static cases have an average score of 2.13 with a standard deviation of 0.33, while the maneuvering cases have an average score of 2.13 with a standard deviation of 0.29. The average results are equivalent for the static and maneuvering circular cases, but the best overall case remains the static circular -50 km offset constellation with a score of 2.63. The best performing maneuvering case is the -80 km



**Fig. 24 Cluster 1 Circular RAAN Maneuver Total Score**



**Fig. 25 Cluster 1 Elliptical RAAN Maneuver Total Score**

offset with a total score of 2.62. For the elliptical constellations, the static cases have an average score of 2.28 with a standard deviation of 0.19, while the maneuvering cases have an average score of 2.25 with a standard deviation of 0.19. There are minor differences in all of the metrics between the static and maneuvering cases, but the results are virtually identical. RAAN maneuvering cases, though, require a large  $\Delta V$  of roughly 650 m/s per maneuver, meaning the maneuvering constellations require a significant improvement in performance metrics to be considered successful.



## 5. Conclusion

This research effort aims to address two investigative research questions: can a constellation of observer satellites engage in meaningful SSA and collision mitigation of massive orbital debris clusters, and how successful is the employed methodology at optimizing constellation designs. The results of the analysis contrasted with the hypothesized performance of the various constellation architectures, with maneuvering cases ultimately underperforming static cases. The methodology and metrics used for the analysis were specifically geared for the mission objectives, and intended to reward traits that improve both SSA and LDR intervention. The difference between the hypothesized results and the actual results highlights the effectiveness of the methodology at identifying the key aspects of the constellation design that provide the best environment for meaningful debris management and optimize debris remediation. While maneuvering cases and elliptical orbits were expected to provide performance improvements, the methodology identified constellations that most closely reflect the orbits of the debris objects, circular and static, as the ideal design. These much simpler orbits reduce the cost associated with deploying such a constellation, meaning larger constellations could be launched than would otherwise be possible. Were the clusters less uniformly distributed, I would expect more complex orbits to have improved performance and maneuvering constellations to be more useful. All constellations analyzed included eight observer satellites, but increasing the number of satellites would improve overall performance.

For a constellation to be effective, it must provide adequate coverage and interaction between the OBSs and RSOs. The constellation must be capable of monitoring every object within the cluster with enough quality and timeliness to predict all potential collisions accurately and have the time necessary to reliably intervene. The results show that a constellation of circular, non-

maneuvering observer satellites placed at the ideal offset would provide highly effective coverage of the debris clusters. For an eight object constellation, each debris object would have an adequate LDR engagement opportunity every hour with a conjunction duration over eight minutes, and a close range conjunction every day for roughly one-minute. Based on the LDR performance figures noted in section III.B.2, roughly 52 eight-minute conjunctions are required to successfully nudge the SMA of a 1000kg object by 40 km. The results suggest this would be achievable in under three days with an eight object constellation. While still capable of providing adequate and effective coverage, maneuvering cases provided inferior performance compared to the non-maneuvering cases, in addition to adding major mission constraints to fuel and time resources.

The methodology is successful in demonstrating its value as a systems engineering tool in constellation design and analysis of alternatives. The method is modular and can be modified and focused to fit various scenarios in which an evaluation of constellation coverage is required. The system additionally allows for easy manipulation of the weighing scheme as mission success criteria change. For example, if it were determined that duration gaps are more important than average conjunction duration due to initial LDR commissioning time being an issue, an engineer could recalculate scoring with TAG weighed heavier than MD, and a new constellation may be found to achieve superior performance. The results and processes explored in this research effort can be applied to various areas of ongoing research in an effort to develop the best practices and solutions to modern space situational awareness and satellite traffic management problems.

## References

- [1] Johnson, N., “The Collision of Iridium 33 and Cosmos 2251: The Shape of Things to Come,” *60<sup>th</sup> International Astronautical Congress*, Daejeon, Republic of Korea, 16 Oct. 2009
- [2] McKnight, D., Walbert, K., Ohriner, E., Fairbanks, J., Lobo, A., “Proposed Series of Orbital Debris Remediation Activities,” *7<sup>th</sup> European Conference on Space Debris*, Vol. 7, Darmstadt, Germany, June 2017  
doi: 10.4172/2618-9792-C1-017
- [3] Bonnal, C., McKnight, D., Phipps, C., Dupont, C., Missonnier, S., Lequette, L., Merle, M., Rommelaere, S., “Just in time collision avoidance – A review,” *Acta Astronautica*, Vol. 170, May 2020, pp. 637-651  
doi: 10.1016/j.actaastro.2020.02.016
- [4] Phipps, C., “LADROIT- A Spaceborne Ultraviolet Laser System for Space Debris Clearing,” *Acta Astronautica*, Vol. 104, Nov 2014, pp. 243-255  
doi: 10.1016/j.actaastro.2014.08.0057
- [5] Yates, J., Spanbauer, B., Black, J.T., “Geostationary Orbit Development and Evaluation for Space Situational Awareness,” *Acta Astronautica*, Vol. 81, Iss. 1, Dec. 2012, pp. 256-272  
doi: 10.1016/j.actaastro.2012.05.011
- [6] McKnight, D., Rosenblatt, J., Garber, D., “Responsible Behavior for Constellations and Clusters,” *Space Traffic Management Conference*. 8. 2018
- [7] Phipps, C., Bonnal, C., “A Spaceborne, Pulsed UV Laser System for Re-entering or Nudging LEO Debris, and Re-orbiting GEO Debris,” *Acta Astronautica*, Vol. 118, Jan 2016, pp. 224-236  
doi: 10.1016/j.actaastro.2015.10.005
- [8] Bekey, I., “Project ORION: Orbital Debris Removal Using Ground-Based Sensors and Lasers”, *2<sup>nd</sup> European Conference on Space Debris*, ESA-SP 393, Vol. 2, 17-19 Mar. 1997, pp.699-701
- [9] Cambell, J., Taylor, C., “Project ORION: results of a feasibility study on removing orbital debris using ground-based lasers and sensors”, *Proc. SPIE*, Vol. 3126, 17 Oct. 1997  
doi: 10.1117/12.290176
- [10] Souldard, R., Quinn, M., “ICAN: A Novel Laser Architecture for Space Debris Removal,” *Acta Astronautica*, Vol. 105, Dec. 2014, pp.192-200  
doi: 10.1016/j.actaastro.2014.09.004
- [11] Wertz, J. R., Larson, W. J., *Space Mission Analysis and Design*, 3<sup>rd</sup> ed., Microcosm Press, Kluwer Academic Publishers, 1999, pp.159-202
- [12] Vallado, D. A., *Fundamentals of Astrodynamics and Applications*, 4<sup>th</sup> ed., Mar. 2013, pp.345-350



## Appendix A: Cluster Information

### Cluster 1

SAT#	Name	Intl Desig.	Period	Inclination	Apogee	Perigee	Mass (kg)
<b>SL-16 Rocket Bodies</b>							
16182	SL-16 R/B	1985-097B	101.68	71	845	832	8,300
17590	SL-16 R/B	1987-027B	101.64	71	841	832	8,300
17974	SL-16 R/B	1987-041B	101.61	71.01	846	823	8,300
19120	SL-16 R/B	1988-039B	101.47	71.02	842	814	8,300
19650	SL-16 R/B	1988-102B	101.71	71	849	831	8,300
20625	SL-16 R/B	1990-046B	101.8	71	855	833	8,300
22220	SL-16 R/B	1992-076B	101.67	71	846	829	8,300
22285	SL-16 R/B	1992-093B	101.77	71.02	845	839	8,300
22566	SL-16 R/B	1993-016B	101.77	71.01	850	835	8,300
22803	SL-16 R/B	1993-059B	101.64	70.99	850	822	8,300
23088	SL-16 R/B	1994-023B	101.79	71	847	840	8,300
23405	SL-16 R/B	1994-077B	101.75	70.98	845	839	8,300
23705	SL-16 R/B	1995-058B	101.76	71.02	851	833	8,300
24298	SL-16 R/B	1996-051B	101.95	70.83	860	842	8,300
25407	SL-16 R/B	1998-045B	101.71	71.01	844	836	8,300
26070	SL-16 R/B	2000-006B	101.74	71	854	828	8,300
28353	SL-16 R/B	2004-021B	101.83	71	847	843	8,300
31793	SL-16 R/B	2007-029B	101.81	70.97	846	843	8,300
<b>SL-16 Payloads</b>							
16181	COSMOS 1697	1985-097A	101.88	70.96	860	836	3,250
17589	COSMOS 1833	1987-027A	101.92	70.92	866	833	3,250
17973	COSMOS 1844	1987-041A	101.84	70.9	868	823	3,250
19119	COSMOS 1943	1988-039A	101.76	71	852	832	3,250
19649	COSMOS 1980	1988-102A	101.79	71	848	839	3,250
20624	COSMOS 2082	1990-046A	101.82	71.04	858	832	3,250
22219	COSMOS 2219	1992-076A	101.87	71.06	861	833	3,250

22284	COSMOS 2227	1992-093A	101.89	70.98	861	835	3,250
22565	COSMOS 2237	1993-016A	101.95	70.84	857	846	3,250
22802	COSMOS 2263	1993-059A	101.9	70.93	864	834	3,250
23087	COSMOS 2278	1994-023A	101.86	71.05	852	842	3,250
23404	COSMOS 2297	1994-077A	101.88	71.02	858	837	3,250
23704	COSMOS 2322	1995-058A	101.89	70.98	856	839	3,250
24297	COSMOS 2333	1996-051A	101.89	70.9	865	832	3,250
25406	COSMOS 2360	1998-045A	101.95	70.85	855	847	3,250
26069	COSMOS 2369	2000-006A	101.89	71	855	841	3,250
28352	COSMOS 2406	2004-021A	102.02	71	865	844	3,250
31792	COSMOS 2428	2007-029A	101.96	70.94	856	846	3,250
Other Payloads							
8519	METEOR 1-23	1975-124A	102.07	81.24	866	848	1200
7574	METEOR 1-20	1974-099A	102.03	81.23	866	843	1200
4419	METEOR 1-5	1970-047A	101.74	81.22	870	812	1200
11288	METEOR 2-4	1979-021A	102	81.21	870	837	2750
5731	METEOR 1-10	1971-120A	102.02	81.26	872	837	2300
10514	METEOR 2-3	1977-117A	102.1	81.21	874	842	2750
7209	METEOR 1-16	1974-011A	101.85	81.23	875	817	1200
8026	METEOR 2-1	1975-064A	102.11	81.28	875	842	2750
9481	METEOR 1-26	1976-102A	102.15	81.22	877	843	1200
7274	METEOR 1-17	1974-025A	102.25	81.23	877	853	1200
11605	METEOR 2-5	1979-095A	102.34	81.21	878	861	2750
6659	METEOR 1-15	1973-034A	102.14	81.19	879	841	1200
8799	METEOR 1-24	1976-032A	102.02	81.26	879	830	1200
6392	METEOR 1-14	1973-015A	102.31	81.25	879	856	1200
13718	METEOR 2-9	1982-116A	101.74	81.25	880	802	2750
7490	METEOR 1-19	1974-083A	102.13	81.19	882	837	1200
8845	METEOR 1-25	1976-043A	102.03	81.26	882	827	1200
6256	METEOR 1-13	1972-085A	102.21	81.27	884	843	1200
11962	METEOR 2-6	1980-073A	102.09	81.22	884	831	2750
5917	METEOR 1-11	1972-022A	102.23	81.22	886	843	1200

7714	METEOR 1-21	1975-023A	102.28	81.21	888	845	1200
9661	METEOR 2-2	1977-002A	102.6	81.27	889	875	2750
6079	METEOR 1-12	1972-049A	102.63	81.23	891	876	1200
9903	METEOR 1-27	1977-024A	102.25	81.26	892	839	1200
12456	METEOR 2-7	1981-043A	102.11	81.27	893	824	2750
11165	COSMOS 1066	1978-121A	102.01	81.24	889	819	2750
15334	SL-12 R/B(2)	1984-106B	101.77	71	844	841	2458
15772	SL-12 R/B(2)	1985-042D	101.32	71.11	847	795	2458
32958	FENGYUN 3A	2008-026A	101.44	98.45	834	819	2295
20322	COBE	1989-089A	102.51	98.97	884	870	2260
37214	FENGYUN 3B	2010-059A	101.71	98.85	852	827	2234
22823	SPOT 3	1993-061A	101.47	98.9	841	815	1907
37849	NPP	2011-061A	101.44	98.72	828	826	1842
15427	NOAA 9	1984-123A	101.7	98.76	850	829	1712
19531	NOAA 11	1988-089A	101.75	98.6	849	834	1712
28654	NOAA 18	2005-018A	101.96	99.2	861	842	1479
11166	SL-3 R/B	1978-121B	101.86	81.24	895	798	1440
13719	SL-3 R/B	1982-116B	101.8	81.26	895	792	1440
11289	SL-3 R/B	1979-021B	102.02	81.25	910	799	1440

## **Cluster 2**

SAT#	Name	Intl Desig	Period	Inclination	Apogee	Perigee	Mass (kg)
SL-8 Rocket Bodies							
5707	SL-8 R/B	1971-114B	100.09	74.03	781	745	1,434
6061	SL-8 R/B	1972-043B	99.97	74.06	771	743	1,434
6324	SL-8 R/B	1972-104B	99.77	74.08	755	740	1,434
6966	SL-8 R/B	1973-098B	99.8	74.05	765	733	1,434
7434	SL-8 R/B	1974-071B	100.24	74.04	785	755	1,434
8344	SL-8 R/B	1975-094B	100.07	74.06	776	747	1,434
8459	SL-8 R/B	1975-112B	100.23	74.06	781	758	1,434
8924	SL-8 R/B	1976-061B	100.21	74.06	778	759	1,434

9023	SL-8 R/B	1976-069B	100.04	74.04	773	747	1,434
9444	SL-8 R/B	1976-098B	100.15	74.05	775	757	1,434
10121	SL-8 R/B	1977-059B	100.3	74.05	786	759	1,434
10521	SL-8 R/B	1977-119B	99.96	74.03	772	741	1,434
10677	SL-8 R/B	1978-019B	100	74.04	769	748	1,434
10962	SL-8 R/B	1978-063B	99.93	74.08	773	737	1,434
11112	SL-8 R/B	1978-105B	100.2	74.03	792	744	1,434
11427	SL-8 R/B	1979-060B	100.19	74.02	782	753	1,434
11511	SL-8 R/B	1979-078B	100.23	74.04	781	758	1,434
11574	SL-8 R/B	1979-089B	99.96	74.07	768	745	1,434
11870	SL-8 R/B	1980-056B	100.22	74.05	781	757	1,434
12443	SL-8 R/B	1981-041B	100.37	74.05	780	772	1,434
12792	SL-8 R/B	1981-084B	100.18	74.03	777	757	1,434
13028	SL-8 R/B	1982-001B	100.12	74.04	778	750	1,434
13149	SL-8 R/B	1982-037B	100.34	74.04	783	766	1,434
13242	SL-8 R/B	1982-051B	100.29	74.04	791	754	1,434
13649	SL-8 R/B	1982-109B	100.21	74	782	755	1,434
13992	SL-8 R/B	1983-031B	100.28	74.05	775	768	1,434
14241	SL-8 R/B	1983-079B	100.27	74.06	784	759	1,434
14402	SL-8 R/B	1983-103B	100.29	74.05	791	754	1,434
14760	SL-8 R/B	1984-019B	100.29	74.04	792	753	1,434
15032	SL-8 R/B	1984-056B	100.37	74.07	789	763	1,434
15483	SL-8 R/B	1985-006B	100.27	74.05	785	758	1,434
16012	SL-8 R/B	1985-079B	100.27	74.06	781	761	1,434
16682	SL-8 R/B	1986-030B	100.3	74.02	784	761	1,434
16864	SL-8 R/B	1986-052B	99.97	74.03	781	733	1,434
16953	SL-8 R/B	1986-070B	100.19	74.01	776	759	1,434
17304	SL-8 R/B	1987-006B	100.17	74.06	788	745	1,434
18096	SL-8 R/B	1987-049B	100.25	74.04	785	756	1,434
18586	SL-8 R/B	1987-098B	100.23	74.01	784	755	1,434
19039	SL-8 R/B	1988-029B	100.12	74.05	781	747	1,434

19257	SL-8 R/B	1988-053B	100.19	74.05	782	753	1,434
19770	SL-8 R/B	1989-005B	100.09	74.05	766	759	1,434
21015	SL-8 R/B	1990-111B	100.29	74.05	787	757	1,434
22676	SL-8 R/B	1993-036B	100.43	74.04	793	764	1,434
23432	SL-8 R/B	1994-083B	100.46	74.03	784	776	1,434
SL-8 Payloads							
5705	COSMOS 468	1971-114A	100.31	74.02	785	762	750
6059	COSMOS 494	1972-043A	100.31	74.06	782	765	750
6323	COSMOS 540	1972-104A	100.26	74.08	783	758	750
6965	COSMOS 614	1973-098A	100.08	74.06	778	746	750
7433	COSMOS 676	1974-071A	100.53	74.05	794	773	750
8343	COSMOS 773	1975-094A	100.36	74.05	784	767	750
8458	COSMOS 783	1975-112A	100.51	74.06	791	775	750
8923	COSMOS 836	1976-061A	100.49	74.05	795	768	750
9022	COSMOS 841	1976-069A	100.3	74.04	781	764	750
9443	COSMOS 858	1976-098A	100.42	74.05	789	768	750
10120	COSMOS 923	1977-059A	100.57	74.05	796	775	750
10520	COSMOS 968	1977-119A	100.28	74.03	784	760	750
10676	COSMOS 990	1978-019A	100.27	74.04	783	760	750
10961	COSMOS 1023	1978-063A	100.25	74.08	783	758	750
11111	COSMOS 1048	1978-105A	100.41	74.03	789	767	750
11425	COSMOS 1110	1979-060A	100.48	74.02	792	770	750
11510	COSMOS 1125	1979-078A	100.48	74.04	790	773	750
11573	COSMOS 1140	1979-089A	100.24	74.07	782	758	750
11869	COSMOS 1190	1980-056A	100.45	74.05	791	769	750
12442	COSMOS 1269	1981-041A	100.55	74.05	792	777	750
12791	COSMOS 1302	1981-084A	100.42	74.03	791	766	750
13027	COSMOS 1331	1982-001A	100.24	74.05	787	753	750
13148	COSMOS 1354	1982-037A	100.57	74.04	793	778	750
13241	COSMOS 1371	1982-051A	100.59	74.04	796	777	750
13648	COSMOS 1420	1982-109A	100.44	74	794	764	750

13991	COSMOS 1452	1983-031A	100.49	74.05	794	770	750
14240	COSMOS 1486	1983-079A	100.43	74.06	789	769	750
14401	COSMOS 1503	1983-103A	100.55	74.05	795	775	750
14759	COSMOS 1538	1984-019A	100.45	74.04	794	766	750
15031	COSMOS 1570	1984-056A	100.58	74.07	795	777	750
15482	COSMOS 1624	1985-006A	100.49	74.04	792	772	750
16011	COSMOS 1680	1985-079A	100.48	74.05	792	771	750
16681	COSMOS 1741	1986-030A	100.5	74.02	796	768	750
16860	COSMOS 1763	1986-052A	100.13	74.03	788	742	750
16952	COSMOS 1777	1986-070A	100.49	74.01	801	762	750
17303	COSMOS 1814	1987-006A	100.36	74.06	793	758	750
18095	COSMOS 1850	1987-049A	100.48	74.04	791	771	750
18585	COSMOS 1898	1987-098A	100.45	74.01	794	766	750
19038	COSMOS 1937	1988-029A	100.34	74.05	792	757	750
19256	COSMOS 1954	1988-053A	100.43	74.05	790	768	750
19769	COSMOS 1992	1989-005A	100.37	74.05	791	760	750
21014	COSMOS 2112	1990-111A	100.47	74.05	800	761	750
22675	COSMOS 2251	1993-036A	100.53	74.04	801	766	750
23431	COSMOS 2298	1994-083A	100.68	74.03	802	780	750

### **Cluster 3**

Sat#	Name	Intl Desig	Period	Inclination	Apogee	Perigee	Mass (kg)
SL-8 Rocket Bodies							
4784	SL-8 R/B	1970-102B	104.6	74.03	995	957	1,434
4800	SL-8 R/B	1970-108B	104.45	74.02	975	962	1,434
5239	SL-8 R/B	1971-046B	104.82	74.03	993	978	1,434
5685	SL-8 R/B	1971-111B	104.59	74.03	993	958	1,434
5847	SL-8 R/B	1972-009B	104.41	74.05	989	944	1,434
6020	SL-8 R/B	1972-035B	104.44	74.02	984	952	1,434

6149	SL-8 R/B	1972-062B	104.13	82.97	960	948	1,434
6207	SL-8 R/B	1972-074B	104.68	65.82	1002	957	1,434
6708	SL-8 R/B	1973-042B	104.8	82.95	994	976	1,434
6829	SL-8 R/B	1973-065B	104.57	82.94	990	958	1,434
7009	SL-8 R/B	1973-109B	104.59	82.95	989	962	1,434
7095	SL-8 R/B	1974-001B	104.46	82.95	997	941	1,434
7350	SL-8 R/B	1974-048B	104.52	82.94	984	960	1,434
7477	SL-8 R/B	1974-079B	104.8	82.94	1011	959	1,434
7594	SL-8 R/B	1974-105B	104.44	82.95	980	956	1,434
7737	SL-8 R/B	1975-028B	104.32	83	976	949	1,434
7769	SL-8 R/B	1975-034B	104.74	82.96	996	969	1,434
8073	SL-8 R/B	1975-074B	104.66	82.9	995	962	1,434
8421	SL-8 R/B	1975-103B	104.6	82.97	991	960	1,434
8597	SL-8 R/B	1976-005B	104.72	82.97	999	964	1,434
8646	SL-8 R/B	1976-011B	104.82	82.97	989	983	1,434
8874	SL-8 R/B	1976-051B	104.74	82.96	999	965	1,434
9044	SL-8 R/B	1976-070B	104.64	82.99	987	968	1,434
9062	SL-8 R/B	1976-078B	104.47	82.93	990	949	1,434
9510	SL-8 R/B	1976-108B	104.54	82.93	992	954	1,434
9613	SL-8 R/B	1976-122B	104.55	82.95	994	952	1,434
9638	SL-8 R/B	1976-128B	104.48	82.94	993	948	1,434
9738	SL-8 R/B	1977-004B	104.83	82.96	998	975	1,434
9848	SL-8 R/B	1977-013B	104.69	82.95	991	969	1,434
10020	SL-8 R/B	1977-039B	104.5	82.94	993	949	1,434
10138	SL-8 R/B	1977-062B	104.82	82.94	1002	970	1,434
10142	SL-8 R/B	1977-064B	104.45	82.96	1001	937	1,434
10355	SL-8 R/B	1977-087B	104.67	82.97	1005	953	1,434
10461	SL-8 R/B	1977-107B	104.59	82.95	1000	950	1,434
10513	SL-8 R/B	1977-116B	104.46	65.83	995	943	1,434
10537	SL-8 R/B	1977-122B	104.71	82.93	996	966	1,434
10600	SL-8 R/B	1978-007B	104.47	82.94	1004	935	1,434

10693	SL-8 R/B	1978-022B	104.54	82.99	990	956	1,434
10732	SL-8 R/B	1978-028B	104.7	82.93	994	967	1,434
10745	SL-8 R/B	1978-031B	104.46	82.93	996	942	1,434
10777	SL-8 R/B	1978-034B	104.55	82.94	992	954	1,434
10918	SL-8 R/B	1978-053B	104.55	82.92	996	951	1,434
10992	SL-8 R/B	1978-074B	104.51	82.93	987	957	1,434
11239	SL-8 R/B	1979-003B	104.67	82.94	1010	948	1,434
11309	SL-8 R/B	1979-026B	104.57	82.97	989	959	1,434
11321	SL-8 R/B	1979-028B	104.62	82.92	990	963	1,434
11327	SL-8 R/B	1979-030B	104.58	82.95	995	954	1,434
11379	SL-8 R/B	1979-046B	104.55	82.95	988	958	1,434
11586	SL-8 R/B	1979-090B	104.43	82.94	987	948	1,434
11668	SL-8 R/B	1980-003B	104.68	82.95	995	964	1,434
11681	SL-8 R/B	1980-007B	104.7	82.93	1007	954	1,434
11736	SL-8 R/B	1980-022B	104.62	82.94	1002	951	1,434
11751	SL-8 R/B	1980-026B	104.57	65.84	987	962	1,434
11804	SL-8 R/B	1980-039B	104.64	82.94	992	963	1,434
12088	SL-8 R/B	1980-097B	104.58	82.94	1012	938	1,434
12092	SL-8 R/B	1980-099B	104.58	82.94	998	952	1,434
12298	SL-8 R/B	1981-013B	104.61	82.95	997	955	1,434
12508	SL-8 R/B	1981-053B	104.63	82.96	1004	950	1,434
12682	SL-8 R/B	1981-077B	104.46	82.92	994	944	1,434
12836	SL-8 R/B	1981-091B	104.62	82.92	993	960	1,434
13034	SL-8 R/B	1982-003B	104.7	82.94	1004	957	1,434
13066	SL-8 R/B	1982-012B	104.56	82.9	1005	943	1,434
13111	SL-8 R/B	1982-024B	104.67	82.93	1010	948	1,434
13128	SL-8 R/B	1982-030B	104.67	82.92	1001	957	1,434
13260	SL-8 R/B	1982-055B	104.78	65.83	1018	950	1,434
13618	SL-8 R/B	1982-102B	104.6	82.97	1000	951	1,434
13758	SL-8 R/B	1983-001B	104.45	82.91	988	949	1,434
13917	SL-8 R/B	1983-021B	104.59	82.94	995	955	1,434



13950	SL-8 R/B	1983-023B	104.59	82.96	1001	949	1,434
14059	SL-8 R/B	1983-042B	104.46	82.97	999	939	1,434
14085	SL-8 R/B	1983-048B	104.63	82.95	1003	952	1,434
14451	SL-8 R/B	1983-108B	104.5	82.93	996	946	1,434
14547	SL-8 R/B	1983-120B	104.57	82.93	1008	941	1,434
14625	SL-8 R/B	1984-003B	104.78	82.93	1001	967	1,434
14680	SL-8 R/B	1984-010B	104.61	82.95	1005	948	1,434
14966	SL-8 R/B	1984-043B	104.77	82.97	996	971	1,434
14974	SL-8 R/B	1984-046B	104.58	82.94	1008	941	1,434
15056	SL-8 R/B	1984-062B	104.63	82.96	997	958	1,434
15078	SL-8 R/B	1984-067B	104.57	82.96	994	955	1,434
15293	SL-8 R/B	1984-100B	104.73	82.94	999	964	1,434
15360	SL-8 R/B	1984-109B	104.6	82.94	1007	944	1,434
15399	SL-8 R/B	1984-118B	104.65	82.94	1003	953	1,434
15506	SL-8 R/B	1985-011B	104.64	82.92	1005	950	1,434
15598	SL-8 R/B	1985-022B	104.61	82.94	993	959	1,434
15752	SL-8 R/B	1985-041B	104.87	82.95	1007	970	1,434
16292	SL-8 R/B	1985-110B	104.58	82.93	998	952	1,434
16369	SL-8 R/B	1985-116B	104.59	82.94	1003	948	1,434
16494	SL-8 R/B	1986-005B	104.62	82.93	990	963	1,434
16511	SL-8 R/B	1986-008B	104.67	82.94	996	962	1,434
16728	SL-8 R/B	1986-037B	104.6	82.96	998	953	1,434
17067	SL-8 R/B	1986-086B	104.53	82.95	997	947	1,434
17160	SL-8 R/B	1986-093B	104.76	82.93	1012	954	1,434
17240	SL-8 R/B	1986-100B	104.81	82.93	1007	964	1,434
17360	SL-8 R/B	1987-009B	104.6	82.92	999	952	1,434
17526	SL-8 R/B	1987-017B	104.59	82.9	1004	946	1,434
18130	SL-8 R/B	1987-054B	104.61	82.92	989	964	1,434
18161	SL-8 R/B	1987-057B	104.58	82.93	997	952	1,434
18710	SL-8 R/B	1987-106B	104.65	82.91	996	960	1,434
18986	SL-8 R/B	1988-023B	104.45	82.95	999	939	1,434

19325	SL-8 R/B	1988-062B	104.54	82.95	997	949	1,434
19827	SL-8 R/B	1989-017B	104.8	82.95	1007	963	1,434
19922	SL-8 R/B	1989-028B	104.56	82.96	1000	948	1,434
20046	SL-8 R/B	1989-042B	104.49	82.94	1003	939	1,434
20104	SL-8 R/B	1989-050B	104.56	82.96	1005	942	1,434
20150	SL-8 R/B	1989-059B	104.68	82.94	1000	959	1,434
20509	SL-8 R/B	1990-017B	104.69	82.95	1012	948	1,434
20528	SL-8 R/B	1990-023B	104.89	82.93	1013	965	1,434
20578	SL-8 R/B	1990-036B	104.63	82.94	986	968	1,434
20805	SL-8 R/B	1990-083B	104.67	82.94	1002	956	1,434
21088	SL-8 R/B	1991-006B	104.57	82.94	990	958	1,434
21090	SL-8 R/B	1991-007B	104.63	82.92	993	961	1,434
21153	SL-8 R/B	1991-019B	104.66	82.92	1001	957	1,434
21231	SL-8 R/B	1991-029B	104.67	82.95	1004	954	1,434
21667	SL-8 R/B	1991-059B	104.72	82.9	996	967	1,434
21797	SL-8 R/B	1991-081B	104.55	82.95	1002	944	1,434
21876	SL-8 R/B	1992-008B	104.68	82.93	1006	953	1,434
21903	SL-8 R/B	1992-012B	104.77	82.94	1016	951	1,434
21938	SL-8 R/B	1992-020B	104.71	82.93	1002	960	1,434
22007	SL-8 R/B	1992-036B	104.51	82.93	993	950	1,434
22208	SL-8 R/B	1992-073B	104.72	82.92	1007	955	1,434
22308	SL-8 R/B	1993-001B	104.68	82.93	996	963	1,434
22488	SL-8 R/B	1993-008B	104.52	82.94	990	954	1,434
22591	SL-8 R/B	1993-020B	104.55	82.93	992	954	1,434
22889	SL-8 R/B	1993-070B	104.51	82.95	1007	936	1,434
23093	SL-8 R/B	1994-024B	104.52	82.95	980	964	1,434
23180	SL-8 R/B	1994-041B	104.5	82.95	992	951	1,434
23190	SL-8 R/B	1994-045B	104.8	74.03	999	971	1,434
23466	SL-8 R/B	1995-002D	104.78	82.93	1009	959	1,434
23527	SL-8 R/B	1995-012B	104.84	82.94	1001	973	1,434
23604	SL-8 R/B	1995-032B	104.78	82.9	1001	967	1,434

23774	SL-8 R/B	1996-004B	104.62	82.98	1009	944	1,434
24306	SL-8 R/B	1996-052C	104.73	82.93	1002	962	1,434
24678	SL-8 R/B	1996-071B	104.83	82.94	1004	969	1,434
24773	SL-8 R/B	1997-017B	104.84	82.92	1004	970	1,434
24955	SL-8 R/B	1997-052C	104.24	82.92	981	936	1,434
25569	SL-8 R/B	1998-072C	104.81	82.95	1002	969	1,434
25592	SL-8 R/B	1998-076B	104.8	82.94	1004	967	1,434
25893	SL-8 R/B	1999-045B	104.62	82.92	998	954	1,434
26819	SL-8 R/B	2001-023B	104.69	82.93	997	963	1,434
27437	SL-8 R/B	2002-026B	104.61	82.95	1009	943	1,434
27535	SL-8 R/B	2002-046B	104.78	82.93	1012	956	1,434
27819	SL-8 R/B	2003-023B	104.79	82.95	1020	949	1,434
28381	SL-8 R/B	2004-028B	104.49	82.96	994	946	1,434
32053	SL-8 R/B	2007-038B	104.63	82.98	998	957	1,434
SI-8 Payloads							
4783	COSMOS 381	1970-102A	104.75	74.03	1005	961	700
4799	COSMOS 385	1970-108A	104.6	74.02	978	973	700
5238	COSMOS 422	1971-046A	104.95	74.02	1003	981	700
5683	COSMOS 465	1971-111A	104.79	74.03	1004	965	700
5846	COSMOS 475	1972-009A	104.64	74.05	994	961	700
6019	COSMOS 489	1972-035A	104.66	74.02	997	960	700
6148	COSMOS 514	1972-062A	104.22	82.97	966	949	700
6206	COSMOS 521	1972-074A	104.92	65.83	995	987	700
6707	COSMOS 574	1973-042A	104.95	82.95	1008	976	700
6828	COSMOS 586	1973-065A	104.72	82.94	1002	961	700
7008	COSMOS 627	1973-109A	104.89	82.95	1014	965	700
7094	COSMOS 628	1974-001A	104.67	82.96	1006	953	700
7349	COSMOS 663	1974-048A	104.69	82.95	999	960	700
7476	COSMOS 689	1974-079A	104.95	82.94	1013	971	700
7593	COSMOS 700	1974-105A	104.6	82.95	994	957	700
7736	COSMOS 726	1975-028A	104.49	83	988	952	700

7768	COSMOS 729	1975-034A	104.85	82.96	1004	971	700
8072	COSMOS 755	1975-074A	104.81	82.9	1005	966	700
8419	COSMOS 778	1975-103A	104.76	82.97	1000	966	700
8591	COSMOS 789	1976-005A	104.88	82.98	1011	967	700
8645	COSMOS 800	1976-011A	104.96	82.97	1009	976	700
8873	COSMOS 823	1976-051A	104.86	82.96	1005	971	700
9025	COSMOS 842	1976-070A	104.8	82.99	1007	964	700
9061	COSMOS 846	1976-078A	104.62	82.93	1007	946	700
9509	COSMOS 864	1976-108A	104.7	82.94	1002	959	700
9610	COSMOS 883	1976-122A	104.66	82.95	1005	952	700
9637	COSMOS 887	1976-128A	104.64	82.94	1012	943	700
9737	COSMOS 890	1977-004A	104.99	82.96	1014	974	700
9846	COSMOS 894	1977-013A	104.81	82.94	1008	963	700
10019	COSMOS 911	1977-039A	104.71	82.95	999	962	700
10137	COSMOS 926	1977-062A	104.94	82.94	1016	967	700
10141	COSMOS 928	1977-064A	104.61	82.97	1003	949	700
10352	COSMOS 951	1977-087A	104.8	82.97	1010	960	700
10459	COSMOS 962	1977-107A	104.75	82.95	1003	963	700
10512	COSMOS 967	1977-116A	104.73	65.83	1004	960	700
10536	COSMOS 971	1977-122A	104.87	82.94	1004	972	700
10599	COSMOS 985	1978-007A	104.6	82.94	1015	936	700
10692	COSMOS 991	1978-022A	104.63	82.99	1005	950	700
10731	COSMOS 994	1978-028A	104.87	82.93	1006	970	700
10744	COSMOS 996	1978-031A	104.62	82.93	1003	950	700
10776	COSMOS 1000	1978-034A	104.7	82.94	1005	956	700
10917	COSMOS 1011	1978-053A	104.71	82.92	1009	953	700
10991	COSMOS 1027	1978-074A	104.62	82.94	996	958	700
11238	COSMOS 1072	1979-003A	104.79	82.94	1013	957	700
11308	COSMOS 1089	1979-026A	104.72	82.97	997	965	700
11320	COSMOS 1091	1979-028A	104.76	82.92	1005	961	700
11326	COSMOS 1092	1979-030A	104.7	82.95	1001	960	700

11378	COSMOS 1104	1979-046A	104.67	82.95	1004	954	700
11667	COSMOS 1150	1980-003A	104.85	82.95	1012	963	700
11680	COSMOS 1153	1980-007A	104.83	82.93	1015	958	700
11735	COSMOS 1168	1980-022A	104.73	82.94	1008	956	700
11750	COSMOS 1171	1980-026A	104.83	65.84	1009	964	700
11803	COSMOS 1181	1980-039A	104.81	82.95	1003	968	700
12087	COSMOS 1225	1980-097A	104.77	82.94	1024	943	700
12091	COSMOS 1226	1980-099A	104.77	82.94	1008	960	700
12297	COSMOS 1244	1981-013A	104.73	82.95	1004	959	700
12504	COSMOS 1275	1981-053A	104.78	82.96	1013	955	700
12681	COSMOS 1295	1981-077A	104.62	82.92	1010	943	700
12835	COSMOS 1308	1981-091A	104.7	82.92	1000	961	700
13033	COSMOS 1333	1982-003A	104.87	82.94	1012	965	700
13065	COSMOS 1339	1982-012A	104.69	82.9	1011	949	700
13110	COSMOS 1344	1982-024A	104.81	82.92	1007	964	700
13127	COSMOS 1349	1982-030A	104.82	82.93	1009	964	700
13259	COSMOS 1375	1982-055A	104.14	65.83	974	934	600
13757	COSMOS 1428	1983-001A	104.59	82.91	1002	949	810
13916	COSMOS 1447	1983-021A	104.72	82.95	1009	954	810
13949	COSMOS 1448	1983-023A	104.66	82.96	1000	958	810
14057	COSMOS 1459	1983-042A	104.61	82.97	1013	939	810
14084	COSMOS 1464	1983-048A	104.77	82.95	1006	962	810
14450	COSMOS 1506	1983-108A	104.64	82.93	1009	946	810
14546	COSMOS 1513	1983-120A	104.79	82.94	1014	955	810
14624	COSMOS 1531	1984-003A	104.95	82.93	1006	978	810
14679	COSMOS 1535	1984-010A	104.72	82.96	1013	950	810
14965	COSMOS 1550	1984-043A	104.9	82.98	1009	970	810
14973	COSMOS 1553	1984-046A	104.71	82.94	1005	956	810
15055	COSMOS 1574	1984-062A	104.78	82.96	1004	965	810
15077	COSMOS 1577	1984-067A	104.7	82.96	1007	954	810
15292	COSMOS 1598	1984-100A	104.88	82.95	1013	965	810

15359	COSMOS 1605	1984-109A	104.72	82.94	1016	946	810
15398	COSMOS 1610	1984-118A	104.83	82.95	1009	964	810
15505	COSMOS 1627	1985-011A	104.78	82.92	1016	952	810
15597	COSMOS 1634	1985-022A	104.72	82.94	1007	956	2200
15751	COSMOS 1655	1985-041A	104.98	82.95	1013	974	810
16291	COSMOS 1704	1985-110A	104.76	82.93	1006	961	810
16368	COSMOS 1709	1985-116A	104.77	82.94	1008	959	810
16493	COSMOS 1725	1986-005A	104.76	82.93	1000	967	810
16510	COSMOS 1727	1986-008A	104.78	82.95	1013	955	810
16727	COSMOS 1745	1986-037A	104.79	82.96	1008	962	810
17066	COSMOS 1791	1986-086A	104.67	82.95	1010	948	810
17159	COSMOS 1802	1986-093A	104.9	82.93	1020	960	810
17239	COSMOS 1808	1986-100A	104.96	82.93	1016	969	810
17359	COSMOS 1816	1987-009A	104.77	82.93	1008	960	810
17525	COSMOS 1821	1987-017A	104.83	82.91	1015	958	810
18129	COSMOS 1861	1987-054A	104.88	82.92	999	979	810
18160	COSMOS 1864	1987-057A	104.69	82.93	1004	956	810
18709	COSMOS 1904	1987-106A	104.79	82.91	1005	964	810
18985	COSMOS 1934	1988-023A	104.62	82.96	1007	947	810
19324	COSMOS 1959	1988-062A	104.65	82.95	1002	954	810
19826	COSMOS 2004	1989-017A	104.94	82.95	1014	969	810
19921	COSMOS 2016	1989-028A	104.73	82.96	1011	952	810
20045	COSMOS 2026	1989-042A	104.65	82.94	1008	948	810
20103	NADEZHDA 1	1989-050A	104.76	82.96	1010	957	825
20149	COSMOS 2034	1989-059A	104.85	82.94	1011	964	810
20508	NADEZHDA 2	1990-017A	104.79	82.96	1016	953	825
20527	COSMOS 2061	1990-023A	104.95	82.94	1015	969	825
20577	COSMOS 2074	1990-036A	104.76	82.94	1003	963	825
20804	COSMOS 2100	1990-083A	104.78	82.94	1012	956	825
21087	INFORMATOR 1	1991-006A	104.71	82.94	1008	954	825
21089	COSMOS 2123	1991-007A	104.76	82.92	1006	960	825

21152	NADEZHDA 3	1991-019A	104.79	82.92	1014	955	825
21230	COSMOS 2142	1991-029A	104.87	82.96	1017	960	825
21666	COSMOS 2154	1991-059A	104.86	82.9	1006	970	825
21796	COSMOS 2173	1991-081A	104.69	82.96	1017	944	825
21875	COSMOS 2180	1992-008A	104.83	82.93	1015	958	825
21902	COSMOS 2181	1992-012A	104.93	82.94	1012	971	825
21937	COSMOS 2184	1992-020A	104.87	82.93	1012	965	825
22006	COSMOS 2195	1992-036A	104.74	82.93	1010	954	825
22207	COSMOS 2218	1992-073A	104.89	82.92	1014	965	825
22307	COSMOS 2230	1993-001A	104.84	82.94	1004	970	825
22487	COSMOS 2233	1993-008A	104.67	82.95	1006	952	825
22590	COSMOS 2239	1993-020A	104.7	82.93	998	962	825
22888	COSMOS 2266	1993-070A	104.74	82.95	1018	947	825
23092	COSMOS 2279	1994-024A	104.63	82.95	1004	950	825
23179	NADEZHDA 4	1994-041A	104.61	82.95	1001	951	825
23189	COSMOS 2285	1994-045A	104.94	74.03	1010	973	825
23463	TSIKADA	1995-002A	104.92	82.93	1018	963	825
23526	COSMOS 2310	1995-012A	104.97	82.94	1010	976	825
23603	COSMOS 2315	1995-032A	104.89	82.9	1012	967	825
23773	COSMOS 2327	1996-004A	104.77	82.98	1020	947	795
24304	COSMOS 2334	1996-052A	104.84	82.93	1010	964	825
24677	COSMOS 2336	1996-071A	104.99	82.94	1012	976	795
24772	COSMOS 2341	1997-017A	105	82.92	1014	976	795
24953	COSMOS 2346	1997-052A	104.38	82.92	994	937	795
25567	NADEZHDA 5	1998-072A	104.97	82.95	1011	975	825
25590	COSMOS 2361	1998-076A	104.89	82.94	1011	967	825
25892	COSMOS 2366	1999-045A	104.77	82.93	1007	960	795
26818	COSMOS 2378	2001-023A	104.81	82.93	1009	962	795
27436	COSMOS 2389	2002-026A	104.73	82.95	1017	947	795
27534	NADEZHDA 7	2002-046A	104.91	82.93	1018	962	825
27818	COSMOS 2398	2003-023A	104.95	82.95	1016	968	795

28380	COSMOS 2407	2004-028A	104.65	82.96	1008	948	820
32052	COSMOS 2429	2007-038A	104.74	82.98	1011	953	795
Other Payloads							
12409	COSMOS 1266	1981-037A	103.57	64.76	963	891	1295
12783	COSMOS 1299	1981-081A	103.94	65.12	968	922	1295
13243	COSMOS 1372	1982-052A	103.9	64.9	973	913	1237
10358	COSMOS 952	1977-088A	104.08	64.94	975	928	1295
13600	COSMOS 1412	1982-099A	103.88	64.81	979	905	1295
7005	COSMOS 626	1973-108A	103.95	65.44	983	907	1295
16917	COSMOS 1771	1986-062A	104.16	64.98	983	927	1295
15085	COSMOS 1579	1984-069A	103.89	65.05	984	901	1295
18122	COSMOS 1860	1987-052A	103.99	65.01	989	905	1295
9486	COSMOS 860	1976-103A	104.25	64.7	989	930	1295
15930	COSMOS 1670	1985-064A	104.07	64.94	991	910	1295
18957	COSMOS 1932	1988-019A	104.37	65.04	994	937	1295
6206	COSMOS 521	1972-074A	104.92	65.83	995	987	750
5050	COSMOS 400	1971-020A	104.95	65.83	997	987	750
12149	COSMOS 1241	1981-006A	104.94	65.82	997	986	750



## Appendix B: Simulation Code

```
function [] = Cluster_Analysis_Function(filename, apogee_array, perigee_array, Tier, Man_Flag, Cluster)
```

### Debris Cluster Conjunction Analysis

Author: Ethan Ohriner

```
% This code will load an debris cluster in STK using an array of SSC
% numbers. It will then compare each debris object against every observer
% satellite in the constellation, storing the miss data in a structure
% named conjunctionData. It will then calculate the performance metrics
% for the constellation and save off the data.

% Inputs
% - filename      : Name for the performance metrics save file.
% - apogee_array  : Array of constellation apogee values.
% - perigee_array : Array of constellation perigee values.
% - Tier          : Tier being analyzed. Options = {1,2,3}
% - Man_Flag      : Maneuver flag. Options = {0,1,2}
% - Cluster       : Cluster being analyzed. Options={1,2,3}
```

### Inputs

```
% Set the scenario start and stop time
StartTime = '1 Jan 2019 00:00:00.000' ;
StopTime  = '1 Jan 2020 00:00:00.000' ;

ScenarioLength = 3600*24*365 ; %sec

% Range Selection
if Tier == 1
    Range = 100000 ; %m
elseif Tier == 2
    Range = 600000 ; %m
elseif Tier == 3
    Range = 2400000 ; %m
end
```

### RSO Selection

```
if Cluster==1
    % SL-8 Cluster (775 km) (88 Objects)
    SSC = [05707, 06061, 06324, 06966, 07434, 08344, 08459, 08924, ...
           09023, 09444, 10121, 10521, 10677, 10962, 11112, 11427, 11511, ...
           11574, 11870, 12443, 12792, 13028, 13149, 13242, 13649, 13992, ...
           14241, 14402, 14760, 15032, 15483, 16012, 16682, 16864, 16953, ...
           17304, 18096, 18586, 19039, 19257, 19770, 21015, 22676, 23432, ...
           05705, 06059, 06323, 06965, 07433, 08343, 08458, 08923, 09022, ...
           09443, 10120, 10520, 10676, 10961, 11111, 11425, 11510, 11573, ...
```

```

11869, 12442, 12791, 13027, 13148, 13241, 13648, 13991, 14240, ...
14401, 14759, 15031, 15482, 16011, 16681, 16860, 16952, 17303, ...
18095, 18585, 19038, 19256, 19769, 21014, 22675, 23431] ;

cluster_alt = 7146 ; %km
cluster_inc = 74 ; %deg

elseif Cluster==2
% SL-16 Cluster with Plds and Miscellaneous Debris (850 km) (75 Objects)
SSC = [16182, 16181, 22285, 22284, 23405, 23404, 22220, 22219, ...
31793, 31792, 28353, 28352, 23088, 23087, 19650, 19649, 22803, ...
22802, 23705, 23704, 26070, 26069, 20625, 20624, 22566, 22565, ...
17974, 17973, 17590, 17589, 25407, 25406, 24298, 24297, 19120, ...
19119, 08519, 07574, 04419, 11288, 05731, 10514, 07209, 08026, ...
09481, 07274, 11605, 06659, 08799, 06392, 13718, 07490, 08845, ...
06256, 11962, 05917, 07714, 09661, 06079, 09903, 12456, 11165, ...
15334, 15772, 32958, 20322, 37214, 22823, 37849, 15427, 19531, ...
28654, 11166, 13719, 11289] ;

cluster_alt = 7210 ; %km
cluster_inc = 71 ; %deg

elseif Cluster==3
% SL-8 Cluster (975km Cluster) (304 Objects)
SSC = [04784, 04800, 05239, 05685, 05847, 06020, 06149, 06207, ...
06708, 06829, 07009, 07095, 07350, 07477, 07594, 07737, 07769, ...
08073, 08421, 08597, 08646, 08874, 09044, 09062, 09510, 09613, ...
09638, 09738, 09848, 10020, 10138, 10142, 10355, 10461, 10513, ...
10537, 10600, 10693, 10732, 10745, 10777, 10918, 10992, 11239, ...
11309, 11321, 11327, 11379, 11586, 11668, 11681, 11736, 11751, ...
11804, 12088, 12092, 12298, 12508, 12682, 12836, 13034, 13066, ...
13111, 13128, 13260, 13618, 13758, 13917, 13950, 14059, 14085, ...
14451, 14547, 14625, 14680, 14966, 14974, 15056, 15078, 15293, ...
15360, 15399, 15506, 15598, 15752, 16292, 16369, 16494, 16511, ...
16728, 17067, 17160, 17240, 17360, 17526, 18130, 18161, 18710, ...
18986, 19325, 19827, 19922, 20046, 20104, 20150, 20509, 20528, ...
20578, 20805, 21088, 21090, 21153, 21231, 21667, 21797, 21876, ...
21903, 21938, 22007, 22208, 22308, 22488, 22591, 22889, 23093, ...
23180, 23190, 23466, 23527, 23604, 23774, 24306, 24678, 24773, ...
24955, 25569, 25592, 25893, 26819, 27437, 27535, 27819, 28381, ...
32053, 04783, 04799, 05238, 05683, 05846, 06019, 06148, 06206, ...
06707, 06828, 07008, 07094, 07349, 07476, 07593, 07736, 07768, ...
08072, 08419, 08591, 08645, 08873, 09025, 09061, 09509, 09610, ...
09637, 09737, 09846, 10019, 10137, 10141, 10352, 10459, 10512, ...
10536, 10599, 10692, 10731, 10744, 10776, 10917, 10991, 11238, ...
11308, 11320, 11326, 11378, 11667, 11680, 11735, 11750, 11803, ...
12087, 12091, 12297, 12504, 12681, 12835, 13033, 13065, 13110, ...
13127, 13259, 13757, 13916, 13949, 14057, 14084, 14450, 14546, ...
14624, 14679, 14965, 14973, 15055, 15077, 15292, 15359, 15398, ...
15505, 15597, 15751, 16291, 16368, 16493, 16510, 16727, 17066, ...
17159, 17239, 17359, 17525, 18129, 18160, 18709, 18985, 19324, ...
19826, 19921, 20045, 20103, 20149, 20508, 20527, 20577, 20804, ...
21087, 21089, 21152, 21230, 21666, 21796, 21875, 21902, 21937, ...
22006, 22207, 22307, 22487, 22590, 22888, 23092, 23179, 23189, ...

```

```

23463, 23526, 23603, 23773, 24304, 24677, 24772, 24953, 25567, ...
25590, 25892, 26818, 27436, 27534, 27818, 28380, 32052, 12409, ...
12783, 13243, 10358, 13600, 07005, 16917, 15085, 18122, 09486, ...
15930, 18957, 05050, 12149] ;

```

```

cluster_alt = 7346 ; %km
cluster_inc = 83 ; %deg

```

```
end
```

### Open STK and connect

```

app = actxserver('STK11.Application');
root = app.Personality2 ;

scenario = root.Children.New('escenario','SSA_Analysis') ;

% Set scenario start and stop time
root.BeginUpdate();
scenario.SetTimePeriod(StartTime,StopTime) ;
root.ExecuteCommand('Animate * Reset');
root.EndUpdate(); %Graphics will not update until the end, saves time.

```

### Define data storage structure:

```

conjunctionData = struct('PrimarySatellite', {}, 'ConjunctionInfo', {});
conjInfoStruct = struct('ConjunctingSatellite', {}, 'TCA', {}, 'RangeMag', {}, ...
    'Radial', {}, 'InPlane', {}, 'Normal', {}, 'VelocityMag', {}, 'V_Radial', {}, ...
    'V_InPlane', {}, 'V_Normal', {}, 'Longitude', {}, 'Latitude', {}, 'Altitude', {}, ...
    'AccessStart', {}, 'AccessStop', {}, 'Duration', {});

subptElems = {'Lat'; 'Lon'; 'Alt'};

```

### RSO Initialization

Load the satellites into STK.

```

h = waitbar(0,'RSO Initialization') ;

% Change time to Epoch Seconds
root.UnitPreferences.Item('DateFormat').SetCurrentUnit('EPSEC');

root.BeginUpdate();
for i=1:length(SSC)

    % Grab the satellite ID
    SSCinc = SSC(i) ;

    % Load satellite in STK
    satellite= scenario.Children.New('esatellite',num2str(SSCinc,'%05d')) ;
    cmd = ['SetState */Satellite/' num2str(SSCinc,'%05d') ' SGP4 ',StartTime,...
        ' ', StopTime, ' 60 ' num2str(SSCinc,'%05d') ' TLESource Automatic'] ;
    root.ExecuteCommand(cmd);

```

```

    % Set the range constraint
    rangeconst = ['SetConstraint */Satellite/' num2str(SSCinc,'%05d') ' Range Min 0 Max '
num2str(Range)] ;
    root.ExecuteCommand(rangeconst) ;

    % Set the illumination constraint
    lightconst = satellite.accessConstraints.AddConstraint('eCstrLighting');
    lightconst.Condition = 'ePenumbraorDirectSun';

    waitbar((i/length(SSC)),h) ;
end
root.EndUpdate();

close(h) % close waitbar
disp('RSO Initialization: Complete')
disp(i)

```

### OBS Initialization

Load the constellation into STK.

```

if Man_Flag == 0 % non-maneuvering flag

EarthRad = 6371 ; %km
alt = cluster_alt - EarthRad; %km
OBSperigee = perigee_array + alt ; %km
OBSapogee = apogee_array + alt ; %km
OBSlocation = 0:(360/length(perigee_array)):359 ;
OBSinc = ones(1,length(perigee_array))*cluster_inc ;

root.BeginUpdate();
for i=1:length(perigee_array)

OBSnum = sprintf('OBS%d',i) ;
satellite= scenario.Children.New('esatellite',OBSnum) ;
satellite.SetPropagatorType('ePropagatorHPOP'); % Set Propagator to HPOP
keplerian = satellite.Propagator.InitialState.Representation.ConvertTo('eOrbitStateClassical');
keplerian.SizeShapeType = 'eSizeShapeAltitude'; % Changes from Ecc/Inc to Perigee/Apogee
Altitude
keplerian.LocationType = 'eLocationTrueAnomaly'; % Makes sure True Anomaly is being used
keplerian.Orientation.AscNodeType = 'eAscNodeLAN'; % Use LAN instead of RAAN for data entry
keplerian.SizeShape.PerigeeAltitude = OBSperigee(i); % km
keplerian.SizeShape.ApogeeAltitude = OBSapogee(i); % km
keplerian.Orientation.Inclination = OBSinc(i); % deg
keplerian.Orientation.ArgOfPerigee = 0; % deg
keplerian.Orientation.AscNode.Value = OBSlocation(i); % deg
keplerian.Location.Value = 0; % deg
satellite.Propagator.InitialState.Representation.Assign(keplerian);
satellite.Propagator.Propagate;

% Set the range constraint
rangeconst = ['SetConstraint */Satellite/' OBSnum ' Range Min 0 Max ' num2str(Range)] ;
root.ExecuteCommand(rangeconst) ;

```

```

end
root.EndUpdate();

disp('OBS Initialization: Complete')
disp(i)

end

```

## Maneuver Manager 1

```

% Phasing Maneuver

if Man_Flag == 1 % phasing maneuver flag

alt = cluster_alt; %km
OBSperigee = perigee_array + alt ; %km
OBSapogee = apogee_array + alt ; %km
OBSlocation = 0:(360/length(perigee_array)):359 ;
OBSinc = ones(1,length(perigee_array))*cluster_inc ;
circular_con = (OBSperigee(1) == OBSapogee(1)) ;

for i=1:length(OBSlocation)

% Start Satellite
OBSnum = sprintf('OBS%d',i) ;
satellite= scenario.Children.New('esatellite',OBSnum) ;

% Start Waitbar
OBSstring = strcat(OBSnum,' Loading Maneuvers');
h2 = waitbar(0,OBSstring) ;

% Set propagator type to Astrogator
satellite.SetPropagatorType('ePropagatorAstrogator');
ASTG = satellite.Propagator;
ASTG.MainSequence.RemoveAll(); %Clear all segments from the MCS

% Insert Initial State Segment into MCS and configure
initState = ASTG.MainSequence.Insert('eVASegmentTypeInitialState', 'Initial State', '-');
initState.InitialState.Epoch = scenario.StartTime;
initState.SetElementType('eVAElementypeKeplerian');
kep = initState.Element;
kep.PeriapsisRadiusSize = OBSperigee(i);
kep.Eccentricity = 1 - 2/((OBSapogee(i)/OBSperigee(i)) + 1);
kep.ArgOfPeriapsis = 0;
kep.RAAN = OBSlocation(i);
kep.Inclination = OBSinc(i);
kep.TrueAnomaly = 0;

% Propagate to start
propagate1 = ASTG.MainSequence.Insert('eVASegmentTypePropagate', 'Propagate 1', '-');
propagate1.PropagatorName = 'Earth Point Mass';
propagate1.Properties.Color = 255; % Red

```

```

propagate1.StoppingConditions.Item('Duration').Properties.Trip = 3600*24*10 ;

if circular_con
    % Insert a Propagate State Segment into the MCS and Add/Remove Stopping Conditions
    propagate2 = ASTG.MainSequence.Insert('evASegmentTypePropagate', 'Propagate 2', '-');
    propagate2.PropagatorName = 'Earth Point Mass';
    propagate2.Properties.Color = 255; % Red
    propagate2.StoppingConditions.Add('AscendingNode');
    propagate2.StoppingConditions.Remove('Duration');
else
    % Insert a Propagate State Segment into the MCS and Add/Remove Stopping Conditions
    propagate2 = ASTG.MainSequence.Insert('evASegmentTypePropagate', 'Propagate 2', '-');
    propagate2.PropagatorName = 'Earth Point Mass';
    propagate2.Properties.Color = 255; % Red
    propagate2.StoppingConditions.Add('Apoapsis');
    propagate2.StoppingConditions.Remove('Duration');
end

PropCount = 2;

% Run the MCS
ASTG.RunMCS;

% Set the range constraint
rangeconst = ['SetConstraint */Satellite/' OBSnum ' Range Min 0 Max ' num2str(Range)] ;
root.ExecuteCommand(rangeconst) ;

% Get time of apoapsis
EndTime = satellite.Propagator.MainSequence.Item(2).FinalState.Epoch ;
EndTime_old = scenario.StartTime ;

loop_count = 1 ; % Initialize loop counter
while(1)

    % Check access to see if burn is needed
    ConjCount = 0;
    for idx = 1:length(SSC)
        sat1 = scenario.Children.Item(num2str(SSC(idx), '%05d')) ;
        acc=satellite.GetAccessToObject(sat1);
        acc.AccessTimePeriod = 'eUserSpecAccessTime';
        acc.AccessTimePeriodData.AccessInterval.State = 'eCrdrnSmartIntervalStateStartStop';
        accStartEpoch = acc.AccessTimePeriodData.AccessInterval.GetStartEpoch();
        accStartEpoch.SetExplicitTime(EndTime_old) ;
        acc.AccessTimePeriodData.AccessInterval.SetStartEpoch(accStartEpoch);
        accStopEpoch = acc.AccessTimePeriodData.AccessInterval.GetStopEpoch();
        accStopEpoch.SetExplicitTime(EndTime) ;
        acc.AccessTimePeriodData.AccessInterval.SetStopEpoch(accStopEpoch);
        acc.ComputeAccess;
        accessDP = acc.DataProviders.Item('Access Data').Exec(EndTime_old, EndTime) ;
        if acc.ComputedAccessIntervalTimes.Count ~= 0
            ConjCount = ConjCount + acc.ComputedAccessIntervalTimes.Count ;
            Duration(idx) =
sum(cell2mat(accessDP.DataSets.GetDataSetByName('Duration').GetValues));
        end
    end
end

```

```

end

if ConjCount ~= 0
    Idx = find(Duration) ;
    MD(loop_count) = mean(Duration(Idx)) ;

    maneuver = 1 ;
    if loop_count ~= 1
        if (MD(loop_count) > MD_avg)
            maneuver = 0 ;
        end
    end
    MD_avg = mean(MD);
    clear Duration
else
    MD(loop_count) = 0 ;
    MD_avg = mean(MD);
    maneuver = 1 ;
end

if maneuver == 1

    % Check access to see if burn is needed
    OBS_COE_DP = satellite.DataProviders.Item('Astrogator Values').Group.Item('Keplerian
Elems').ExecElements(scenario.StartTime,scenario.StopTime,60,...
    {'Time';'Semimajor_Axis'}) ;
    SMA = OBS_COE_DP.DataSets.GetDataSetByName('Semimajor_Axis').GetValues ;

    mu_earth = 3.986004418E14 ; %m^3/s^2
    a_old_m = cell2mat(SMA(end))*1000 ; %km (with the *1000)
    CurrentPeriod = 2*pi*sqrt(a_old_m^3/mu_earth) ; %sec
    PhaseAngle = 10 ; %deg to phase
    PhaseTime = CurrentPeriod*(PhaseAngle/360); %sec to phase
    T = CurrentPeriod - PhaseTime ;
    a_new_m = (mu_earth*(T/(2*pi))^2)^(1/3) ;

    % STK wants km units
    a_old = a_old_m/1000 ; %km
    a_new = a_new_m/1000 ; %km

    % Insert a target sequence with nested maneuver segment
    ts = ASTG.MainSequence.Insert('evASegmentTypeTargetSequence','Start Transfer','-');
    dv1 = ts.Segments.Insert('evASegmentTypeManeuver','DV1','-');
    dv1.SetManeuverType('evAManeuverTypeImpulsive');
    % Create a handle to the impulsive properties of the maneuver
    impulsive = dv1.Maneuver;
    impulsive.SetAttitudeControlType('evaAttitudeControlThrustVector');
    % Create a handle to the Attitude Control - Thrust Vector properties of the
    % maneuver and set the appropriate axes
    thrustVector = impulsive.AttitudeControl;
    thrustVector.ThrustAxesName = 'Satellite VNC(Earth)';
    % For the targeter to vary a given segment property, it must be
    % enabled as a control parameter.
    dv1.EnableControlParameter('evaControlManeuverImpulsiveCartesianX');

```

```

    % Segment Results, which can be used as targeter goals, are also stored in a
collection
    dv1.Results.Add('Keplerian Elems/Semimajor Axis');
    % Targeter Profiles are also stored as a collection
    dc = ts.Profiles.Item('Differential Corrector');

    % Create a handle to the targeter control and set its properties
    xControlParam = dc.ControlParameters.GetControlByPaths('DV1',
'ImpulsiveMnvr.Cartesian.X');
    xControlParam.Enable = true;
    xControlParam.MaxStep = 0.3;

    % Create a handle to the targeter results and set its properties
    Result = dc.Results.GetResultByPaths('DV1', 'Semimajor Axis');
    Result.Enable = true;
    Result.DesiredValue = a_new ;
    Result.Tolerance = 0.1;

    % Set final DC and targeter properties and run modes
    dc.MaxIterations = 50;
    dc.EnabledDisplayStatus = true;
    dc.Mode = 'evAProfileModeIterate';
    ts.Action = 'evATargetSeqActionRunActiveProfiles';

    % Propagate the Transfer Orbit to Apogee
    transferEllipse = ASTG.MainSequence.Insert('evASegmentTypePropagate', 'Transfer
Ellipse', '-');
    transferEllipse.PropagatorName = 'Earth Point Mass';
    propagate2.Properties.Color = 65280;
    % Add an Apoapsis Stopping Condition and remove the Duration Stopping Condition
    transferEllipse.StoppingConditions.Add('Apoapsis');
    transferEllipse.StoppingConditions.Remove('Duration');

    if circular_con
        % Propagate the Transfer Orbit to Apogee
    transferEllipse = ASTG.MainSequence.Insert('evASegmentTypePropagate', 'Transfer
Ellipse', '-');
        transferEllipse.PropagatorName = 'Earth Point Mass';
        propagate2.Properties.Color = 65280;
        %Add an Apoapsis Stopping Condition and remove the Duration Stopping Condition
        transferEllipse.StoppingConditions.Add('AscendingNode');
        transferEllipse.StoppingConditions.Remove('Duration');
    else
        % Propagate the Transfer Orbit to Apogee
    transferEllipse = ASTG.MainSequence.Insert('evASegmentTypePropagate', 'Transfer
Ellipse', '-');
        transferEllipse.PropagatorName = 'Earth Point Mass';
        propagate2.Properties.Color = 65280;
        %Add an Apoapsis Stopping Condition and remove the Duration Stopping Condition
        transferEllipse.StoppingConditions.Add('Apoapsis');
        transferEllipse.StoppingConditions.Remove('Duration');
    end

    % Maneuver into the Outer Orbit

```



```

ts = ASTG.MainSequence.Insert('eVASegmentTypeTargetSequence','Finish Transfer','-');
dv2 = ts.Segments.Insert('eVASegmentTypeManeuver','DV2','-');

% Select Variables
dv2.SetManeuverType('eVAManeuverTypeImpulsive');
impulsive = dv2.Maneuver;
impulsive.SetAttitudeControlType('eVAAttitudeControlThrustVector');
thrustVector = impulsive.AttitudeControl;
thrustVector.ThrustAxesName = 'Satellite VNC(Earth)';
dv2.EnableControlParameter('eVAControlManeuverImpulsiveCartesianX');
dv2.Results.Add('Keplerian Elems/Semimajor Axis');

% Set up the Targeter
dc = ts.Profiles.Item('Differential Corrector');
xControlParam = dc.ControlParameters.GetControlByPaths('DV2',
'ImpulsiveMnvr.Cartesian.X');
xControlParam.Enable = true;
xControlParam.MaxStep = 0.3;
Result2 = dc.Results.GetResultByPaths('DV2', 'Semimajor Axis');
Result2.Enable = true;
Result2.DesiredValue = a_old;
Result2.Tolerance = 0.01;

% Set final DC and targeter properties and run modes
dc.EnabledDisplayStatus = true;
dc.Mode = 'eVAProfileModeIterate';
ts.Action = 'eVATargetSeqActionRunActiveProfiles';

% Propagate the Outer Orbit
outerOrbit = ASTG.MainSequence.Insert('eVASegmentTypePropagate','Outer Orbit','-');
outerOrbit.PropagatorName = 'Earth Point Mass';
outerOrbit.StoppingConditions.Item('Duration').Properties.Trip = 3600*24*10;

if circular_con
    % Propagate the Transfer Orbit to Apogee
    outerOrbit_apo =
ASTG.MainSequence.Insert('eVASegmentTypePropagate','Transfer_Ellipse','-');
    outerOrbit_apo.PropagatorName = 'Earth Point Mass';
    outerOrbit_apo.Properties.Color = 65280;
    % Add an Apoapsis Stopping Condition and remove the Duration Stopping Condition
    outerOrbit_apo.StoppingConditions.Add('AscendingNode');
    outerOrbit_apo.StoppingConditions.Remove('Duration');
else
    % Propagate the Transfer Orbit to Apogee
    outerOrbit_apo =
ASTG.MainSequence.Insert('eVASegmentTypePropagate','Transfer_Ellipse','-');
    outerOrbit_apo.PropagatorName = 'Earth Point Mass';
    outerOrbit_apo.Properties.Color = 65280;
    % Add an Apoapsis Stopping Condition and remove the Duration Stopping Condition
    outerOrbit_apo.StoppingConditions.Add('Apoapsis');
    outerOrbit_apo.StoppingConditions.Remove('Duration');
end

%Execute

```

```

ASTG.RunMCS;

else

    % Propagate
    PropCount = PropCount+1;
    prop_string = ['Propagate' num2str(PropCount)];
    propagate = ASTG.MainSequence.Insert('eVASegmentTypePropagate', prop_string, '-');
    propagate.PropagatorName = 'Earth Point Mass';
    propagate.StoppingConditions.Item('Duration').Properties.Trip = 3600*24*10 ;

    if circular_con
        % Propagate the Transfer Orbit to Apogee
        outerOrbit_apo =
ASTG.MainSequence.Insert('eVASegmentTypePropagate','Transfer_Ellipse','-');
        outerOrbit_apo.PropagatorName = 'Earth Point Mass';
        outerOrbit_apo.Properties.Color = 65280;
        % Add an Apoapsis Stopping Condition and remove the Duration Stopping Condition
        outerOrbit_apo.StoppingConditions.Add('AscendingNode');
        outerOrbit_apo.StoppingConditions.Remove('Duration');
    else
        % Propagate the Transfer Orbit to Apogee
        outerOrbit_apo =
ASTG.MainSequence.Insert('eVASegmentTypePropagate','Transfer_Ellipse','-');
        outerOrbit_apo.PropagatorName = 'Earth Point Mass';
        outerOrbit_apo.Properties.Color = 65280;
        % Add an Apoapsis Stopping Condition and remove the Duration Stopping Condition
        outerOrbit_apo.StoppingConditions.Add('Apoapsis');
        outerOrbit_apo.StoppingConditions.Remove('Duration');
    end

    % Execute
    ASTG.RunMCS;

end

% Get end time
EndTime_old = EndTime ;
count = satellite.Propagator.MainSequence.count;
EndTime = satellite.Propagator.MainSequence.Item(count-1).FinalState.Epoch ;

waitbar((EndTime/ScenarioLength),h2,OBSstring) ;

if EndTime > (ScenarioLength-(3600*24))
    break
end

loop_count = loop_count+1;
end

propagate_end = ASTG.MainSequence.Insert('eVASegmentTypePropagate', 'Propagate End', '-');
propagate_end.PropagatorName = 'Earth Point Mass';
propagate_end.StoppingConditions.Add('Epoch');
propagate_end.StoppingConditions.Remove('Duration');

```

```

propagate_end.StoppingConditions.Item('Epoch').Properties.Trip = ScenarioLength;

ASTG.RunMCS;

% Close waitbar
close(h2)
end

end

```

## Maneuver Manager 2

```

% RAAN Maneuver

if Man_Flag == 2 % maneuver flag

alt = cluster_alt; %km
OBSperigee = perigee_array + alt ; %km
OBSapogee = apogee_array + alt ; %km
OBSlocation = 0:(360/length(perigee_array)):359 ;
OBSinc = ones(1,length(perigee_array))*cluster_inc ;

for i=1:length(OBSlocation)

% Start Satellite
OBSnum = sprintf('OBS%d',i) ;
satellite= scenario.Children.New('esatellite',OBSnum) ;

% Start waitbar
OBSstring = strcat(OBSnum,' Loading Maneuvers');
h2 = waitbar(0,OBSstring) ;

% Set propagator type to astrogator
satellite.SetPropagatorType('ePropagatorAstrogator');
ASTG = satellite.Propagator;
ASTG.MainSequence.RemoveAll(); %Clear all segments from the MCS

% Insert Initial State Segment into MCS and configure
initState = ASTG.MainSequence.Insert('eVASegmentTypeInitialState', 'Initial State', '-');
initState.InitialState.Epoch = scenario.StartTime;
initState.SetElementType('eVAElementypeKeplerian');
kep = initState.Element;
kep.PeriapsisRadiusSize = OBSperigee(i);
kep.Eccentricity = 1 - 2/((OBSapogee(i)/OBSperigee(i)) + 1);
kep.ArgOfPeriapsis = 0;
kep.RAAN = OBSlocation(i);
kep.Inclination = OBSinc(i);
kep.TrueAnomaly = 0;

% Propagate for a full day
propagate1 = ASTG.MainSequence.Insert('eVASegmentTypePropagate', 'Propagate 1', '-');
propagate1.PropagatorName = 'Earth Point Mass';
propagate1.Properties.Color = 255; % Red

```

```

propagate1.StoppingConditions.Item('Duration').Properties.Trip = 3600*24*5 ;

dRAAN = 5 ;
vu = acosd(cosd(OBSinc(i))^2 + sind(OBSinc(i))^2*cosd(dRAAN)) ;
ArgLat_i = acosd(tand(OBSinc(i))*((cosd(dRAAN)-cosd(vu)) / (sind(vu)))) ;
ArgLat_f = acosd(cosd(OBSinc(i))*sind(OBSinc(i))*((1-cosd(dRAAN))/(sind(vu)))) ;

% Insert a Propagate State Segment into the MCS and Add/Remove Stopping Conditions
propagate2 = ASTG.MainSequence.Insert('eVASegmentTypePropagate', 'Propagate 2', '-');
propagate2.PropagatorName = 'Earth Point Mass';
propagate2.Properties.Color = 255; % Red
propagate2.StoppingConditions.Add('Argument of Latitude');
propagate2.StoppingConditions.Remove('Duration');
propagate2.StoppingConditions.Item('Argument_of_Latitude').Properties.Trip = ArgLat_i ;

PropCount = 2;

% Run the MCS
ASTG.RunMCS;

% Set the range constraint
rangeconst = ['SetConstraint */Satellite/' OBSnum ' Range Min 0 Max ' num2str(Range)] ;
root.ExecuteCommand(rangeconst) ;

% Get time of apoapsis
EndTime = satellite.Propagator.MainSequence.Item(2).FinalState.Epoch ;

loop_count = 1 ;
maneuver=1;
while(1)
    if maneuver == 1

        % Insert a target sequence with nested maneuver segment
        ts = ASTG.MainSequence.Insert('eVASegmentTypeTargetSequence', 'Start Transfer', '-');
        dv1 = ts.Segments.Insert('eVASegmentTypeManeuver', 'DV1', '-');
        dv1.SetManeuverType('eVAManeuverTypeImpulsive');
        % Create a handle to the impulsive properties of the maneuver
        impulsive = dv1.Maneuver;
        impulsive.SetAttitudeControlType('eVAAttitudeControlThrustVector');
        % Create a handle to the Attitude Control - Thrust Vector properties of the
        % maneuver and set the appropriate axes
        thrustVector = impulsive.AttitudeControl;
        thrustVector.ThrustAxesName = 'Satellite VNC(Earth)';
        % For the targeter to vary a given segment property, it must be
        % enabled as a control parameter.
        dv1.EnableControlParameter('eVAControlManeuverImpulsiveCartesianX');
        dv1.EnableControlParameter('eVAControlManeuverImpulsiveCartesianY');
        % Segment Results, which can be used as targeter goals, are also stored in a
collection
        dv1.Results.Add('Keplerian Elems/Argument of Latitude');
        dv1.Results.Add('Keplerian Elems/Radius of Apoapsis');
        % Targeter Profiles are also stored as a collection
        dc = ts.Profiles.Item('Differential Corrector');
    end
end

```

```

        % Create a handle to the targeter control and set its properties
        xControlParam = dc.ControlParameters.GetControlByPaths('DV1',
'ImpulsiveMnvr.Cartesian.X');
        xControlParam.Enable = true;
        xControlParam.MaxStep = 0.1;
        yControlParam = dc.ControlParameters.GetControlByPaths('DV1',
'ImpulsiveMnvr.Cartesian.Y');
        yControlParam.Enable = true;
        yControlParam.MaxStep = 0.1;

        % Create a handle to the targeter results and set its properties
        Result = dc.Results.GetResultByPaths('DV1', 'Argument of Latitude');
        Result.Enable = true;
        Result.DesiredValue = ArgLat_f ;
        Result.Tolerance = 0.001;
        Result2 = dc.Results.GetResultByPaths('DV1', 'Radius Of Apoapsis');
        Result2.Enable = true;
        Result2.DesiredValue = OBSapogee(i) ;
        Result2.Tolerance = 0.001;

        % Set final DC and targeter properties and run modes
        dc.MaxIterations = 50;
        dc.EnabledDisplayStatus = true;
        dc.Mode = 'evAProfileModeIterate';
        ts.Action = 'evATargetSeqActionRunActiveProfiles';

        % Propagate the Outer Orbit
        outerOrbit = ASTG.MainSequence.Insert('evASegmentTypePropagate','Outer Orbit','-');
        outerOrbit.PropagatorName = 'Earth Point Mass';
        outerOrbit.StoppingConditions.Item('Duration').Properties.Trip = 3600*24*15;

        % Insert a Propagate State Segment into the MCS and Add/Remove Stopping Conditions
        PropCount = PropCount+1;
        prop_string = ['Propagate' num2str(PropCount)];
        propagate = ASTG.MainSequence.Insert('evASegmentTypePropagate', prop_string, '-');
        propagate.PropagatorName = 'Earth Point Mass';
        propagate.StoppingConditions.Add('Argument of Latitude');
        propagate.StoppingConditions.Remove('Duration');
        propagate.StoppingConditions.Item('Argument_of_Latitude').Properties.Trip = ArgLat_i
;

        % Execute
        ASTG.RunMCS;

else

        % Propagate for a full day
        PropCount = PropCount+1;
        prop_string = ['Propagate' num2str(PropCount)];
        propagate = ASTG.MainSequence.Insert('evASegmentTypePropagate', prop_string, '-');
        propagate.PropagatorName = 'Earth Point Mass';
        propagate.StoppingConditions.Item('Duration').Properties.Trip = 3600*24*15 ;

        % Execute

```

```

        ASTG.RunMCS;
    end

    % Get end time
    count = satellite.Propagator.MainSequence.count;
    EndTime = satellite.Propagator.MainSequence.Item(count-1).FinalState.Epoch ;

    waitbar((EndTime/ScenarioLength),h2,OBSstring) ;

    if EndTime > (ScenarioLength-(3600*24))
        break
    end

    loop_count = loop_count+1;
end

propagate_end = ASTG.MainSequence.Insert('eVASegmentTypePropagate', 'Propagate End', '-');
propagate_end.PropagatorName = 'Earth Point Mass';
propagate_end.StoppingConditions.Add('Epoch');
propagate_end.StoppingConditions.Remove('Duration');
propagate_end.StoppingConditions.Item('Epoch').Properties.Trip = ScenarioLength;

ASTG.RunMCS;

% Close waitbar
close(h2)
end

end

```

### Conjunction Data Generation

```

h = waitbar(0,'Conjunction Analysis In Progress...') ;

for i=1:length(SSC)

    SSCinc = SSC(i) ;
    sat1 = scenario.Children.Item(num2str(SSCinc,'%05d')) ;

    %Set up data storage, in structure, for current satellite
    conjunctionData(i).PrimarySatellite = SSCinc;
    conjunctionData(i).ConjunctionInfo = conjInfoStruct;

    % Compare to each other satellite in SSC vector
    numConjunctions = 0;
    for j=1:length(apogee_array) %length(OBS)
        OBSinc = sprintf('OBS%d',j) ;
        sat2 = scenario.Children.Item(OBSinc) ;
        acc=sat1.GetAccessToObject(sat2);
        acc.ComputeAccess;

        % Create displacement vector between the two satellites and a
        % corresponding vector Magnitude calculation scalar to query the

```

```

% time of min and min range values:
if (sat1.Vgt.Vectors.Contains('ToSat2') == 0)
    relativePositionVector = sat1.Vgt.Vectors.Factory.Create('ToSat2', 'Displacement
vector', 'eCrndVectorTypeDisplacement');
else
    relativePositionVector = sat1.Vgt.Vectors.Item('ToSat2');
end
relativePositionVector.Origin.SetPoint(sat1.Vgt.Points.Item('Center'));

% Create vector parameter set in the RIC frame to get access to the
% vector components:
if (sat1.Vgt.ParameterSets.Contains('ToSat2_RIC') == 0)
    positionVectorSetRIC =
sat1.Vgt.ParameterSets.Factory.CreateParameterSetVector('ToSat2_RIC', 'Vector parameter set
expressing relative position in the RIC frame');
else
    positionVectorSetRIC = sat1.Vgt.ParameterSets.Item('ToSat2_RIC');
end
positionVectorSetRIC.Vector = relativePositionVector;
positionVectorSetRIC.ReferenceAxes = sat1.Vgt.Axes.Item('RIC');

    relativePositionMagnitude =
positionVectorSetRIC.EmbeddedComponents.Item('ToSat2_RIC.Cartesian.Magnitude');
    relativePositionX =
positionVectorSetRIC.EmbeddedComponents.Item('ToSat2_RIC.Cartesian.X');
    relativePositionY =
positionVectorSetRIC.EmbeddedComponents.Item('ToSat2_RIC.Cartesian.Y');
    relativePositionZ =
positionVectorSetRIC.EmbeddedComponents.Item('ToSat2_RIC.Cartesian.Z');

% Create a velocity vector by taking the derivative of the position
% vector in ECEF:
if (sat1.Vgt.Vectors.Contains('dxToSat2') == 0)
    relativeVelocityVector = sat1.Vgt.Vectors.Factory.Create('dxToSat2', 'Derivative of
relative position vector', 'eCrndVectorTypeDerivative');
    relativeVelocityVector.Vector.SetVector(relativePositionVector);
    relativeVelocityVector.ReferenceAxes.SetAxes(root.Vgt.WellKnownAxes.Earth.Fixed);
    relativeVelocityVector.DifferencingTimeStep = 0.1;
else
    relativeVelocityVector = sat1.Vgt.Vectors.Item('dxToSat2');
end

% Create vector parameter set in the RIC frame to get access to the
% vector components:
if (sat1.Vgt.ParameterSets.Contains('dxToSat2_RIC') == 0)
    velocityVectorSetRIC =
sat1.Vgt.ParameterSets.Factory.CreateParameterSetVector('dxToSat2_RIC', 'Vector parameter set
expressing relative position in the RIC frame');
else
    velocityVectorSetRIC = sat1.Vgt.ParameterSets.Item('dxToSat2_RIC');
end
velocityVectorSetRIC.Vector = relativeVelocityVector;
velocityVectorSetRIC.ReferenceAxes = sat1.Vgt.Axes.Item('RIC');

```

```

        relativeVelocityMagnitude =
velocityVectorSetRIC.EmbeddedComponents.Item('dxToSat2_RIC.Cartesian.Magnitude');
        relativeVelocityX =
velocityVectorSetRIC.EmbeddedComponents.Item('dxToSat2_RIC.Cartesian.X');
        relativeVelocityY =
velocityVectorSetRIC.EmbeddedComponents.Item('dxToSat2_RIC.Cartesian.Y');
        relativeVelocityZ =
velocityVectorSetRIC.EmbeddedComponents.Item('dxToSat2_RIC.Cartesian.Z');

        % Create an event array to find the time of minimum range per access interval:
        if (sat1.Vgt.EventArrays.Contains('TimesOfMinRange') == 0)
            extremaArray =
sat1.Vgt.EventArrays.Factory.CreateEventArrayExtrema('TimesOfMinRange','Times for min range over
access intervals');
            extremaArray.ExtremumType = 'eCrdnExtremumMinimum';
            extremaArray.Calculation = relativePositionMagnitude;
            extremaArray.IsGlobal = true;
        else
            extremaArray = sat1.Vgt.EventArrays.Item('TimesOfMinRange');
        end

        subptDP = sat1.DataProviders.GetDataPrvTimeVarFromPath('LLA State/Fixed');

        if acc.ComputedAccessIntervalTimes.Count ~= 0
            % Update the end point of the position vector to the current
            % satellite and pass the access intervals to the event array:
            relativePositionVector.Destination.SetPoint(sat2.Vgt.Points.Item('Center'));
            intervalCmd = ['TimeTool * Satellite/',sat1.InstanceName,' Modify "Time Array"
TimesOfMinRange "Times of Extrema" "TimeIntervalList" "Access/Satellite-',sat1.InstanceName,'-To-
Satellite-',sat2.InstanceName,' AccessIntervals"'];
            root.ExecuteCommand(intervalCmd);
            localMinTimes = extremaArray.FindTimes().Times;

            % Compute Duration of Access Intervals
            accDP = acc.DataProviders.Item('Access
Data').Exec(scenario.StartTime,scenario.StopTime) ;

            DurationStartTimes = accDP.DataSets.GetDataSetByName('Start Time').GetValues ;
            DurationStopTimes = accDP.DataSets.GetDataSetByName('Stop Time').GetValues ;
            DurationTimes = accDP.DataSets.GetDataSetByName('Duration').GetValues ;

            for nRows = 1:length(localMinTimes)
                numConjunctions = numConjunctions + 1;
                minTime = localMinTimes{nRows};
                % Evaluate the relative range and velocity at the
                % minimum range time:
                rangeAtMinTime = relativePositionMagnitude.Evaluate(minTime).Value;
                rangeXAtMinTime = relativePositionX.Evaluate(minTime).Value;
                rangeYAtMinTime = relativePositionY.Evaluate(minTime).Value;
                rangeZAtMinTime = relativePositionZ.Evaluate(minTime).Value;

                velocityAtMinTime = relativeVelocityMagnitude.Evaluate(minTime).Value;
                velocityXAtMinTime = relativeVelocityX.Evaluate(minTime).Value;
                velocityYAtMinTime = relativeVelocityY.Evaluate(minTime).Value;

```



```

velocityZAtMinTime = relativeVelocityZ.Evaluate(minTime).Value;

subptRes = subptDP.ExecSingleElements(minTime, subptElems);
deticLatitude = cell2mat(subptRes.DataSets.GetDataSetByName('Lat').GetValues);
deticLongitude = cell2mat(subptRes.DataSets.GetDataSetByName('Lon').GetValues);
wgs84Alt = cell2mat(subptRes.DataSets.GetDataSetByName('Alt').GetValues);

% Populate conjunction data structure:
conjunctionData(i).ConjunctionInfo(numConjunctions).ConjunctingSatellite =
num2str(OBSinc);

conjunctionData(i).ConjunctionInfo(numConjunctions).TCA = minTime;

conjunctionData(i).ConjunctionInfo(numConjunctions).RangeMag = rangeAtMinTime;
conjunctionData(i).ConjunctionInfo(numConjunctions).Radial = rangeXAtMinTime;
conjunctionData(i).ConjunctionInfo(numConjunctions).InPlane = rangeYAtMinTime;
conjunctionData(i).ConjunctionInfo(numConjunctions).Normal = rangeZAtMinTime;

conjunctionData(i).ConjunctionInfo(numConjunctions).VelocityMag =
velocityAtMinTime;
conjunctionData(i).ConjunctionInfo(numConjunctions).V_Radial =
velocityXAtMinTime;
conjunctionData(i).ConjunctionInfo(numConjunctions).V_InPlane =
velocityYAtMinTime;
conjunctionData(i).ConjunctionInfo(numConjunctions).V_Normal =
velocityZAtMinTime;

conjunctionData(i).ConjunctionInfo(numConjunctions).Latitude = deticLatitude;
conjunctionData(i).ConjunctionInfo(numConjunctions).Longitude = deticLongitude;
conjunctionData(i).ConjunctionInfo(numConjunctions).Altitude = wgs84Alt;

conjunctionData(i).ConjunctionInfo(numConjunctions).AccessStart =
cell2mat(DurationStartTimes(nRows));
conjunctionData(i).ConjunctionInfo(numConjunctions).AccessStop =
cell2mat(DurationStopTimes(nRows));
conjunctionData(i).ConjunctionInfo(numConjunctions).Duration =
cell2mat(DurationTimes(nRows));
    end
end
end

% Remove computed access to free up memory
acc.RemoveAccess;

% Remove created components before moving on to next object:
sat1.Vgt.CalcScalars.Remove(positionVectorSetRIC.Name);
sat1.Vgt.CalcScalars.Remove(velocityVectorSetRIC.Name);
sat1.Vgt.EventArrays.Remove(extremaArray.Name);
sat1.Vgt.Vectors.Remove(relativePositionVector.Name);
sat1.Vgt.Vectors.Remove(relativeVelocityVector.Name);
clear acc;

waitbar(i/length(SSC),h) ;
fprintf('Sat %d Complete\n',i)

```

```

end
close(h)
disp('Data Generation: Complete')

```

## Post Process of Results

```

DataStruct = struct('PrimarySatellite', {}, 'Metrics', {});
Metrics = struct('PC', {}, 'MD', {}, 'MnD', {}, 'TAG', {}, 'MRT', {});

TotalSimTime = (scenario.StopTime - scenario.StartTime) ;

for ii = 1:length(conjunctionData)

    if isempty(conjunctionData(ii).ConjunctionInfo) ~= 1
        %Set up data storage, in structure, for current satellite
        DataStruct(ii).PrimarySatellite = SSC(ii);
        DataStruct(ii).Metrics = Metrics;

        %Create Duration Metrics
        for jj = 1:length(conjunctionData(ii).ConjunctionInfo)
            Duration(jj) = conjunctionData(ii).ConjunctionInfo(jj).Duration;

            AccessStartTimes(jj) = (conjunctionData(ii).ConjunctionInfo(jj).AccessStart) ;
            AccessStopTimes(jj) = (conjunctionData(ii).ConjunctionInfo(jj).AccessStop) ;
        end

        [AccessStartTimesSort, Idx] = sort(AccessStartTimes) ;
        AccessStopTimesSort = AccessStopTimes(Idx);

        % Sort Duration Gaps and eliminate access overlaps
        jj=1; EndGapFlag = 0 ;
        while jj < length(conjunctionData(ii).ConjunctionInfo)
            if jj>1
                if (AccessStartTimesSort(jj) - AccessStopTimesSort(jj-1)) > 0
                    DurationGaps(jj) = (AccessStartTimesSort(jj) - AccessStopTimesSort(jj-1)) ;
                    jj=jj+1;
                else
                    kk = jj ;
                    while(1)
                        kk=kk+1;
                        if kk > length(AccessStartTimesSort)
                            EndGapFlag = 1 ;
                            break
                        end
                        if (AccessStartTimesSort(kk) - AccessStopTimesSort(jj-1)) > 0
                            DurationGaps(jj) = (AccessStartTimesSort(kk) -
AccessStopTimesSort(jj-1)) ;
                            jj = kk;
                            break
                        end
                    end
                    jj=jj+1;
                end
            end
        end
    end
end

```

```

        else
            DurationGaps(jj) = (AccessStartTimesSort(jj) - scenario.StartTime) ;
            jj=jj+1;
        end
    end

    if EndGapFlag
        DurationGaps(jj) = (scenario.StopTime - AccessStopTimesSort(jj-1)) ;
    else
        DurationGaps(jj) = (scenario.StopTime - AccessStopTimesSort(end)) ;
    end

    DurationTotal = TotalSimTime - sum(DurationGaps) ;

    % Percent Coverage
    PC = ((DurationTotal) / TotalSimTime)*100 ;
    DataStruct(ii).Metrics(1).PC = PC ;
    PCMetrics(ii) = PC ;

    % Avg Duration
    MeanDuration = mean(Duration) ;
    DataStruct(ii).Metrics(1).MnD = MeanDuration ;
    MnDMetrics(ii) = MeanDuration ;

    % Time Average Gap
    TAG = (sum(DurationGaps.^2) / TotalSimTime) ;
    DataStruct(ii).Metrics(1).TAG = TAG ;
    TAGMetrics(ii) = TAG ;

    % Mean Response Time
    for qq = 1:length(DurationGaps)
        MRTmetric(qq) = (DurationGaps(qq)*(DurationGaps(qq) + 1))/2 ; % 1+2+3+...n = n(n+1)/2
    end
    MRT = sum(MRTmetric)/TotalSimTime ;
    DataStruct(ii).Metrics(1).MRT = MRT ;
    MRTMetrics(ii) = MRT ;

else

    % if no conjunctions
    PCMetrics(ii) = 0 ;
    MnDMetrics(ii) = 0 ;
    TAGMetrics(ii) = TotalSimTime ;
    MRTMetrics(ii) = TotalSimTime ; %365 day duration

end

% Clear variables
clear DurationGaps
clear DurationTotal
clear Duration
clear AccessStartTimes
clear AccessStopTimes
clear AccessStartTimesSort

```

```
clear AccessStopTimesSort

end

% Mean Statistics For Constellation Set
PCavg = mean(PCMetrics); %percent
MnDavg = mean(MnDMetrics); %seconds
TAGavg = mean(TAGMetrics); %seconds
MRTavg = mean(MRTMetrics); %seconds

% Save off results for post-processing
save([filename '_DataStruct'],'DataStruct')
save([filename '_conjunctionData'],'conjunctionData')
save([filename '_averages'],'PCavg','MnDavg','TAGavg','MRTavg') ;

end
```

*Published with MATLAB® R2016b*